Suffusion Evaluation - Comparison of Current Approaches

Olivier Semar[1], Dipl.-Ing., Prof. Dr.-Ing. Karl Josef Witt[2], and Prof. Dr. R. Jonathan Fannin[3]

[1]Lahmeyer International GmbH, Hydropower and Water Resources, olivier.semar@lahmeyer.de
[2]Bauhaus-Universität Weimar, Germany, Department of Geotechnical Engineering, kj.witt@uni-weimar.de
[3]University of British Columbia, Canada, Department of Civil Engineering, jonathan.fannin@ubc.ca

ABSTRACT

The paper gives an evaluation of current practice to assess the vulnerability to suffusion. Therefore comparisons of different approaches concepts are summarized. Suffusion is characterized by the phenomena that the fines can move inside a soil skeleton. In practice the vulnerability to suffusion is evaluated in two steps. First the geometrical possibility of fine movement is analysed. If the fine particles are mobile the hydraulic conditions come into focus as triggering force. In this contribution the authors concentrate on the geometrical criteria used in current design practice. A comparison of limit state conditions and an evaluation of laboratory studies will be delivered. In addition new approaches based on statistical and stochastically methods are discussed.

Key words: suffusion, filter criteria, internal erosion, soil structure

INTRODUCTION

Internal erosion of soil structures is an essential problem for the long-term stability of earth structures impacted by seepage. One particular phenomenon of internal erosion, the displacement of fines in the grain skeleton, is called suffusion. When suffusion occurs than the permeability and the porosity will increase while the bulk density decreases. The consequences are a decrease of resistance against external load and settlement as well as significant change in the state of pore pressure [10].

In dependency of the location where suffusion might occur Ziems [34] distinguishes three types i. e. internal suffusion, external suffusion and contact suffusion (Figure 1). The mechanics of the process is very similar. The focus in this paper is located at the phenomena of internal suffusion. Good reviews to several kinds of internal erosion were published among others in [2, 19, 24, 25].

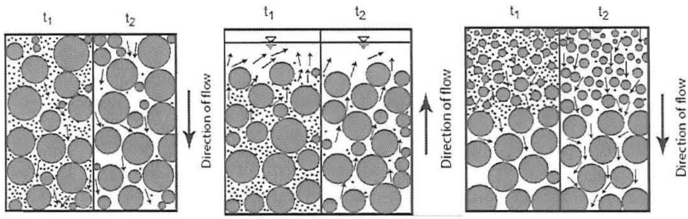

Figure 1: illustration of Suffusion by Ziems [34] for time steps t_1 and t_2.

Internal suffusion might be spatially restricted as a local phenomena where the fines will be trapped in dependency of particle size and hydrodynamic forces (colmatation). But suffusion can grow to a global wash out of fines from the grain skeleton. To exclude that internal suffusion of soils can occur it is necessary to satisfy two criteria. The sufficient criterion is the proof whether it is possible that fine material is able to pass through the smallest constrictions along the relevant pore path without clogging (geometrical criteria). The fundamental criterion is satisfied when it can be excluded that the hydrodynamic load in the pore structure provides a critical energy needed to mobilize and transport the fines (hydraulic criteria).

Geometrical suffusion criteria

The first researchers who concentrate on suffusive soils were motivated by creating mix filters in embankment dams instead of layered filters. Therefore they developed optimal mixture relationships. The concept was the creation of soils with minimum porosity based by experiences in the field of concrete technology. Such non suffusive soil mixtures were described e. g. by Pavčič, Talbot, Ochotin, Lupinskij (cited in [12]) and Sichardt [31]. With an absolute minimum of porosity two fundamental aspects are fulfilled,

- an uniform distribution of constriction sizes with a small mean value and therefore a minimum effective opening size
- a structure in which the majority of grains are fixed by a certain contact stress. This can bee assumed for homogeneous soils with a steady curved grain size distribution, a low porosity and therefore an uniform distribution of constriction sizes within the pore structure.

With this idealised packing providing a minimum porosity as propagated by Patrašev laboratory tests are carried out by Pavčič [22], Čištin [4] and Lubočkov [12, 13, 14, 15] developed empirical relationships (equation 1) to calculate perfect non-suffusive grain size distributions while taking into account the factor of uniformity C_U.

$$\frac{d_i}{d_{max}} = f(p_i, C_U) \qquad \text{respective} \qquad \frac{d_i}{d_{min}} = f(p_i, C_U) \tag{1}$$

p_i finer by weight of the grain diameter d_i

d_{max}, d_{min} maximum respectively minimum grain size diameter

In Europe the graphical approach by Lubočkov is used [12, 13, 14, 15] by comparing the normalized grain size distribution with empirical thresholds (Figure 2). Another empirical graphical approach is published by Burenkova [1] (Figure 3). This approach is valid for convex, concave and linear grain size distributions in semi-logarithmic scale. Gap graded grain size distributions can not be analysed.

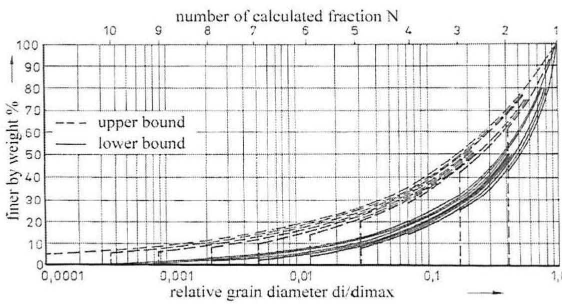

Figure 2: Upper and lower bound of non-suffusive soils by Lubočkov [13]

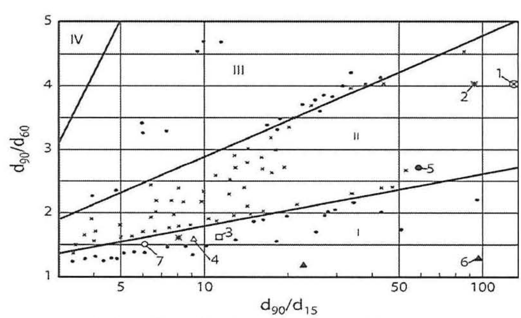

Zone I and III: suffusive

Zone II: non-suffusive

Zone IV: zone of artificial soils

Figure 3: Criterion of Burenkova [1]

Recognising the internal stability of a granular material results from an ability to prevent the loss of its own small particles due to disturbing influences such as seepage and vibration, Kenney and Lau [7] conducted a series of tests to define a threshold between stable and potentially unstable gradations. The base soils were well-graded sandy gravels and the filter materials a uniform medium or coarse gravel, or uniform distribution of coarse gravel and cobbles. Interpretation of the results based on a method of describing the shape of the grading curve and, therefore, is insensitive to grain size of the soil (see Figure 4).

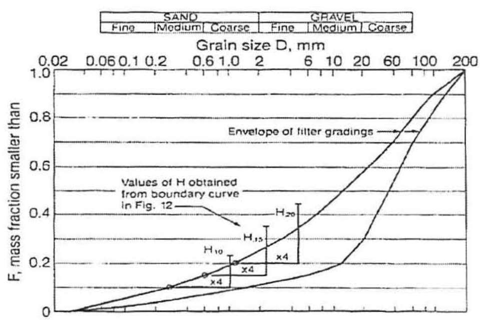

Figure 4: Shape analysis (after [7])

As illustrated, a discrete envelope of points (H) is established for selected intervals on the grading curve (F). If the grading curve lies below this envelope of points, over a designated portion of its finer end, then the gradation is deemed potentially unstable. The concept follows from that originally advanced by Lubočkov. The postulated boundary between stable and potentially unstable grading curves was firstly defined as $H/F = 1.3$ [7].

The experimental study of Kenney and Lau [7] generated significant discussion. Comments by Milligan [17], and additional work by Sherard and Dunnigan [30], led Kenney and Lau [8] to perform additional tests and redefine the postulated boundary between stable and potentially unstable grading curves as $H/F = 1$. Skempton and Brogan [32] report findings from piping tests on well graded and gap graded sandy gravels that broadly confirm the Kenney and Lau [8] criterion for internal stability. They found that there is an abrupt transition from stable to suffusive behaviour at about the limits defined by Kenney and Lau as well as those defined by Kezdi [9].

The above mentioned methods do not deliver sharp criteria in the classical engineering sense defining limit state conditions with a physical background. This empirical considerations give an idea whether a soil is vulnerable to be suffusive or not by analysing the heterogeneity and comparing the grain size distribution to thresholds.

The first geometric suffusion criterion based an physical considerations of the pore space was developed by Patrašev [21]. It is based on the idea that suffusion is impossible if the largest mobile particle d_s would not be able to pass through an equivalent pore size d_{po} (equation 2). This consideration introduces the fundamental approach, that there is a pore structure constituted by coarser fractions and a potentially mobile portion of grains, which are prone to erode.

$$d_s \geq d_{po} \tag{2}$$

This kind of criteria is considered of several technical guidelines. The Russian guideline [20] denotes two criteria on this basis.

Alternative 1: Mobility of particles

$$\begin{aligned} & d_s \geq 0{,}77 \cdot d_{po} \text{ with} \\ & d_{po} = 0.455 \cdot (1 + 0.05 \cdot C_u) \cdot \sqrt[6]{C_u \cdot e \cdot d_{17}} \quad \text{for } C_u \leq 25 \\ & d_{po} = 0.16 \cdot \left(3 + \sqrt[3]{C_u \cdot \lg(C_u)}\right) \cdot \sqrt[6]{C_u \cdot e \cdot d_{17}} \quad \text{for } C_u > 25 \end{aligned} \tag{3}$$

d_s largest suffusive grain size diameter

d_{po} effective opening size of the structure

d_{17} grain size diameter with 17% finer by weight

Alternative 2: Condition of suffusion

$$\frac{d_{3-5\%}}{d_{17}} \geq 0.32 \cdot (1 + 0.05 \cdot C_u) \cdot \sqrt[6]{C_u \cdot e} \tag{4}$$

$d_{3-5\%}$ accepted loss from 3 to 5% finer by weight

In Germany the inequation 5 by Ziems [34] is used.

$$\begin{aligned} & d_{min} \geq 1.5 \cdot 0.6 \cdot 0.455 \cdot \sqrt[6]{C_u \cdot e \cdot d_{17}} \\ & \Leftrightarrow \frac{d_{0-3\%}}{d_{17}} \geq 0.41 \cdot \sqrt[6]{C_u \cdot e} \end{aligned}$$

In a study of filtration phenomena, Sherard et al. [28] concluded the filter design criterion, which Karl Terzaghi had formulated from his theoretical studies and companion special technical advising [5], is conservative, but not unduly so, for filters with a D_{15} greater than 1.0 mm. Alternative recommendations were made for finer filters suitable for base soils comprising fine-grained silts and clays [29]. Importantly, the authors noted that based on Terzaghi's criteria [33] the limit proposed by Kezdi [9] involves dividing the soil into a fine and coarse component, using select fines content on the grading curve. If the two components satisfy the filtration rule of Terzaghi [33], where $D_{15}/d_{85} < 4$, then the composite gradation will be self-filtering and therefore internally stable.

The Federal Waterways Engineering and Research Institute (BAW) in Germany as well recommend in a guideline [18] first to separate the grain size distribution into a finer and coarser part and to proof the stability with the geometrical filter criterion of Čištin/Ziems (Figure 5) afterwards. Steady grain size distributions, should be separate, at the inflection point. In case of gap graded grain size distributions it is reasonable to separate in the range of the gap (saddle point) [24]. The criterion of Čištin/Ziems was initially developed to analyse contact erosion phenomena. The geometrical criterion - i. e. no filtration - is satisfied if the relation $A50 = d_{50,II}/d_{50I}$ is less than the ultimate-relation $A_{50,ult}$ given at the y-axis of the chart in Figure 5. The index I indicates the base-material (fines), the index II is referred to the coarser material (filter).

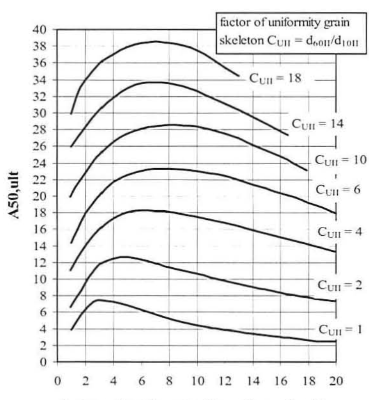

Figure 5: Criterion of Čištin/Ziems (cited in [2])

A unified approach combining the method of Kezdi and Kenney and Lau was established by Li and Fannin [11]. The common feature of both methods is the examination of the slope of the gradation curve over a discrete interval of its length [3]. The difference arises from the criterion used to establish the size of that interval: one approach uses a constant increment of percent finer by mass while, in contrast, the other uses a variable increment of grain size. More specifically, the D'_{15}/d'_{15} filter ratio of Kezdi [9] is calculated, by its very definition, over the constant increment of $H = 15\%$ at any point along the gradation curve. It implies a theoretical boundary to instability that is a linear relation on the semi-log plot of grain size. In contrast, the H/F stability index of Kenney and Lau [8] is calculated over the increment D to 4D, which increases in magnitude with progression along the gradation curve. It therefore implies a theoretical boundary to instability that is a non-linear relation and concave upwards in shape [11].

A plot of the respective Kezdi and Kenney and Lau boundaries, in F:H space, is given in Figure 6. At values of $F > 15\%$, the method of Kenney and Lau defines a boundary to internal stability which locates above that of the Kezdi method. Conversely, the method of Kezdi defines a boundary above that of the Kenney and Lau method at $F < 15\%$. The suggested limit values to stability of $D'_{15}/d'_{85} = 4$ and $H/F = 1$ yield a unique point on the gradation curve, where both criteria converge at $F \approx 15\%$. By inspection, the Kenney and Lau criterion is the more conservative of the two methods at $F > 15\%$, while the Kezdi criterion is more conservative at $F < 15\%$.

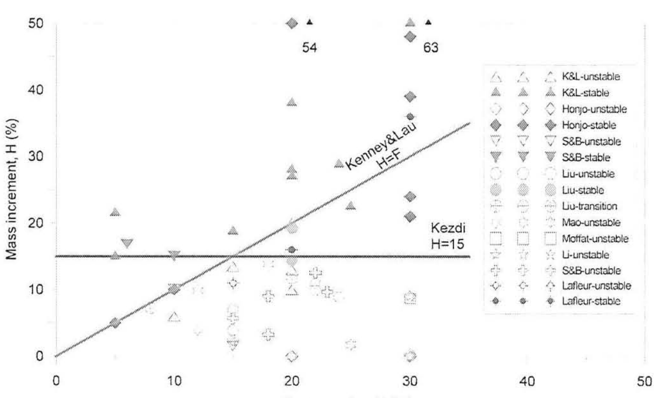

Figure 6: A unified approach for geometric analysis [11]

Merits of unifying some aspects of the two empirical methods are further examined in Figure 6. The data are those compiled by Li and Fannin [11] for 41 unstable soils and 22 stable soils. Inspection of the plot suggests the Kenney and Lau criterion of instability at $H/F < 1$ yields a more precise distinction between stable and unstable gradations at $F < 15\%$. In contrast, the Kezdi criterion yields a more precise distinction at $F > 15\%$. The resulting unified approach offers some improvements as a decision-support tool, and is currently being evaluated for adoption in engineering practice.

The above mentioned criteria allow permitting in advance which soils are definitely not vulnerable to suffusion. Therefore characteristically non-suffusive soils are [2, 25]:

- Soils with a factor of uniformity $C_U = d_{60}/d_{10} \approx 1$ (d_{60} and d_{10}: diameters of particles for which 60% or 10% are smaller by weight).
- Soils with a rather linear grain size distribution in semi-logarithmic scale with $C_U < 10$ irrespective of density index I_D.
- Non-uniform soils with $C_U > 10$ and $I_D > 0.6$
- Steady curved grain size distribution with $C_U < 8$ irrespective of I_D
- Non-uniform soils which are very close to the Fuller or Talbot grain size distribution. After Lubočkov [13] non-uniform soils with $I_D = 0.3$ till 0.6 and steady curved grain size distribution in border area of Figure 2.

The comparison of the different approaches shows that in general they are limited in their usability. Most of them are of empirical nature so that transferability has to be proofed. Mostly the limitation is the factor of uniformity or the gradation, because the empirical criteria are minimized to a range of soils. Also the empirical criteria do not distinguish between hydraulic and geometrical influences of particle transport. All aspects of transport and clogging phenomena are mixed up. Soils with slightly cohesive character can not be analysed with the common criteria, because the size of the eroded aggregates are unknown. Another disadvantage is that only the vulnerability to suffusion can be estimated or the largest suffusive particle diameter.

CURRENT RESEARCH

Two possibilities to derive better criteria are currently pursued, the empirical and theoretical way. The aim of the empirical way done for example by French project ERINOH and the European working group on internal erosion is the development of methods to a better prediction of the vulnerability to internal erosion. This includes in situ and laboratory studies. The methods regards primarily on the erodibility of soils.

Contrary the German research group "SUFFOS" supported by the German Research Foundation (DFG) are using a theoretical and modern approach to simulate transport and clogging processes inside a void structure, the so called percolation theory (above others [27]). This theory is a branch of the probability theory dealing with properties of random media. Determining the three-dimensional pore structure in advance is necessary to simulate the possibility of locally limited and global particle movement with the percolation theory adequately. In this sieve-analogy the governing soil structure is acting as a spatial sieve while the embedded fines are considered as a randomly distributed base material. The determination of the relevant pore structure is part of current research [6, 16, 27].

First general statements about local and global mobility of fines inside a grain structure can already be made with uncorrelated bond percolation models [27]. The constriction sizes of the grain skeleton are the controlling parameters for the fine movement possibility. A first approach can therefore be derived when using the constriction size distribution of the grain skeleton with Schulers' approach [26], which is the most promising at the moment. Other approaches to determine constriction size distributions and effective pore opening sizes are summarised in Reboul[23].

CONCLUSIONS

The comparison of the different approaches shows that they are limited in their usability. The limitations are the factor of uniformity. The empirical criteria are only valid for soils which are comparable to those analysed. Soils with cohesive fine fractions can not be analysed without uncertainties but resistance against erosion increases dramatically with increasing cohesion. Another disadvantage is that local effects and structural changes are completely neglected. Both can lead to significant settlements or to a negative impact on the hydrodynamic conditions [10].

At present the interest in further research is very high. Further work is required for example by Fannin to better establish the utility that may be derived from combining aspects of the two empirical methods, shown in Figure 6, and to account for relative conservatism in each of those methods. However, it appears:

I. The two methods of Kenney and Lau respectively Kezdi are predicated on a similar approach that involves quantifying the shape of the grain size distribution curve over a defined interval, but differ in how that interval is determined. The Kezdi method establishes it with reference to a constant increment of mass passing, whereas it is established by a variable increment in the Kenney and Lau method. This yields one point on the grain size curve where both methods converge to give the same index value, at $F \approx 15\%$.

II. Comparison indicates the filter ratio (D'_{15}/d'_{85}) of the Kezdi method is relatively more conservative for $F < 15\%$ and the stability index $(H/F)min$ of the Kenney and Lau method is more conservative for $F > 15\%$.

A spatial sieve approach based on pore networks and percolation theory to simulate transport processes within the pore structure is part of the current research of the research group "SUFFOS". Anyway, all the approaches are based on the assumption that the soil is packed homogeneously. Hence the engineering practice shows that local segregation often is the focal point in suffusion. But up to now this effect cannot be taken into account in any safety consideration.

ACKNOWLEDGEMENT

The authors acknowledge the German Research Foundation (DFG) for supporting the research project "Conditions of suffusive erosion phenomena in soils" and the Wasser- und Schifffahrtsamt Freiburg for financial support of the research and development project "Beurteilung der Gefährdung der Rheinseitendämme durch suffossiven Materialtransport.

REFERENCES

[1]V. V. Burenkova. Assessment of Suffosion in Non-Cohesive and Graded Soils. In J. Brauns, U. Schuler, and M. Heibaum, editors, *Filters in Geotechnical and Hydraulic Engineering on the First International Conference Geo-Filters*, Karlsruhe, 20.-22. Oktober, pages 357-367, Rotterdam, 1992, Balkema.

[2]K.-F. Busch, L. Luckner, and K. Tiemer. *Geohydraulik: Lehrbuch der Hydrogeologie*. Ferdinand Enke Verlag, 3rd edition

[3]R. P. Chapuis, Similarity of Internal Stability Criteria for Granular Soils. *Canadian Geotechnical Journal*, 29:711-713, 1992.

[4]J. Čištin. Zum Problem mechanischer Deformation nichtbindiger Lockergesteine durch die Sickerwassserströmung in Erddämmen. *Wasserwirtschaft Wassertechnik*, 2:45-49, 1967.

[5] R. J. Fannin. Karl Terzaghi: from theory to practice in geotechnical filter design. ASCE Journal of Geotechnical and Geoenvironmental Engineering, 134:267.276, 2008

[6]U. Homberg, R. Binner, and S. Prohaska. Determining geometric grain structure from x-ray micro-tomograms of gradated soil. In K. J. Witt, editor, *Workshop Internal Erosion, volume 21* of *Schriftenreihe Geotechnik*, Witt, K. J., Nov. 2008

[7]T. C. Kenney and D. Lau, Internal Stability of Granular Filters. *Canadian Geotechnical Journal*, 22:32-43, 1985.

[8]T. C. Kenney and D. Lau. Internal Stability of Granular Filters: Reply. *Canadian Geotechnical Journal*, 23:420-423, 1986.

[9]A. Kezdi. *Soil physics – selected topics*. Elsevier Scientific Publishing Company, Amsterdam 1979.

[10] H. Leussink, T. G. Visweswaraiya, and H. Brendlin. Beitrag zur Kenntnis der bodenphysikalischen Eigenschaften von Mischböden. Veröffentlichung des Institutes für Bodenmechanik und Felsmechanik, Universität Karlsruhe, 1964, Heft 15.

[11] M. Li and R. J. Fannin. A comparison of two criteria for internal instability of granular soils. *Canadian Geotechnical Journal*, 45:1303-1309, 2008.

[12] E. A. Lubočkov. Nesuffozionnye nesvjaznye grunty. Technical Report 71, Izv. VNIIG, Leningrad, 1965.

[13] E. A. Lubočkov. Grafičeskie I analitičeskij sposoby opredelenija suffozionnych svojstv nesvjaznych gruntov. Technical Report 78, Izv. VNIIG, Leningrad, 1965

[14] E. A. Lubočkov. Calculation of the piping properties of cohesionless soils with the use of nonpiping analog. 2(3):233-237, Mar. 1968. Translation, original Gidrotechničeskoe stroitel'stvo.

[15] E. A. Lubočkov. The Calculation of Suffosion Properties of Non-Cohesive Soils when using the Non-Suffosion Analogue (russian). In *Internatinal Conference on Hydraulic Research*, pages 135-148, Brno, Czeckoslovakai, 1969.

[16] T. Mehlhorn, S. Prohaska, and V. Slowik. Modelling and analysis of particle and pore structures in soils. In K. J. Witt, editor, *Workshop Internal Erosion*, volume 21 of *Schriftenreihe Geotechnik*. Witt, K. J., Nov. 2008.

[17] V. Milligan. Internal stability of granular filters: Discussion. *Canadian Geotechnical Journal*, 23:414-418, 1986.

[18] MSD. Merkblatt: Standsicherheit von Dämmen an Bundeswasserstraßen. Technical Report, Bundesanstalt für Wasserbau, 2005.

[19] P. Muckenthaler. *Hydraulische Sicherheit von Staudämmen*. PhD thesis, TU München, 1989. Bericht Nr. 61.

[20] P-92-80. Instrukcija po proektirovaniju obratnyh fil'trov gidroehniceskih sooruzenij. VSN-02-65, 1981.

[21] A. N. Patrašev. Motedika podbora granulometričeskogo sostava obratnych fil'trov. Technical Report, Sbornik trudov Lengiprorečtransa, 1957.

[22] M. Pavčič. Sposob opredelenija nesuffozionych granulometričeskich sostavov grunta, 1961.

[23] N. Reboul. *Transport de particules dans les milieux granulaires. Application á l'érosin interne*. PhD thesis, L'école centrale de Lyon, Nov. 2008.

[24] U. Saucke. Nachweis der Sicherheit gegen innere Erosion für körnige Erdstoffe. *Geotechnik*: 4.-53, 2006.

[25] H. J. Schaef. Örtliche Standsicherheit (Suffusion und Erosion) bei Sickerwasserströmungen. Erläuterungen zum bodenmechanischen Arbeitsblatt 4.4 der ehemaligen Obersten Bergbehörde Leipzig. Technical Report, TU Bergakademie Freiberg, 1995. Veröffentlichungen des Institutes Geotechnik.

[26] U. Schuler. How to Deal with the Problem of Suffosion. In *Research and Development in the Field of Dams*, Sept. 1995. 7.-9. September.

[27] O. Semar and K. J. Witt. Percolation Theory – Phenomenological Approach to Describe Erosion Processes. In K. J. Witt, editor, *Workshop Internal Ersoion*, volume 21 of *Schriftenreihe Geotechnik*, Weimar. Nov. 2008.

[28] J. L. Sherard, L. P. Dunnigan and J. R. Talbot. Basic properties of sand and gravel filters. *Journal of Geotechnical Engineering-ASCE*, 110(6):684-700, 1984.

[29] J. L. Sherard, L. P. Dunnigan and J. R. Talbot. Filters for silts and clays. *Journal of Geotechnical Engineering-ASCE*, 110(6):701-718, 1984.

[30] J. L. Sherard and L. P. Dunnigan. Internal stability of granular filters: *Discussion. Canadian Geotechnical Journal*, 23:418-420, 1986.

[31] W. Sichardt. Kies und Sandfilter im Grund- und Wasserbau. *Die Bautechnik*, 29 (3/4), 1952.

[32] A. W. Skempton and J. M. Brogan. Experiments on piping in sandy gravels. *Géotechnique*, 44:449-460, 1994.

[33] K. Terzaghi. Soil mechanics: a new chapter in engineering science. *Journal of the Institution of Civil Engineering*. 12:106-141, 1939.

[34] J. Ziems. *Beitrag zur Kontakterosion nichtbindiger Erdstoffe*. PhD thesis, TU Dresden, 1969.

A Life Cycle Approach to Probabilistic Assessment of Levee Erosion

Landris T. Lee[1], P.E., Brian A. Hubel[2], P.E., G.E., and Marc J. Goodhue[3], P.E.

[1]Research Civil Engineer, U.S. Army Engineer Research and Development Center, 3909 Halls Ferry Rd., Vicksburg, MS 39180
[2] Senior Civil Engineer, U.S. Army Corps of Engineer San Francisco District Geo-Sciences Section, 1455 Market Street, San Francisco, CA 94103
[3] Geo-Sciences Section Chief, U.S. Army Corps of Engineer San Francisco District Geo-Sciences Section, 1455 Market Street, San Francisco, CA 94103

ABSTRACT

A methodology to assess the erosion-induced breaching probability (i.e. probability of unsatisfactory performance) of clay levees exposed to coastal and riverine hydrodynamic loading was developed for selected levee reaches, and has application to levee life-cycle maintenance planning. The methodology applies probabilistic erosion relationships including water-side storm surge and wave runup with or without concurrent land-side overtopping. The method provides a means to forecast levee maintenance and flood risk reduction costs by estimating future erosion damage from episodic or cumulative storm events.

INTRODUCTION

The successful long-term performance of an earthen levee structure exposed to flooding, storm surge, river currents, or coastal wave action depends upon its structural resilience to the external hydrodynamic loads (illustrated in **Figure 1**). Erosion of the outer slope (water-side), crest, or inner slope (land-side) requires an initiating external force (energy, pressure, or load). Any levee system that is not adequately designed to withstand a wide range of hydrodynamic loads for extensive durations is susceptible to erosion-induced breaching failure.

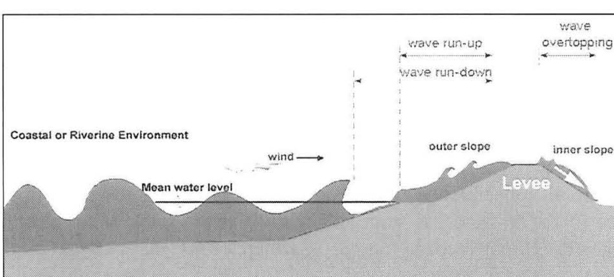

Figure 1. Diagram of potential hydrodynamic forcing on a levee structure.

Erosion effectively reduces the levee cross-sectional area (width) by physically removing soil from either side of the levee, and extensive damage negatively affects the structural integrity. Levee maintainenance provides resilience and perpetuates successful performance.

Levee maintenance costs are not normally resourced using a reliability assessment approach based on analytical models (FEMA 2008, USACE 1996). An erosion-damaged levee reach is generally repaired as a response to a storm event by using fill dirt or riprap from a stockpiled supply source. What-if scenarios of expected levee damage occurring from a storm or flood event are generally subjective, based on local experience or judgement. **Figure 2** illustrates two such possible levee erosion and subsequent damage repair scenarios. If outer slope erosion initiates and progressively damages the levee, a post-storm repair effort (e.g. dump truck and bulldozer) typically mitigates the damage. In lieu of (or in addition to) outer slope damage, the inner slope may be overtopped and eroded. The inner slope or crest is then repaired in a similar fashion. If repairs and maintenance are performed in a timely manner, the levee structure will be ready for exposure to the next storm event.

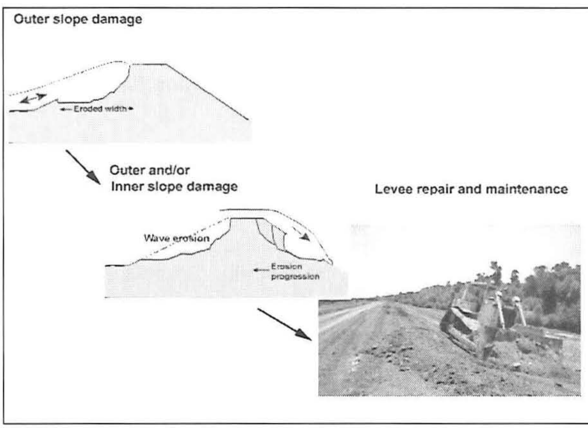

Figure 2. Eroded levee restoration and maintenance.

Utilizing a reliability assessment model to estimate the conditional probability of erosion-induced breaching (i.e. unsatisfactory performance) becomes increasingly important if the levee is protecting property or population. **Figure 3** illustrates the possible eventual consequence of inadequate intervention, restoration, or long-term maintenance of the levee cross sectional width. If the levee's integrity is not maintained, any subsequent hydrodynamic loading event may cause erosion-induced breaching.

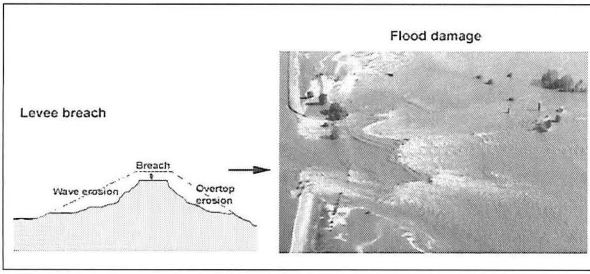

Figure 3. Illustration of a breach possibly due to inadequate levee restoration or long-term maintenance.

Figure 4 shows a framework of steps to estimate levee erodibility, forecast cross section erosion volumes, and assess risk reduction alternatives for minimizing levee life-cycle flood damages.

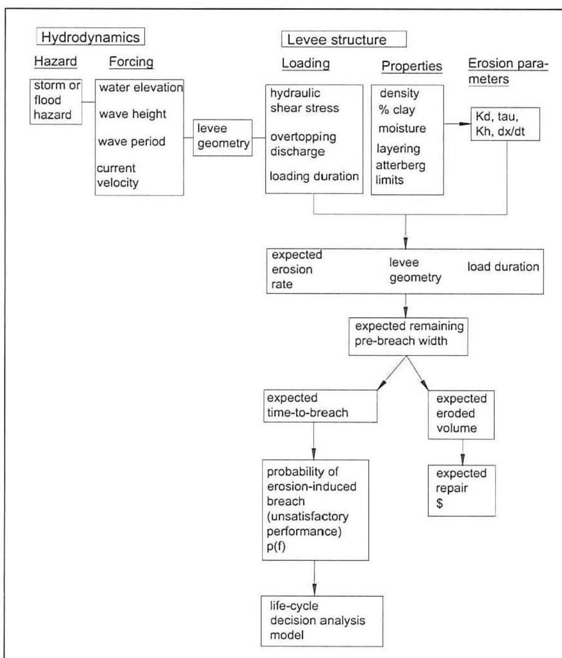

Figure 4. Levee erosion model flow chart showing a framework for addressing (a) expected erosion repair costs and/or (b) life-cycle flood risk reduction analysis.

LEVEE EROSION

In the United States, levee erosion-induced breaching is receiving more attention as a potential failure mode (IPET 2007). Predicting levee erosion and erosion-induced breaching caused by transient hydrodynamic loads is a largely uncertain exercise and the very few models that have been developed (including the one addressed in this paper) have not been validated on existing levees. Very little experimental research has related hydrodynamic (storm surge and wave action) parameters to erosion of fine-grained (cohesive) levees (USACE 2007).

Erosion rate is a function of hydrodynamic loading and soil strength. Eroded volume is a function of erosion rate and hydrodynamic loading exposure time (duration). The longer a storm surge acts on a levee face, the greater the potential eroded volume (width, depth, and length). As the storm progresses and intensifies, loading may also develop on the levee crest and inner slope. Time-dependent hydrodynamic loading on coastal structures is a relatively recent modeling capability (Melby, 2008; Nadal and Melby, 2009; Lynett et al., 2010; Dean et al., 2010). Little is known about the mechanisms of wave-induced time-dependent erosion or modeling of breaking wave runup and overtopping on levees, and empirical erosion parameters were generally developed from steady-state loading scenarios. However, usage of the empirical parameters may arguably be appropriate for reliability modeling if parameter and model uncertainties are addressed. The methodology herein was based on such an assumption and was developed for quantifying erosion damage probabilities along selected coastal levee reaches (Lee 2010).

Erosion-induced breaching of a predominately fine-grained levee (illustrated in **Figure 5**) occurs when either (a) the outer slope erodes up to the levee crest (**Figure 6**), (b) the levee crest erodes (**Figure 6**), (c) the inner slope erodes backwards up to the levee crest (**Figure 7**), or (d) combined erosion (**Figure 8**). These simplified illustrations are patterned after embankment erosion observations and research conducted by Ralston (1987), Temple et. al (2005) and Hanson et. al (2005).

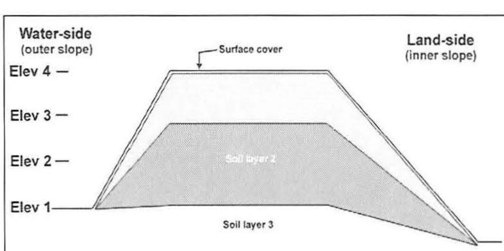

Figure 5. Cross-sectional slice through a multi-layered levee.

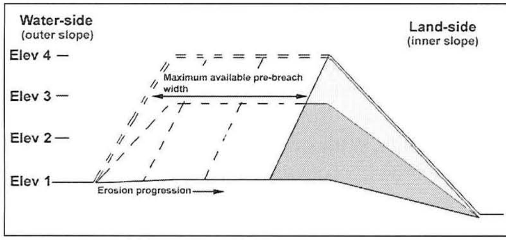

Figure 6. Conceptual outer slope erosion progression scenario

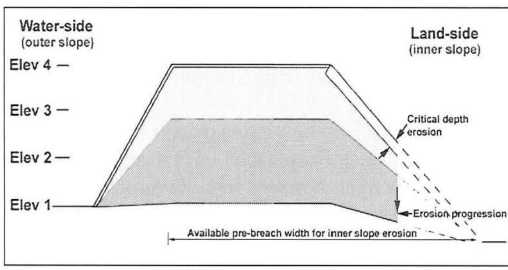

Figure 7. Conceptual inner slope erosion beginning at the levee toe

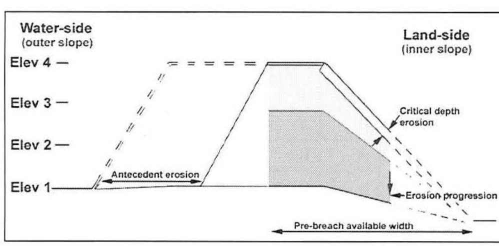

Figure 8. Conceptual combined outer slope and inner slope erosion

Modeling the levee damage from wave action and hydrodynamic loading requires estimation of the erosion rate. The estimation of the erosion rate, ε, is based on the textbook equation

$$\varepsilon = K_d (\tau - \tau_c)$$

K_d = erodibility coefficient
τ = hydrodynamic shear stress
τ_c = limiting, or critical, soil shear strength

The erodibility coefficient and critical shear strength values are based on empirical relationships or experimental data. Procedures for selecting these values are found in Temple et. al (2005) and Hanson et. al (2005). Guidance for estimating headcut advance and other erosion process parameters are found in NRCS (1997, 2001). Uncertainty variables are discussed in URS (2007). The hydrodynamic shear stress, overtopping flow rates, and their uncertainty variables are also needed. Nadal and Melby (2009) discuss the hydrodynamic parameters.

EROSION PROBABILITY

As diagrammed in **Figure 4** above, the expected remaining levee width was calculated first. The expected remaining levee width is a function of expected hydrodynamic parameters (outer slope shear stress, inner slope overtopping flow rate, and exposure time). Estimating the expected remaining levee width is necessary for (a) estimating eroded cross-sectional area (volume) and (b) estimating the probability of unsatisfactory performance for subsequent risk assessment.

Figure 10 is a lookup table showing expected remaining levee widths for a selected levee cross section. The lookup table format allows modeling of cumulative storm events in addition to single storm events. Each tabulated value was developed by calculating expected erosion rate and its uncertainty for a given levee cross-section. Each input variable was assigned as a lognormal probability distribution function and each equation's expected (central tendency or mean) value was calculated using statistical software Monte Carlo simulations.

Hydraulic shear stress, psf	0.1	0.3	0.5	1	2	3	4
Exposure, ,hr	Expected remaining levee width prior to breaching, ft						
0	8	8	8	8	8	8	8
0.2	8	8	7.9	7.8	7.6	7.3	7
0.4	8	8	7.9	7.6	7.1	6.6	6
0.8	8	8	7.8	7.3	6.2	5.2	4.1
1	8	8	7.7	7.1	5.8	4.5	3.2
2	8	8	7.5	6.2	3.6	1	0
3	8	8	7.2	5.3	1.4	0	0

Figure 10. Example lookup table of expected remaining levee widths for a multi-layered clay levee with an 8-ft crest width (Lee 2010).

Probability of Unsatisfactory Performance

Erosion parameters were calculated using the NRCS (1997, 2001) equations within a probabilistic framework. The expected critical times to breach were computed by dividing the tabulated remaining width values by the erosion rate expected value (mean) and standard deviation values, also generated by Monte Carlo simulations. The computed critical breach times were then formulated as limit state functions by comparing critical times to expected exposure times. Next, the conditional probability of erosion-induced breaching failure value was obtained using the text-book limit state method for calculating the reliability index (Harr 1987). The reliability index (β) values were generated as simulation outputs. Each conditional probability value, p(f), was then computed from the standard normal distribution. The conditional probability values represented the erosion-induced breaching conditional probability for either the outer slope, crest, or inner slope, or combinations thereof. **Figure 11** is an example conditional probability lookup table for a selected levee cross section.

Probability of erosion-induced levee failure, p(f)													
Critical time to breach, hr	Exposure time, hr												
	0.2	0.4	0.6	0.8	1	1.2	1.4	1.6	1.8	2	3	4	5
9.2	0.02	0.02	0.02	0.03	0.03	0.03	0.04	0.04	0.05	0.05	0.08	0.12	0.17
3.4	0.03	0.04	0.05	0.06	0.08	0.10	0.12	0.14	0.17	0.20	0.40	0.62	0.81
0.8	0.07	0.17	0.33	0.54	0.72	0.86	0.94	0.98	0.99	1.00	1.00	1.00	1.00

Figure 11. Conditional probability lookup table from an example levee cross section (Lee 2010).

Risk Reduction Analysis

Estimating the probability of unsatisfactory performance is needed to conduct risk reduction simulations. Projecting the hydrodynamic loads (expected values and standard deviations) on a given levee structure allows probabilistic forecasting of subsequent flood damages to property and population. Knowing the probability of failure and the failure consequences allows economic decisions to be quantified. For example, knowing that a given levee reach has a higher probability of failure may justify allocation of additional long-term maintenance resources to prevent that reach from failing due to erosion-induced breaching. Other failure modes (stability, seepage, etc.) may also be included in the risk analysis.

Figure 12 illustrates components needed to conduct long-term erosion risk reduction decision analyses. This flow chart illustrates only one potential approach to life-cycle decision analysis. The level of detail and component sophistication will depend on numerous other factors such as including additional potential failure modes (i.e. underseepage and stability), availability of hydrodynamic data, ability to quantify elevation exceedance curves, methodologies to quantify life-cycle damages (consequence analyses), and quantifying risk reduction costs, to list a few. The purpose of this illustration is to show that the pre-requisite module is a levee erosion model that quantifies the probability of unsatisfactory performance p(f). The p(f) calculations are based on geotechnical evaluation of the soil erodibility linked to expected hydrodynamic loading that explicitly includes uncertainty.

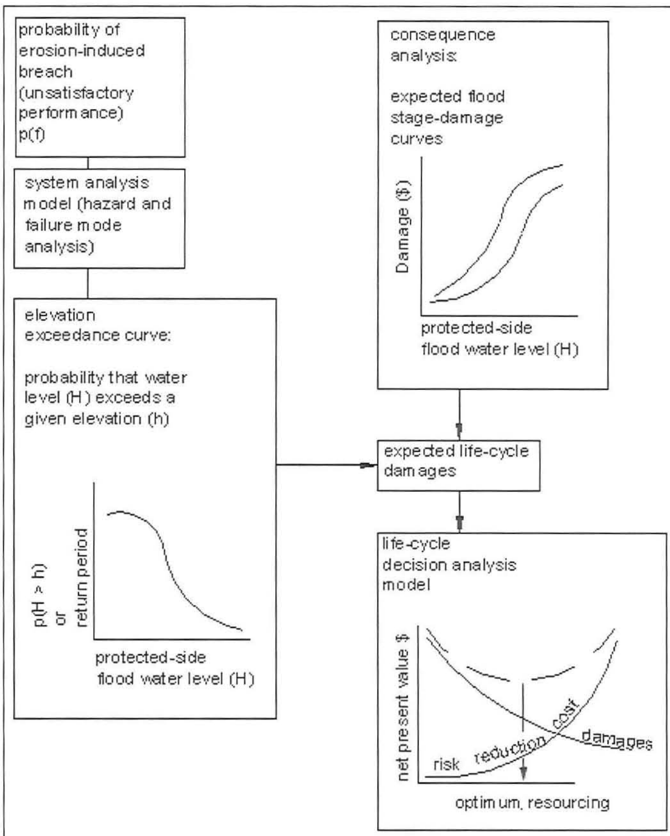

Figure 12. Flow chart illustrating necessary components for one approach to life-cycle flood risk reduction analysis utilizing a probabilistic levee erosion model.

CONCLUSION

Development of a probabilistic erosion model enabled the expected levee erosion damage (caused by episodic or cumulative storm events) to be quantified. The ability to forecast the expected levee maintenance costs and evaluate flood risk reduction economics are logical extensions of this model. Although not addressed in detail herein, these life-cycle issues may be modeled by extending the original erosion model functions to include damage and decision analysis modules.

REFERENCES

Dean, R.G., Rosati, J.D., Walton, T.L., and Edge, B.L. (2010). "Erosional equivalences of levees: Steady and intermittent wave overtopping," *Ocean Engineering* 37, 104 -113.

FEMA (2008). "Guidance for coastal flood hazard analyses and mapping in sheltered waters," Technical Memorandum, Dept. of Homeland Security, February, 22 pages.

Hanson, G.J., Temple, D.M., Morris, M., Hassan, M., and Cook, K.R. (2005). "Simplified breach analysis model for homogeneous embankments: Part II, Parameter inputs and variable scale model comparisons", Proceedings of the 2005 U.S. Society on Dams Annual Meeting and Conference, Salt Lake City, UT, pp: 163 - 174.

Harr, M.E. (1987). *Reliability-based design in civil engineering*, Dover Publications, Mineola, NY.

Interagency Performance Evaluation Team (IPET) (2007). Performance Evaluation of the New Orleans and Southeast Louisiana Hurricane Protection System, Interim Draft Final Report of the Interagency Performance Evaluation Task Force, Volumes 1 through 9, U.S. Army Corps of Engineers, Washington, D.C. http://ipet.wes.army.mil/

Lee, L. T. (2010). "Reliability assessment of South San Francisco Bay shoreline levees," ERDC Technical Report (in publication), U.S. Army Engineer Research and Development Center, Vicksburg, MS.

Lynett, P.J., Melby, J.A., and Kim, D. (2010). "An application of Boussinesq modeling to hurricane wave overtopping and inundation," *Ocean Engineering*, 37, 135 – 153.

Melby, J.A. (2008). "Time-dependent life-cycle analysis of coastal structures," In Press, *Proc. of Coastal Structures 2007*, ASCE, Reston, VA.

Nadal, N. C. and Melby, J. A. (2009). "Wave runup and overtopping analysis for South San Francisco Bay Shoreline Study," ERDC Technical Report (in publication), U.S. Army Engineer Research and Development Center, Vicksburg, MS.

NRCS (1997). Chapter 51, Earth spillway erosion model, in *USDA National Engineering Handbook, Part 628 Dams*

NRCS (2001). Chapter 52, Field procedures guide for the headcut erodibility index, in *USDA National Engineering Handbook, Part 628 Dams*

Ralston, D.C. (1987). "Mechanics of embankment erosion during overflow," *Proc., Hydraulic Engineering*, 1987, ASCE, New York, 733-738.

Temple, D.M., Hanson, G.J., Neilsen, M.L., and Cook, K.R. (2005). "Simplified breach analysis model for homogeneous embankments: Part I, Background and model components", Proceedings of the 2005 U.S. Society on Dams Annual Meeting and Conference, Salt Lake City, UT, pp: 151 - 161.

URS (2007). *Erosion toolbox user's manual: Levee risk assessment methodology*, prepared for US Army Corps of Engineers' Nationwide Levee Risk Assessment Program, Washington, D.C.

USACE (1996). Engineering and design: Risk analysis for flood damage reduction studies," Engineer Manual 1110-2-1619, U.S. Army Corps of Engineers, Washington, D.C.

USACE (2007). "Certification of levee systems for the National Flood Insurance Program," Draft ETL 1110-2-570, U.S. Army Corps of Engineers, Washington, D.C.

A Practical Approach to Assess Combined Levee Erosion, Seepage, and Slope Stability Failure Modes

Brian A. Hubel, P.E., G.E.[1], Joseph V. Letter, Jr., Ph.D., P.E.[2], Marc Goodhue, P.E.[3], Landris T. Lee, P.E.[4]

[1] Senior Civil Engineer, U.S. Army Corps of Engineer San Francisco District Geo-Sciences Section, 1455 Market Street, San Francisco, CA 94103
[2] Research Hydraulic Engineer, U.S. Army Engineer Research and Development Center, 3909 Halls Ferry Rd., Vicksburg, MS 39180
[3] Geo-Sciences Section Chief, U.S. Army Corps of Engineer San Francisco District Geo-Sciences Section, 1455 Market Street, San Francisco, CA 94103
[4] Research Civil Engineer, U.S. Army Engineer Research and Development Center, 3909 Halls Ferry Rd., Vicksburg, MS 39180

ABSTRACT

Probability of unsatisfactory performance (system response) curves were developed for seepage, slope stability, and erosion potential failure modes during a flood reduction feasibility study. The erosion-induced breaching failure mode included water-side storm surge and wave runup with or without concurrent land-side overtopping. Response curves were developed for landside and waterside slope stability and landside seepage failure modes for various hydrostatic water loads. This paper illustrates an approach for evaluating the overall system response considering levee seepage, stability, and erosion response under various hydrodynamic loading and geomorphological uncertainties.

INTRODUCTION

Probabilistic methods to evaluate the geotechnical performance of earthen levees are required to better understand economic and life-safety risks of earthen levee structures for engineers, managers, planners, and the general public. Additionally, proposed legislation will require that in order for levees and floodwall structures to be considered to provide flood reduction benefits by the Federal Emergency Management Agency (FEMA) and the National Flood Insurance Program (NFIP) levees and floodwalls must meet specific reliability performance criteria (FEMA, 2006). Although methods for statistical evaluation of the hydraulic aspects have been widely used, the overall system response is rarely been considered in engineering analyses. Hesitance to apply probabilistic methods by geotechnical practitioners in levee analyses is partially due to:

a. unfamiliarity by geotechnical engineers with probabilistic analyses,
b. a general lack of guidance for incorporating both aleatory and epistemic geotechnical uncertainty,
c. models that have not been calibrated to real world performance, and
d. difficulty in presenting probabilities of unsatisfactory levee performance (Duncan, 2000, Christian et al. 1994).

The overall performance of an earthen levee system is highly sensitive to the geotechnical performance of the levee. USACE guidance for project feasibility studies requires that existing systems be holistically evaluated using probabilistic methods to estimate annual damages over a standard project life cycle (USACE 2006). Damage estimates (risk) for a given event frequency are simplified as shown .

$d=(\rho_e)(\rho_f)(H)$
where
d= damage
ρ_e = probability of a specific event (storm, high tide, etc)
ρ_f = probability of levee system failure under a specific event load
H = hazard due to failure (i.e. dollars at risk)

Damage (d) is integrated over all possible events to find a total estimate of annual damages. Uncertainty of each event and of performance can also be evaluated to estimate a confidence bounds of the damage estimates. Significant analysis is required to define events, parameters and their uncertainties and the relationship between system failure and the loading. Monte-Carlo methodology is a suitable and easy approach to integrate many uncertain parameters with varying distributions, provided the computational power is available. Figure 1 illustrates a holistic approach to evaluating levee system response using a Monte-Carlo methodology.

A practical approach to define the geotechnical inputs of levee performance (erosion, stability, and seepage) is presented in the sections below. The results are curves and tables that relate the probability of unsatisfactory performance to defined loading. Although the performance of the different performance modes (erosion, slope stability and seepage) may be related, convenient, comprehensive models are not available to practicing engineers. The failure modes are treated as independent performance modes for ease of application. For this discussion the erosion modes are "dynamic" failure modes, and specifically consider the time-dependant erosion progression. For stability and seepage, a practical approach is to select index points along a levee reach and evaluate under assumed steady state, static water level conditions.

The term, "Probability of Unsatisfactory Performance" (P_u) was chosen to describe the probability that specific levee states are less than a defined limit state. For seepage analysis, the limit state is defined as a critical seepage gradient, for stability it is defined as a slope stability slip surface that extends half way through the levee crest having a factor of safety less than one, and for erosion P_u was defined as the probability of a levee breach occurrence. Although treated as a probability of failure in damage estimates, in many situations the levee states may indicate failure compared to the critical limit state but the levees may not fail in a way that leads to breach and uncontrolled flooding. For this reason, Probability of Unsatisfactory Performance is preferred terminology. Future research into calibrated failure models and event-tree type analysis may more accurately predict levee breaching and flooding.

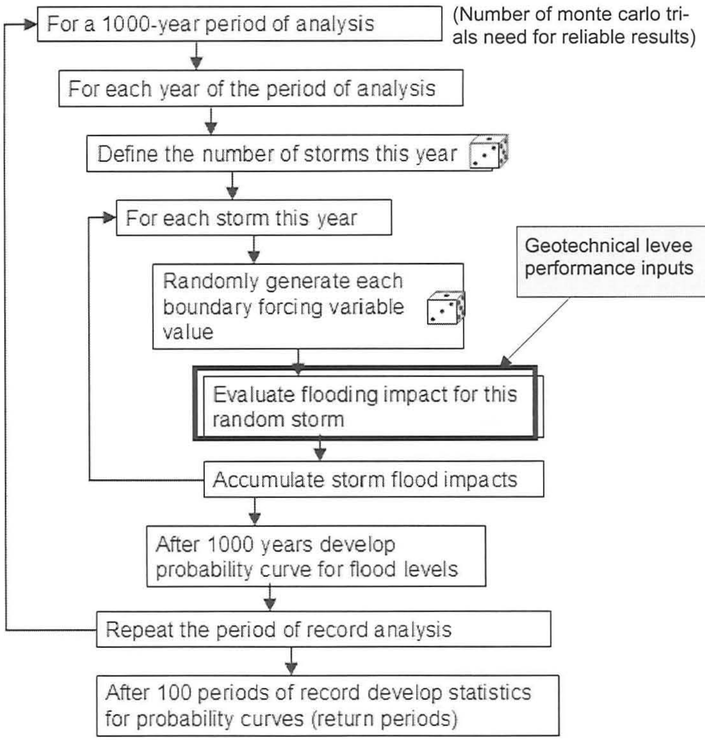

Figure 1. Overall Analysis Structure for a Monte Carlo Analysis

SLOPE STABILITY AND SEEPAGE PROBABILITY OF UNSATISFATORY PERFORMANCE

This example illustrates how levee performance curves may be developed in general accordance with the guidance provided in USACE ETL 1110-2-556 Evaluating the Reliability of Existing Levees (USACE 1999). The purpose of levee performance evaluation is to evaluate the geotechnical slope stability and seepage performance of the study area levees for economic cost/benefit analysis. The resulting performance curves are intended to be used as an input, along with hydraulic, hydrologic, coastal, and economic inputs, to determine the annual economic damages (See Figure 1). The performance levee segments are presented as a probability of unsatisfactory levee performance as a function of still water elevation.

Notes Regarding Index Point Selection and Spatial Variability

Probabilistic analysis in geotechnical engineering applications is not a new concept. Many have illustrated how these concepts are relatively easily applied to problems such as retaining walls, slope stability, and foundation design (Duncan, other references). Most of these problems are relatively small, spatially, when compared to many levee systems that often extend many miles. Research into spatial variability and spatial-correlation functions may one day help solve problems dealing with long geotechnical structures, these methods are not mature or easily applied in engineering practice.

Levee systems are commonly compared to links in a chain, (ie the levee is only as good as it's weakest link). Some have proposed that the weak point in the levee should be identified and evaluated to determine the overall system probability of unsatisfactory performance (Wolff, 1994). These ideas have validity, but the question remains, "How do we know we have identified the weak link?" There are weakness in this methodology, however, with a competent engineering it is reasoned that engineering judgment will guide the analyses such that the weak points of a levee system are identified. Practitioners, at a minimum should:

- Review the project geology and project construction history. Be sure to explore each geologic formation and each different construction history.
- Review past failures, and explore known failure/problem areas.
- Review geomorphology and explore conditions that might result in differing geotechnical conditions in the levee foundation.
- Understand the flood basin in terms of internal topography and economic impact areas to be sure chosen index points do not rule out the possibility of flooding in other areas of the basin.
- Understand the levee geometry.
- Have local experience with the geologic and geotechnical conditions expected at the project site.
- Consider and perform geophysical studies as appropriate

Figure 2 illustrates a practical approach to identifying the weak link of a levee. These steps are:

1) Identify if material properties appear uniformly distributed across the project space. Visually, this may be done by plotting all of the subsurface information on a single plot to look for outlier locations spatially.
2) For locations where subsurface conditions do not fit the general material distribution these locations should be evaluated discretely using the location specific geometry (surface and subsurface layering).
3) The weak geometry (surface and subsurface layering) with distributed soil properties should be used to calculate probability of unsatisfactory performance when the overall soil property distribution does not show clearly weaker locations.
4) The less reliable of steps 2 and 3 is used to estimate the system probability of unsatisfactory performance.

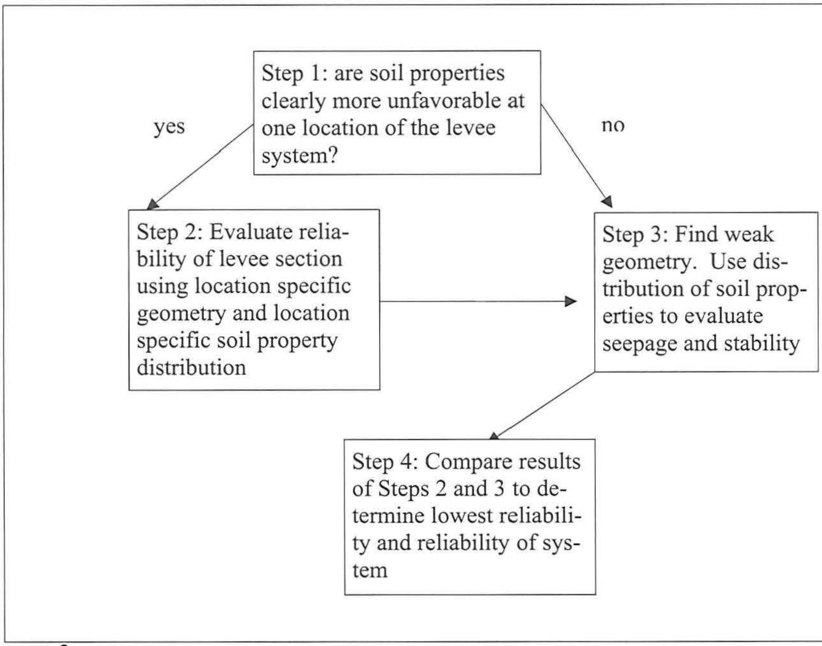

Figure 2: Selecting Index Points for Evaluation of Levee System Stability and Seepage

Slope Stability

Slope stability analyses may be performed using limit equilibrium methods, such as the popular computer software Slope/W by Geoslope International. Soil properties are input for each layer with a defined parameter distribution for Monte Carlo slope stability trials. Careful definition of what constitutes unsatisfactory performance is required. For this example it was judged that slip surfaces that extend atleast ½ way through the levee crest have the potential to cause unsatisfactory performance if the factor of safety is less than 1.0. In general, shallower slip surfaces often have lower factors of safety and surfaces extending further into the levee have higher factors of safety. Searches for the potential surfaces were performed by fixing the surface at the midpoint of the levee crest, and allowing a range of potential exit points, to find the surface with the lowest factor of safety. Figure 3 illustrates the slip surface search range. The green mass has the lowest factor of safety, the other surfaces shown (gray lines) illustrate the wide variety of slip surface trials evaluated to find the surface with the lowest factor of safety.

Thousands of stability trials can quickly be performed using a Monte-Carlo approach. While this approach is different than using closed first-order second-moment solutions, using the computer to perform trials using possible soil properties generates similar factor of safety distributions, provided enough trials are performed. For this example case 2,000 trials were performed. For each trial new soil properties were randomly generated for each soil layer in accordance with defined distributions of soil parameters. Key parameters for stability analysis are shear strength and unit weight. For each trial a factor of safety is calculated and saved. The results of all of the trials are binned to estimate a frequency distribution of factors of safety for the slope. The probability that the factor of safety is less than 1.0 is used as the probability that the levee will experience unsatisfactory performance due to slope instability.

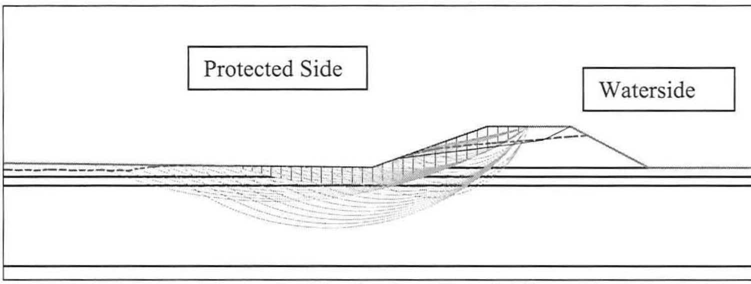

Figure 3. Slip Surface Search Illustration

Each potential slope stability failure mode of concern (ie landside steady state seepage, rapid drawdown, etc) is evaluated in this manner for a wide range of water loading levels to develop curves that relate the performance to the water loading. For practicality, pore pressures used in the slope stability analysis are based on best estimated steady state seepage conditions for the given water load. An example how stability and seepage failure modes are combined to a single function are presented in the Combining Seepage and Stability Section of this paper.

Seepage

The probability of unsatisfactory performance was defined as the probability that a critical seepage gradient was exceeded. Variables important to the seepage analysis included horizontal hydraulic conductivity, horizontal to vertical hydraulic conductivity, layering and layer dimensions, as appropriate. In general high seepage gradients were calculated when there were high contrasts in permeability between two layers (such as a low permeability layer over a high permeability layer). In general hydraulic conductivities were assumed to range over several orders of magnitude.

Seepage calculations were performed using steady-state assumptions and the computer program Seep/W by Geo-Slope International, Inc. Seepage trials were performed with all variables set at the expected values, except one which was varied between plus-one and minus-one standard deviation. The seepage gradients were tabulated and combined using a first-order second-moment solution and an assumed log-normal statistical distribution. A log-normal distribution was judged appropriate due to the wide variability in material properties. As typical seepage gradient contour plot is shown on Figure 4.

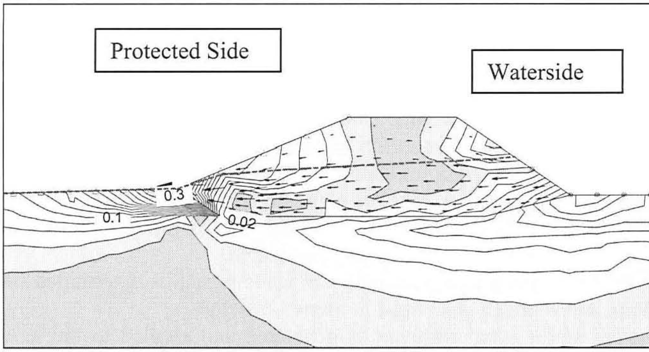

Figure 4. Example Vertical Seepage Gradients and Seepage Vectors

Combining Seepage and Stability

The combined probability of unsatisfactory performance is a combination of individual failure mode probabilities that correspond to the loading that the project will experience. Typically these modes include through seepage, under seepage, drawdown stability and long-term stability. Taylor series formulation is used to determine the combined performance. Figure 5 illustrates the combination of performance functions. Figure 5 includes a with and without drawdown curve. In many cases a drawdown failure mode may not cause economic damages if the levee can be repaired before another high water event.

$$P_u = 1 - \prod (1 - P_i)$$

Pi = the probability of unsatisfactory performance of each potential failure mode

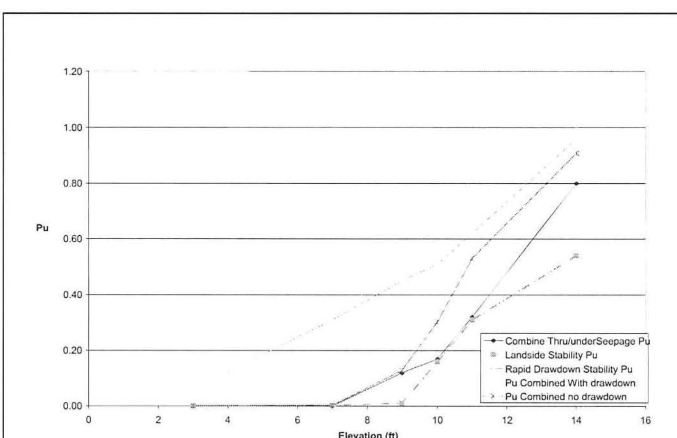

Figure 5. Example of Stability and Seepage Probability of Unsatisfactory Performance

LEVEE EROSION

Army Corps of Engineers (Lee and Wibowo 2007) and European levee erosion models (Steenbergen et al., 2004; Buijs et al., 2004) use the limit state approach for estimating the probability of levee erosion-induced breaching. Soil erosion and breach parameters may be calculated using the NRCS (1997, 2001) equations within a probabilistic framework. All equation variables are assigned a probability distribution function (typically a lognormal distribution). The expected value (mean) and standard deviation values generated are formulated as limit state functions in order to calculate a reliability index (β value). The probability of failure can be determined from the β value within a standard normal distribution.

Figure 6 illustrates how probability of levee breach is determined for a given storm loading, and is briefly discussed in Steps 1-7 below.

1. A given storm event response is generated and applied to the levee. The flood impacts are then integrated over the storm event, beginning at a low water level and rising through the peak surge level at a time step of a tenth of an hour.
2. For each of the levee subsections the erosion analysis is applied, using a relative storm surge elevation, taking into account the time varying surge level and the local subsection levee crest.
3. Based on the generated storm event ,wave runup is determined. From the wave runup data, the water level, wave height and wave period define the shear stress on the outer slope and the overtopping discharge.
4. Given the width of levee crest remaining and the shear stress applied by the hydraulic loading, a table look-up is performed within, which provides the outer slope erosion remaining width as a function of duration and shear stress. The table is interrogated by first interpolating to obtain for the current shear stress the equivalent duration of exposure that gives the current remaining crest width. Then the current time step in added to that equivalent duration and the incremental erosion determined by then re-interpolating the remaining crest width.
5. With the now updated remaining crest width and the current shear stress a look-up is performed which provides the critical time to breaching in hours. The impacts of overtopping erosion at the inside toe of the levee are estimated using critical time to breaching based on the remaining crest width and the current overtopping discharge.
6. The conditional probability of breaching is then determined from the critical time to breaching and the incremental duration (time step) by using tables. The steps 1-7 are repeated for each time step through the storm event, with the maximum probability of failure obtained during the storm.
7. The maximum probability of failure that is generated is tested by the Monte Carlo analysis for failure of the levee.
8. Length and temporal effects can be incorporated using Dutch methods, as appropriate (Vrouwenvelder et al. 2001).

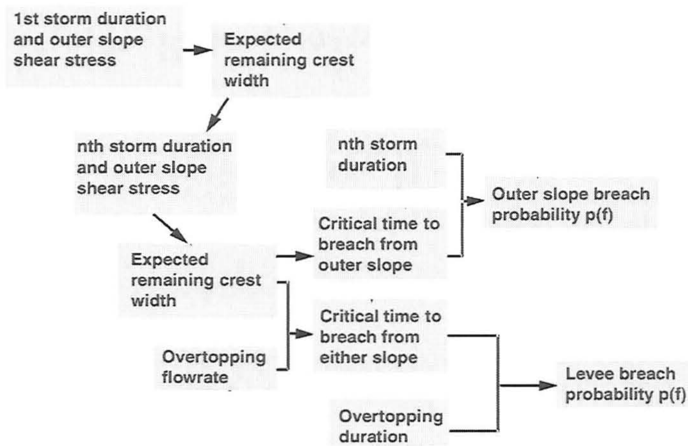

Figure 6. Process for Calculating Probability of Unsatisfactory Erosion Performance

COMBINING P_U FOR SLOPE STABILTY/SEEPAGE AND EROSION FAILURE MODES

Combining the probabilities of failure in the Monte Carlo Analysis is performed by checking both the probability of unsatisfactory performance using stability and seepage failure modes, and using erosion failure modes for each storm trial. Flooding can be mapped when breaches occur using estimated breach dimensions.

For the stability and seepage failure modes, although an index point (weak link) is defined, flooding should be checked to see the sensitivity of the breach location. For the erosion failure modes, the randomness of the breach location is already incorporated into the hydrodynamic loading and erosion progression.

APPLICATION AND CONSIDERATIONS

Although calibration for this methodology is lacking in terms of both actual field performance and laboratory study, the methodology does provide a framework in which consistent decisions can be made regarding project economics (ie comparing different project alternatives to reduce flood damage for example).

Care should be taken by engineers when designing new structures not to design based solely on Probability of Unsatisfactory Performance. Appropriate proven design methods, associated uncertainties and risks, and appropriate redundancy designs should be incorporated in a complete flood protection design.

Future research in these subjects is warranted and needed, especially in light of new legislative requirements that will require engineering analysis in a holistic probabilistic framework. Particular areas of research may include:

- Incorporation of time and length effects in slope and seepage analysis.
- Developing a standard definition of Unsatisfactory Performance in terms of levee failure.

- Incorporation of geotechnical spatial variation
- Calibrating failures to field performance in stability, seepage, and erosion modes

REFERENCES

Buijs, F.A., van Gelder, H.A.J.M., and Hall, J.W. (2004). "Application of reliability-based flood defence design in the UK," HERON, Vol 49, Issue 1, Delft University of Technology, Delft, The Netherlands. http://www.mechanics.citg.tudelft.nl/heron/2004_1/2004_1.html

Christian, John T., Ladd, Charles C., Baecher, Gregory B., (1994), "Reliability Applied to Slope Stability Analysis," Journal of Geotechnical Engineering Vol. 120, No 12 pp. 2180-2207.

Duncan, Michael, J. (2000), "Factors of Safety and Reliability in Geotechnical Engineering," Journal of Geotechnical and Geoenvironmental Engineering, Vol. 126 Issue 4, pp. 307-315.

Interagency Levee Policy Review Committee under contract to FEMA (2006), "The National Levee Challenge, Levees and the FEMA Flood Map Modernization Initiative, " Contract HSFEQ-04-D0025.

Lee, L.T. and Wibowo, J.L. (2007). "Overtopped levee erosion toolbox: Risk assessment methodology and user's guide", Draft Technical Report (in progress), ERDC Geotechnical and Structures Laboratory, Vicksburg, MS.

NRCS (1997). Chapter 51, Earth spillway erosion model, in *USDA National Engineering Handbook, Part 628 Dams*

NRCS (2001). Chapter 52, Field procedures guide for the headcut erodibility index, in *USDA National Engineering Handbook, Part 628 Dams*

Steenbergen, H.M.G.M., Lassing, B.L., Vrouwenvelder, A.C.W.M., and Waarts, P.H. (2004). "Reliability analysis of flood defence systems," HERON, Vol 29, Issue 1, Technische Universiteit Delft, Netherlands. http://www.mechanics.citg.tudelft.nl/heron/2004_1/2004_1.html

USACE (2007). "Certification of levee systems for the National Flood Insurance Program," Draft ETL 1110-2-570, U.S. Army Corps of Engineers, Washington, D.C.

USACE (1999). "Evaluating the reliability of existing levees," Appendix B, ETL 1110-2-556, 28 May, U.S. Army Corps of Engineers, Washington, D.C.

USACE(2006), "Risk Analysis for Flood Damage Reduction Studies, " Engineering Regulation 1105-2-101, U.S. Army Corps of Engineers, Washington. D.C.

Vrouwenvelder, A.C.W.M., Steenbergen, H.M.G.M., and Slijkhuis, K.A.H. (2001). "Theory manual of PC-RING", TNO Building and Construction Research, Delft, The Netherlands.

Wolff, Thomas, F., (1994), "Evaluating the reliability of Existing Levees, Report of Research Project: Reliability of Existing Levees," prepared for US Army Engineer Waterways Experiment Station

Levee Failure Due to Piping: A Full-Scale Experiment

V.M. van Beek[1,2], H.T.J. de Bruijn[1], J.G. Knoeff[1], A. Bezuijen[1,2] and U. Förster[1]

[1]Deltares, P.O. Box 177, 2600 MH, Delft; PH +31(0)88-3357228; email: vera.vanbeek@deltares.nl
[2]Delft University of Technology, Faculty of Civil Engineering and Geosciences

ABSTRACT

Piping is considered as an important failure mechanism for water retaining structures in the Netherlands. A recently performed study on the safety of Dutch levees raised some doubts with respect to the validity of the current calculation model. A large research program has therefore started to investigate the process of piping in more detail. After laboratory experiments and desk studies, the model was validated in a full-scale experiment (seepage length 15 m). This paper describes the piping process as observed in this experiment. Different phases were found: seepage, retrograde erosion, widening of the channel and failure. Once sand craters were formed, stabilization of sand transport was not observed, although quantities of transported sand were very low. Ongoing erosion resulted in a piping channel from the downstream to the upstream side in a few days. Widening of the channel due to continued erosion finally resulted in significant deformation and failure of the levee.

INTRODUCTION

Piping, the process of retrograde internal erosion in sandy layers underneath clay levees, is considered one of the most dominant failure mechanisms of levees in the Netherlands (VNK1, 2005). The process starts with heave and cracking of the soft soil top layer at the land side of the levee, caused by high water pressures which are easily transferred through the permeable sand layer (Figure 1a-b). The cracks in the top soft soil layer allow for seepage. In case the water level difference between river and land side (the hydraulic head) is large enough, sand grains may be transported along with the water flow, thereby creating a pipe underneath the levee (Figure 1c-d). Continuing erosion may finally lead to failure of the levee and breakthrough (Figure 1e-g).

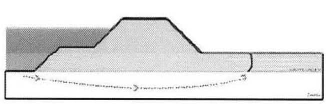

a) Heave

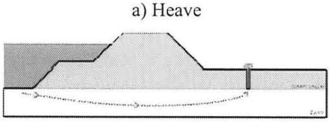

b) Seepage

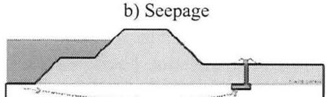

c) Pipe-formation

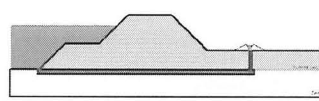

e) Widening of pipe

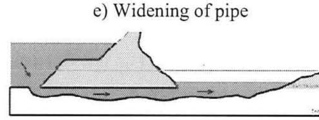

f) Failure of the levee

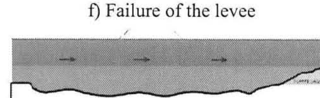

g) Breakthrough

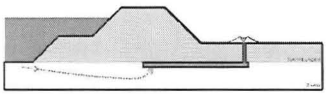

d) Retrograde erosion

Figure 1a-g. Process of retrograde erosion

Several calculation models and empirical relations are available to predict the occurrence of piping by retrograde erosion in order to assess the safety of levees. The most well-known prediction tools are the empirical rule of Bligh [1910] and the model of Sellmeijer [1988], of which the latter describes the process in most detail. However, a discrepancy emerged between calculated probabilities of failure and the opinion of levee managers of the actual resistance to piping (VNK1, 2005) in a recently performed safety assessment of Dutch levees using the model of Sellmeijer. Scepticism existed on whether piping would actually result in failure of the levee and the validity of the model was questioned. A large research program was started to validate and possibly improve the model.

This programme is part of a larger research programme called Strength and Loading of Flood Defence Structures (SBW), in which improvement of prediction models on different failure mechanisms for levees is pursued, in order to improve testing methods for the 6-yearly safety assessment of Dutch levees. SBW Piping specifically focuses on the improvement and applicability of prediction methods for piping. Experiments have been performed to study the process of piping in more detail.

After series of small-scale, medium-scale and centrifuge experiments (Van Beek, 2010[a], Van Beek 2010[b]), in which the process of piping and the influence of sand characteristics and length on the critical head was studied, the calculation model was validated in a full-scale experiment (seepage length 15 m). Three objectives were combined in a total of four tests: validation of different aspects of the calculation model, investigation of the failure process and testing of monitoring equipment. The objective of testing of monitoring equipment is part of the research program of the IJkdijk Foundation (described in De Vries et al., 2010). A cooperation between different parties allowed for the experiments to be performed. In this paper the process of piping in the full-scale experiments is described and compared with the expected process based on the model of Sellmeijer.

The model of Sellmeijer

The model of Sellmeijer is based on the equilibrium of forces of sand grains, flow in the developing channel (pipe flow) and the flow through the aquifer (Darcy). The model of Sellmeijer gives the relation between the pipe length and the hydraulic head at which the sand grains are in equilibrium, resulting in the curve as shown in figure 2. This graph shows the head at which the grains are just in equilibrium (ΔH_{eq}) for different relative pipe lengths (l/L). The graph shows that the growth of the channel will stop at a certain equilibrium length, as long as the critical head (ΔH_c, the maximum head at which grains can be in equilibrium) has not been reached; an increase of hydraulic head is necessary to obtain further growth of the pipe. The growth of the channel will continue once the critical head is reached; no equilibrium is possible unless the hydraulic head is lowered. It is assumed that the continued erosion will lead to failure of the levee within a relatively short time.

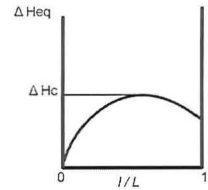

Figure 2. Hydraulic head at equilibrium as a function of the ratio between pipe length (l) and seepage path (L)

The equilibrium curve is of importance for field inspection. Sand transporting seepage wells are often observed and it is important to know whether the sand transport may stop as a result of equilibrium of the sand grains. The equilibrium curve is one of the important items of validation. In the laboratory experiments this curve has not been clearly observed, possibly due to scale or configuration. Below the critical head continuous sand transport has not been observed, although there had been some small signs of sand transport below the critical head, like individual grain transport or formation of very small channels.

FULL-SCALE EXPERIMENT SET UP

The full-scale experiment was performed at the location of the IJkdijk in the Northeast of the Netherlands. Two large basins were created (size 30x15 m), which were filled with two different sands. The sands had a d_{50} of 150 μm and 200 μm and are denoted in the following text as 'fine sand' and 'coarse sand' respectively. The dry sand was applied in layers and densified until a relative density of at least 50% was achieved. After densification, the sand layer was saturated. A clay levee with a height of 3.5 m and slopes of 1:2 was built on top of the sand by densification of smaller clay lumps. A levee with a seepage length of 15 m was obtained.

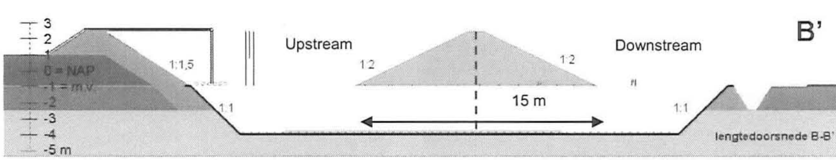

Figure 3. Cross-section of the full-scale experiments

At the downstream side, an overflow was created to keep the downstream water level at a constant level (approx 0.10 – 0.20 m above the sand layer). At the upstream side, the water level could be raised to a level of 3 m above the sand layer and was kept constant. Pumps were installed with a discharge capacity of 150 m^3/h at maximum to keep the water level constant.

Several rows of pore pressure gauges were placed at the interface of sand and clay to be able to monitor the pipe formation. In addition, fiber optics were placed at the interface to measure temperature and strain differences. In two of the four experiments additional monitoring equipment was tested, which is more extensively described in by de Vries et al., (2010). Monitoring wells were placed to measure the head difference and water pressure at both upstream side and downstream side, at depths of 1 and 2 m. A flow meter was connected to the overflow unit.

To fulfill the three objectives of the project, validation of different aspects of the calculation model, investigation of the failure process and testing of monitoring equipment, a total of four tests was performed. Next to validation of the model two types of sand were applied in two different basins. Next to validation of the model, monitoring techniques were tested. As some of the monitoring techniques were invasive and might interfere with the objective of validation of the model, a test program as shown in table 1 was defined.

Table 1: Test program

Test nr.	Sand type	Monitoring equipment	Objective
1	Fine sand	Low disturbance techniques	Validation of model and process / Testing monitoring techniques
2	Coarse sand	No additional monitoring	Validation model and process
3	Fine sand	No additional monitoring	Validation model and process
4	Coarse sand	High disturbance techniques	Testing monitoring techniques

In this article only test 1-3 will be discussed, as the monitoring techniques in test four might have been disturbing for analysis of the process. Each test has been performed in the same way: the head difference was increased with 0.1 m every hour (15 minutes of filling and 45 minutes of monitoring) until sand transport took place. When sand transport was observed, the increase of hydraulic head was delayed until sand transport had ceased. In some cases the hydraulic head had been increased, despite of ongoing sand transport, as a result of time constraints. Sand craters that occurred at the water level were removed by hand to keep a constant gradient through the dike.

Figure 4: Filling the basin with sand and build-up of the clay levee

PIPING PROCESS – FROM SEEPAGE TO FAILURE

Based on observations in the full-scale experiments, the phenomena in the experiment can be divided into four phases: seepage, retrograde erosion, widening of the channel and failure.

Seepage

Seepage underneath the levee was observed during the first steps of increase of hydraulic head, but no transport of sand. This stage allowed for accurate determination of the permeability of the sand layer. Based on the flow measurement, grain size distribution, laboratory permeability measurements and the relative density it was concluded that the degree of saturation was good.

Table 2: Properties of sand layer in test 1-3

Test nr.	Sand type	Relative density [%] [1)]	Permeability [m/s] [2)]
1	Fine sand	60	8E-5
2	Coarse sand	75	1.4E-4
3	Fine sand	60	8E-5

1) +/- 10% 2) T=12°C

Retrograde erosion

The retrograde erosion manifested itself in different forms. Sand traces occurred in an early stage of the experiment (first observed at hydraulic head of 0.10 m to 1.4 m depending on the experiment (gradients of 0.007 – 0.09)). Sand traces are spots of sand, which suddenly appear without any visual movement of sand. No boiling of sand or sand craters were observed. The amount of transported sand is limited (spots are generally around 0.1-0.3 m in diameter with barely any height). Although no sand transport is visible, the sand traces may slightly increase in size, and fines were found to be in suspension near these locations. The sand traces do not notably affect the water pressures and are present at various locations along the downstream toe.

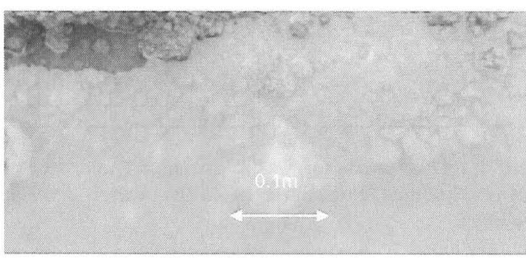

Figure 5. A sand trace

After increase of hydraulic head until 1.6-2.1 m (gradients of 0.11-0.14), depending on the experiment, wells with boiling sand may occur. These wells do lift the sand grains in (small) sand craters, but sand grains are not deposited at or over the rim of the sand crater. A short channel must have been present as the pore pressure meters located near the downstream toe indicated a decrease of water pressure near these wells.

In some cases the wells with boiling sand started to deposit sand over the rim of the crater, after increase of hydraulic head. It also occurred that new wells were created that immediately started to transport sand. In experiment 1 and 3 several well locations were present along the toe of the levee, but in experiment 2 only one well transported sand. It is striking that sand transport at this stage does not cease. Although quantities were limited (approx 0.5 kg/hr) the transport of sand continued at a more or less stable pace.

At this stage the hydraulic head was maintained at a constant level for about 24 hours in each experiment, without any notification of decrease of sand transport. Due to time constraints, the hydraulic head was increased in an attempt to speed up the process. The amount of transported sand increased with each step. Once the transport is such that it was expected that the channel would reach the upstream side within a certain timeframe, the hydraulic head was kept constant.

The channel formation was monitored by the water pressure measurements. A local decrease of water pressure is an indication for channel formation (Figure 7).

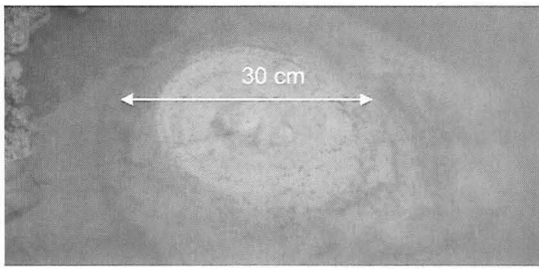

Figure 6. Sand transporting sand boil (sand crater)

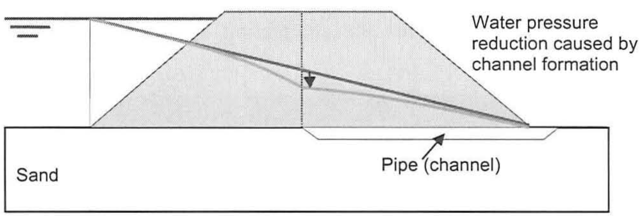

Figure 7. Sketch Local decrease of water pressure (pale blue line) caused by retrograde piping channels compared to initial water level before channel formation (blue line).

Widening of the channel

As soon as the channel reaches the upstream side, a different process starts: widening of the channel. In this process, the channel is enlarged from the upstream side towards the downstream side. The sand, eroded as a result of the widening and deepening of the channel, is pushed forward, causing the backward formed channels to clog. This process therefore takes a considerable amount of time, dependent on the seepage length.

The start of this process cannot be observed in the behavior of the sand boils, as the amount of transported sand does not change initially (Figure 8). The measurement data stops when the widening of the channel reaches the downstream side. It can be seen that no significant increase in transported sand occurs in the transition from retrograde erosion to widening of the channel.

However, the widening process can be observed in the water pressure measurements, as an increase of pressure is observed, caused by the low hydraulic resistance of the enlarged channel, spreading from the upstream side towards the downstream side (figure 9).

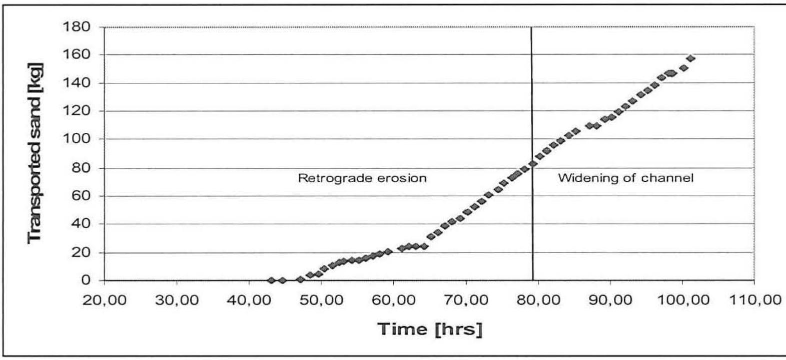

Figure 8: Cumulative amount of transported sand in experiment 3

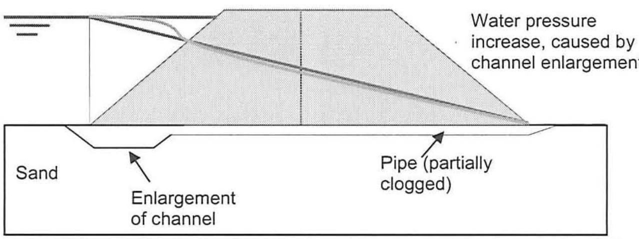

Figure 9: Sketch Change of water level in the sand as a result of channel enlargement (red line) compared to initial water level before channel formation (blue line)

Figure 10: Widening of channel has reached the downstream side, resulting in an increase of sand transport, in this case followed by deformation

A change in the amount of sand transport is observed as soon as the widening process reaches the downstream side: a connection is created between the up- and downstream side of the levee. At this point two things may happen: either the flow and sand transport increase further until the levee fails (which happened in experiments 1 and 3), or the levee deforms (which happened in experiments 2 and 4), thereby partially closing the channel, causing the sand transport to decrease (figure 10). Cracks appear in the levee. In the latter case, it is only a matter of time until the connection between the upstream and downstream side has re-established and sand transport and flow increase again. Several phases of reconnection and deformation may take place before the levee fails.

Failure

In all experiments failure of the levee took place. The process of failure starts with a large increase of turbulent flow and sand transport (mud flow), affecting a large area. Cracks appear in the levee and parts of the toe of the levee are eroded. Due to the large discharge, the water level at the upstream side could not be maintained, a drop of at least 0.60 m was observed in all experiments. In reality this drop of water level will not occur, thereby possibly even further increasing the damage to the levee.

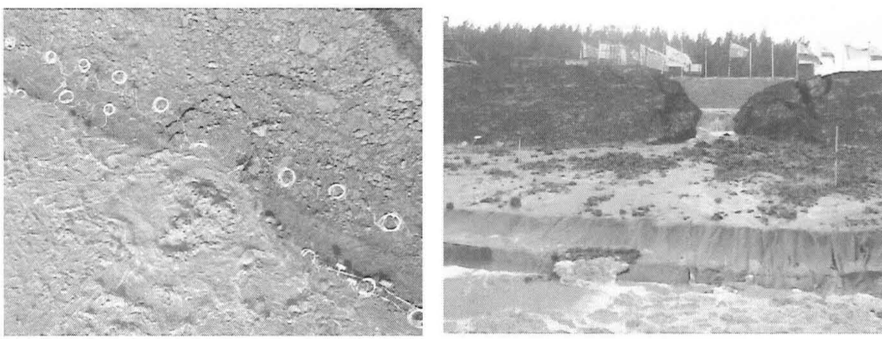

Figure 11: Increase of sand and water transport (mud flow)(left) leading to failure and breakthrough of the levee (right)

Processes in relation to hydraulic head and time

In figure 12 the named processes are related to the applied hydraulic head and the calculated bulk permeability for experiment 2. In table 3 the relation between observed processes, time and hydraulic head is given for test 1-3. An important finding, which results from both figure 12 and table 3, is the fact that the critical head is (almost) reached as soon as sand transporting wells appear. In the experiments the head is increased due to time constraints (after 45, 55 and 65 hours in the test shown in Figure 12), but it is expected that finally the channel would have reached the upstream side at the level at which the first sand transporting wells were observed. As this is uncertain, the critical head is expected to be somewhere between 1.6 and 1.9 m for experiment 2 (gradients 0.11-0.13). The critical head is therefore defined as the head at which it is expected that the channel will reach the upstream side. For the three tests the critical head is estimated to be 2.3, 1.75 and 2.1 m respectively.

Comparing the experimentally obtained critical head with the calculated critical head, it appeared that there was good agreement for the 'fine sand' test. The agreement was less for the 'coarse sand'. The critical head of experiment 2 (coarse sand) is lower than the critical heads of experiment 1 and 3 (fine sand). Based on small-scale experiments (Van Beek, 2010), this was expected, but according to the model of Sellmeijer (1988) the dependency is in the opposite direction. This aspect will be subject to further study.

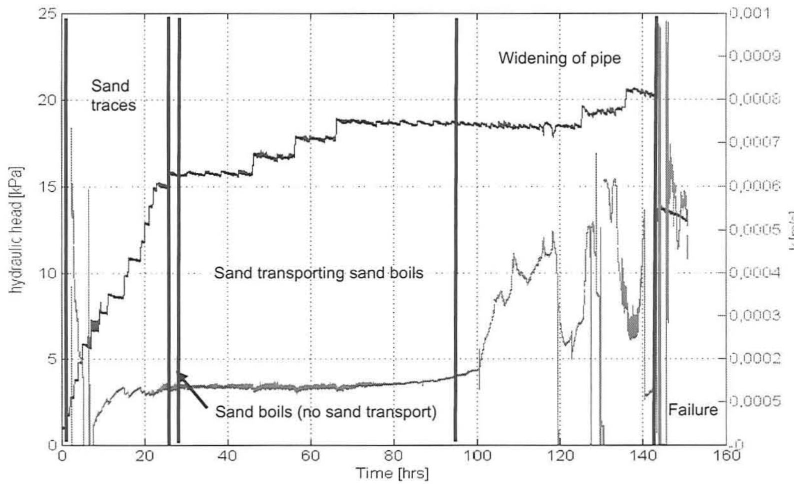

Figure 12. Experiment 2, Relation between processes, time, bulk permeability and hydraulic head

Table 3: Overview of time and hydraulic head in relation to processes in test 1-3

Test		Sand trace	Sand boil	Sand boil	Widening	Failure
1	Time [hrs]	5.3-20.5	20.5-25.7	25.7-95*	95-100.3	100.3
	Head [m]	0.6-1.6	1.6-2.0	2.0-2.7	2.7	2.7
2	Time [hrs]	2-26.3	26.3-27.5	27.5-94.5	94.5-143.3	143.3
	Head [m]	0.2-1.6	1.6	1.6-1.9	1.9-2.1	2.1
3	Time [hrs]	24.6*-42.5	-	42.5-79.2	79.2-111.8	111.8
	Head [m]	1.5-2.1	-	2.1	2.1-2.3	2.3

* value unclear due to limited monitoring

The retrograde erosion phase takes several days, but will proceed faster when the head difference is further increased. Exceeding the critical head with more than several tens of centimetres could possibly result in rapid failure. The relation between time and erosion should be investigated.

The equilibrium curve, as shown in figure 2, might still be correct, although the amount of transported sand is very limited until the critical head is reached. In practice, this amount of transported sand may even not be visible.

It was expected that as soon as the channel reaches the upstream side, the flow and sand transport would increase significantly, quickly followed by failure of the levee. In figure 12 and table 3 it can be seen that the time necessary for the widening process can take up to a few days, which is longer than expected. The process can be well monitored using pore pressure transducers, but in a field situation, without any monitoring equipment, there may be little warning for the failure, as the situation may suddenly change from small sand boils to mud flows and failure. It would therefore be recommended to take immediate measures as soon as sand boils appear.

CONCLUSIONS

The process of piping was studied in a full-scale experiment at the location of the IJkdijk in the Netherlands. Four phases have been observed: seepage, retrograde erosion, widening of the channel and failure of the levee. The phase of retrograde erosion is modelled by Sellmeijer (1988). In this phase channel formation is observed as sand traces, clean wells and sand transporting wells (sand craters). Sand traces, which are sandy spots without any crater formation, appear at a hydraulic head that is below the critical head. In contrary to what was expected, the amount of transported sand below the critical head was very limited. As soon as sand transporting craters appear, the critical head was (almost) reached. The start of the next phase, widening of the channel (cleaning of channel from upstream to downstream), can be monitored only by using pore pressure transducers. The amount of transported sand increases only significantly when the channel reaches the downstream side. The widening process may directly result in failure as soon as the channel reaches the downstream side, but may also result in deformation of the clay levee, partially closing the channel, thereby extending the duration of the widening phase. Failure takes place by significant increase of sand and water transport and deformation of the levee. It appears that failure caused by piping is a realistic threat for levees.

As soon as sand craters appear in the field, most likely the critical head has been reached, and it is recommended to take measures. Based on the amount of transported sand the time to failure cannot be predicted. Water pressure measurements give an indication of the phase.

ACKNOWLEDGEMENTS

The full-scale experiments are a combined effort of Deltares, TNO ICT, NV NOM and STOWA. The research was partly funded by Rijkswaterstaat – Centre for Water Management – on behalf of the Ministry for Transport, Public Works and Water Management. This funding was realized in the framework of the research program “Strength and Loading on Flood Defence Structures”(SBW). The project was realized with the contribution of Samenwerkingsverband Noord Nederland (SNN) and was also partly financed by the European Regional Development Fund.

REFERENCES

Bligh, W.G. (1910). “Dams Barrages and weirs on porous foundations” Engineering News 64 (26).

De Vries, G. , Koelewijn, A.R., Hopman, V. (2010), “IJkdijk Full Scale Underseepage Erosion (Piping) Test: Evaluation of Innovative Sensor Technology”, Fifth international conference on Scour and erosion, 2010 San Francisco.

Sellmeijer, J. B. (1988). "On the mechanism of piping under impervious structures," Delft University of Technology, Delft.

Van Beek, V.M., Bezuijen, A., Zwanenburg, C., (2010a). Piping: Centrifuge experiments on scaling effects and levee stability, 7th International Conference on Physical Modelling in Geotechnics, Zurich.

Van Beek, V.M., Knoeff, J.G., Rietdijk, J., Sellmeijer, J.B., Lopez De La Cruz, J. (2010b). Influence of sand characteristics and scale on the piping process – experiments and multivariate analysis, 7th Int. Conf. on Physical Modelling in Geotechnics, Zurich.

VNK1, (2005). “Flood Risks and Safety in the Netherlands (Floris), Floris study - Full report”, www.helpdeskwater.nl.

Levee Erosion Prediction Equations Calibrated with Laboratory Testing

Scott Shewbridge[1] M. ASCE, Juan Perri[1] M. ASCE, Philip Mineart[1] M. ASCE, Richard Millet[2] M. ASCE, Wilbur Huang[2] M. ASCE, Juan Vargas[2] M. ASCE, Mike Inamine[3] M. ASCE, and Steve Mahnke[3] M. ASCE,

[1] URS Corporation URS Corporation, 1333 Broadway, Suite 800, Oakland, CA 94612,email: scott_shewbridge@urscorp.com and juan_perri@urscorp.com
[2] URS Corporation, 2870 Gateway Oaks Drive, Suite 150, Sacramento, CA, email: richard_millet@urscorp.com, wilbur_huang@urscorp.com and juan_vargas@urscorp.com
[3] Department of Water Resources, Division of Flood Management, 2825 Watt Avenue #100, Sacramento, CA 95821, email: inamine@water.ca.gov and gmahnke@water.ca.gov

ABSTRACT:

A physical and mathematical model used in the third tier of the California Department of Water Resources' Urban Levee Geotechnical Evaluations Program Erosion Screening Process (ESP) is described. It has been developed and calibrated based on the results of Erosion Function Apparatus (EFA) test results of California river and levee soil samples, confirming the relationships relating general soil classification to erosion resistance as a function of water-induced shear stresses. The model is used to assess erosion during normal and/or flood conditions for combined wind and current loads. An example calculation using the method is provided.

INTRODUCTION

The California Department of Water Resources' Urban Levee Geotechnical Evaluations Program is evaluating urban levees in the Sacramento and San Joaquin river systems. As described in a companion paper, a three-tiered Erosion Screening Process (ESP) has been developed to qualitatively and quantitatively assess the risk of current and wind wave induced erosion failure on a levee's waterside slope. This paper describes the fluid and soil mechanics-based model developed for the quantitative third tier analyses.

EROSION SCREENING PROCESS COMPUTATIONS METHODOLOGY

To conduct the third tier quantitative analyses, an Erosion Screening Process (ESP) spreadsheet was developed to estimate the surface erosion potential on the waterside of a levee. It is a tool for use during screening level assessments of levee vulnerability; it is not a design tool. The ESP spreadsheet uses the same physical process model used to develop an erosion risk model for the US Army Corps of Engineers (URS, 2007).

In essence, the erosion potential assessment is conducted using six pieces of information: levee geometry, water/stream/river current characteristics, wind characteristics, armor characteristics, vegetation characteristics and soil type. Erosion risks to riverine levees will most likely be due to a weakened levee cross section coupled with high flow velocity and/or wave action. In large, open bodies of water like a bypass, wind-wave damage is expected to be a dominant cause of erosion. Erosion caused by factors like surface runoff, boat wakes, and embankment overtopping during a flood were not considered for this erosion analysis methodology.

Erosion Rate Model

Several erosion studies have been performed in the past that focus on identifying the erosion parameters and correlating those parameters to formulate an expression (i.e., a physical model) for erosion rates (Hanson and Temple, 2002, Hanson and Cook, 2004). The governing equation for this model is:

$$\dot{\varepsilon} = (k\,(\tau - \tau_c)) > 0 \qquad (1)$$

where:

$\dot{\varepsilon}$ = erosion rate (ft/hr)
k = erodibility coefficient or detachment rate coefficient (ft^3/lb-hr)
τ = effective hydraulic stress on the soil boundary (psf)
τ_c = critical shear stress (psf) i.e., the shear stress at which erosion starts

The erosion rate ($\dot{\varepsilon}$) is a function of both hydraulic (τ) and geotechnical (k, τ_c) parameters. τ mainly depends on characteristics of water-soil boundary, current/stream velocity and/or wind wave height and period. Both k and τ_c are functions of the engineering properties of the levee and the foundation materials.

The following subsections describe the hydraulic and geotechnical parameters in the above model and how they are used and modeled in the spreadsheet.

Hydraulic Loading

Two general types of erosion that are common for levees are current erosion (sometimes called scour) and wave erosion. In the erosion calculation, the shear stresses associated with each are calculated separately to estimate the combined erosion rate.

Current/Stream Velocity Erosion Parameters

The estimation of erosion rate due to shear stresses imparted to the levee and its foundation due to current/stream velocity requires information on the hydraulic parameters of stream velocity and water-soil interface roughness. Using the conventional assumption of a logarithmic velocity profile (USACE, 1994), the average hydraulic shear stress due to currents (τ_s) can be calculated using Equation 2.

$$\tau_s = \tfrac{1}{2}\,\rho\, f_c\, V^2 \qquad (2)$$

Where:

ρ = mass density of water (lbm/ft^3)
f_c = current friction factor (also referred to as the Fanning friction factor which is dimensionless) = $2(2.5(\ln(30h/k_b)-1))^{-2}$ (Danish Hydraulic Institute (DHI), 2007)

where:

h = water depth (ft)

k_b = bed roughness (ft)

V = current speed (ft/s)

Wind Wave Erosion Parameters

Erosion by waves can occur from two mechanisms; by generating excess shear stress on the soil underneath the waves (i.e., bottom currents) or by wave breaking on the levee slope. The estimation of the wave induced erosion rate requires estimates of wave height and period.

Wave Height and Period

Wind waves are generated by wind blowing over water and their height and period are a function of the wind speed, duration, water depth and fetch length. For the erosion spreadsheet it was assumed that the wind blows for sufficient duration for fully developed waves to form in deep water, making wave height and period a function of fetch length and wind speed only, a reasonable assumption for a screening-level assessment.

The waves generated by the wind are not all the same size or have the same period, so a spectra of values are generated. Typically a value of wave height is picked to represent the spectra called the significant wave height. Traditionally, the significant wave height is calculated as the average of one-third of the highest wave heights measured from the troughs to the peaks. Using this definition of significant wave height, the wave height can be estimated using the equations below (USACE, 1984, often referred to as SPM – The Shore Protection Manual):

$$\frac{gH_s}{U_A^2} = 1.6 \cdot 10^{-3}\left(\frac{gF}{U_A^2}\right)^{1/2} < 2.433 \cdot 10^{-1} \tag{3}$$

$$\frac{gT_m}{U_A} = 2.857 \times 10^{-1}\left(\frac{gF}{U_A^2}\right)^{\frac{1}{3}} < 8.134 \tag{4}$$

where,

H_s = significant wave height (ft)

T_m = average period of the wave (s)

F = fetch length (ft)

U_A = the wind-stress factor (ft/s)

$U_A = 2.329\,(0.447\,U)^{1.23}$ (ft/s)

where, U = wind speed in miles/hour

g = acceleration due to gravity (32.2 ft/s^2)

The wave height is limted to approximately 60 percent of the water depth. Therefore in the spreadsheet if H_s is greater than the 0.6 times the water depth, then it is set equal to 0.6 times the water depth.

Hydraulic Shear Stress Due to Waves

The wind-driven waves will generate bottom currents with a corresponding shear stress. If this shear stress exceeds the critical shear stress of the soil, erosion will occur. The bottom current shear stress (τ_w) can be estimated from Equation 5 below.

$$\tau_w = \tfrac{1}{2}\, \rho\, f_w\, U^2_b \qquad (5)$$

where:

ρ = mass density of water (lbm/ft^3)

f_w = wave friction factor (Fanning - dimensionless)

$$= \exp\left(5.213\left(\frac{a}{k_l}\right)^{-0.194} - 5.977\right) \quad \text{(Swart, 1974)} \qquad (6)$$

$$\textit{if} \quad \frac{a}{k_l} \leq 1, \qquad f_w = 0.47$$

k_l = levee slope roughness (ft)

a = horizontal mean wave orbital motion at the bed (ft) (DHI, 2007)

$$a = \frac{H}{\pi}\frac{1}{\sinh(\frac{2\pi h}{L})} \qquad (7)$$

L = wave length (ft)

$$L = \frac{gT^2}{2\pi}\left\{\tanh\left[\left(\frac{2\pi}{T}\sqrt{\frac{h}{g}}\right)^{3/2}\right]\right\}^{2/3} \qquad (8)$$

h = water depth (ft)

U_b = horizontal mean orbital wave velocity at water-soil interface (ft/sec)

$$U_b = \frac{2H}{T}\frac{1}{\sinh(\frac{2\pi h}{L})} \qquad (9)$$

H = wave height (ft)

For levee erosion calculations, $H=H_s$ and $T=T_m$

The orbital wave velocity, U_b, is dependent on the significant wave height, the wave period, and the water depth. The roughness, k_l, is often related to some measure of the grain size of the slope (i.e., levee or foundation) materials. Puleo and Holland (2001) provide a summary of common relationships used to define k_l.

Shear Stress Due to Wave Breaking

The science of estimating the shear stress on a levee due to wave breaking is much less advanced than the estimation of shear stress due to wave orbital velocities. To provide an estimate of the shear stress, the following assumptions are made:

- The rate of energy dissipation due to wave breaking can be estimated as a shear stress (τ) times a velocity, where the shear stress is the force per unit area on the levee surface due to the wave breaking, and the velocity is the rate at which energy is conveyed to the levee by the waves. The velocity at which energy is propagated is called the group wave speed and is represented by c_g. The rate of energy dissipation is then:

$$\text{Rate of energy dissipation} = \tau \cdot c_g \qquad (10)$$

The rate of energy dissipation is assessed in units of lbs-ft per feet^2 per second (a more familiar unit may be BTU or calorie per ft^2 per second)

- Only a portion of the wave energy dissipated by the wave breaking causes sediment erosion due to bed shear stress. That portion (i.e., the efficiency) is considered low because most of the wave energy is lost in the generation of turbulence.

Energy dissipation in the surf zone can be estimated from Equation 11 (Zou, Bowen and Hay, 2006):

$$\Delta = \frac{1}{4}\rho g f \frac{(BH_{max})^3}{h} \qquad (11)$$

Where: Δ = energy dissipation rate (lbf-ft/ft^2/s)
ρ = density of water (lbm/ft^3)
g = gravitational acceleration (ft/s^2)
f = wave frequency (1/s)
= $1/T_p$
T_p = wave period (s)
B = empirical coefficient often set equal to one
H_{max} = wave height at breaking (ft)
h = local water depth (ft)

This form is similar to the form presented by USACE (2003), Lim and Chan (2003), and others.

H_{max}, the wave height at breaking can be estimated from:

$$H_{max} = \frac{0.88}{k}\tanh(\gamma_b \frac{kh}{0.88}) \qquad (12a)$$

Simplified to approximately:

$$H_{max} = 0.14 \cdot L \cdot \tanh\left(\frac{2\pi \cdot h}{L}\right) \qquad (12b)$$

Where: k = wave number = $2\pi/L$ (ft^{-1})
γ_b = ratio between wave height and water depth in shallow water (depth-limited breaking) and can vary from 0.4 to 1.2 (Zou et al. 2006) but is typically taken to be 0.78 (Larson and Kraus, 2000). A value of 0.78 is used in this analysis.
h = local water depth (ft)

To estimate the shear stress due to wave breaking it is necessary to estimate the group velocity. The group velocity, c_g, can be estimated as (Kinsman, 1984):

$$c_g = 0.5 \cdot \sqrt{\frac{g}{k}\tanh\left(2\pi\frac{h}{L}\right)} \cdot \left(1+\frac{2kh}{\sinh(2kh)}\right) \tag{13}$$

In most scenarios Equation 3-20 can be simplified assuming deep water (i.e., h/L>~0.5) to:

$$c_{gd}^2 = \frac{g \cdot L}{8\pi} \tag{14}$$

The shear stress is then estimated as:

$$\tau = \varepsilon\, \Delta / c_g \tag{15}$$

Where

ε = portion of the energy dissipated by wave breaking that is dissipated as bed shear stress.

To estimate wave energy bed shear stress dissipation rates, a limited number of case histories were evaluated during testing of a similar erosion evaluation tool developed for the United States Army Corps of Engineers (URS, 2007). Based on those limited results, energy dissipated as bed shear stress appears to be between 5 and 10 percent. Therefore, the analyses performed for the DWR ULE program used an estimated wave breaking bed shear stress dissipation value of 7.5 percent. Additional work in this area seems warranted.

Geotechnical Parameters

Once the hydraulic stress on the levee material due to either the stream velocity or wind generated waves is known, the next step is the estimation of the geotechnical parameters that influence the erosion potential (erosion rate) of a levee.

Armoring and Vegetation

Physical armoring and vegetation have both been observed to have an impact on the initiation and continuation of erosion of levee slopes. The erosion calculation uses four generic categories: presence and absence of armoring and presence and absence of vegetation. Depending on the presence or absence of either, and the design critical armor/vegetation velocity and critical armor/vegetation wave height, the erosion rate computed using Equation 1 is modified. If armoring and or vegetation is present, and the flow velocity does not exceed either critical velocity, and the wave height does not exceed either critical wave height then, zero erosion is computed. If armoring or vegetation is present, but the flow velocity associated with an analyzed flood level (i.e., water surface elevation) exceeds either critical velocity, or if the wave heights exceed the critical wave heights, the armor and or vegetation is considered eroded and Equation 1 is used to calculate erosion.

Special note - armor and vegetation erosion resistance is a significant factor in the analyses, but due to space limitations, cannot be more fully discussed in this paper. The "Erosion Toolbox: Levee Risk Assessment Methodology" (URS, 2007) can be consulted for additional information and discussion regarding armor-types and vegetation classes and associated modeling parameters.

Levee and Foundation Materials

The characteristics of the levee and foundation materials have a significant impact on the expected erosion rates. Typically, dense coarse-grained materials and stiff fine-grained materials are generally more resistant to erosion than loose coarse-grained materials and soft fine-grained materials, respectively. Therefore, it is important to identify the levee and foundation materials and classify them appropriately. The calculation incorporated five main soil types, generally categorized under ASTM D 2488 (Standard Practice for Description and Identification of Soils) as boulders and cobbles (very resistant), gravel (resistant), sand (erodible), silt (very erodible) and clay (moderately resistant). Note, clays and silts are not differentiated based on particle size alone, but rather by limiting percentage of a maximum particle size and plasticity characteristics.

Critical Shear Stress as a Function of Soil Type

Erosion rates as a function of flow velocity / induced shear stress can be measured in the laboratory using one of several devices such as the Erosion Function Apparatus (EFA, Briaud et. al, 2001a and b). The critical shear stress, τ_c, is defined as the shear stress corresponding to a rate of erosion of 1 mm/hr in the EFA. While useful for analytical studies, this method is impractical for rapid surveys. Alternatively, the critical shear stress can be estimated using empirical correlations between the critical shear stress and soil index properties. Several empirical correlations between critical shear stress (τ_c) and soil index properties such as grain size, plasticity index and shear strength are available in the literature to estimate the value of τ_c (URS, 2007). In order to simplify the analyses, erosion resistance of the levee and foundation material has been divided into five broad classes related to their ASTM classifications, as shown in Table 1. The erosion calculations used these typical values for critical shear. The values shown are based on the experimental and field-testing results as reported by Briaud et al. (2001a, 2003) and Hanson and Simon (2001).

Erodibility Coefficient as a Function of Soil Type

One method to estimate the coefficient of erodibility, k, used in Equation 1, is by performing the jet index test (ASTM D 5852). However performing site-specific tests will be impractical for rapid assessment of conditions. Therefore, in a manner similar to the method used to evaluate critical shear stresses, to simplify the analyses, erodibility of the levee and foundation materials has been divided into five broad classes related to the material's ASTM classification, as shown in Table 1. The erosion calculations used typical values for erodibility coefficients. The values presented in Table 1 are based on the experimental and field-testing results as reported by Briaud et. al (2001a, 2003) and Hanson and Simon (2001).

Table 1 - Typical Values for Critical Shear Stress and Coefficient of Erodibility of Soils

Levee/Foundation Material	ASTM Typical Soil Types	Critical Shear Stress, τ_c (psf)	Erodibility Coefficient, k (ft^3/lb-hr)
Very Resistant	BOULDERS and COBBLES	4.869	0.005
Resistant	GRAVEL (GP-GW)	1.058	0.021
Moderately Resistant	CLAY (CL, CH, SC, GC)	0.094	0.094
Erodible	SAND (SP, SM and mixtures)	0.014	0.409
Very Erodible	SILT (ML)	0.003	1.867

Levee Geometry

Figure 1 illustrates the geometric characteristics of a given levee that influence the erosion analyses. Erosion of the foundation and/or levee waterside slope materials is considered in the analysis. For the DWR studies, overtopping is considered as a separate failure mode. Erosion due to overtopping is not evaluated in this process, though the soil-water model used in this analysis can be expanded for such analyses.

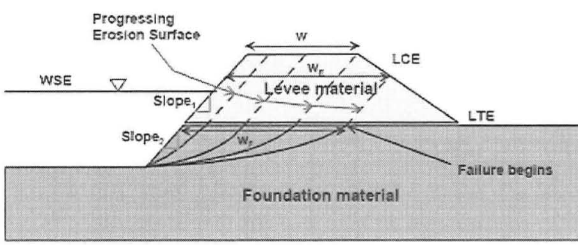

Notes:

1) LCE: Maximum water surface or levee crest elevation
2) LTE: Landside toe elevation
3) WSE: Water surface elevation
4) w: Levee crest width
5) w_E: Effective levee width
6) w_F: Width of levee at the LTE that must be eroded for failure to occur
7) For failure to occur, WSE must be greater than LTE

Figure 1 – Levee and Foundation Geometry

CALIBRATION TESTING

To validate the soil type categorizations of critical shear stress and erodibility coefficients (i.e., Table 1), soil samples were collected throughout the DWR ULE study areas. Soil Characterization tests, including gradation, Atterberg limits, moisture contents and density tests were performed on the samples. These samples were then tested in an Erosion Function Apparatus or EFA (Figure 2, Briaud et al., 2001a). The 75mm outside diameter sampling tube is placed through the bottom of the conduit where water flows at a constant velocity. The soil is pushed out of the sampling tube only as fast as it is eroded by the water flowing over it. For each velocity, an erosion rate is measured and a shear stress is calculated.

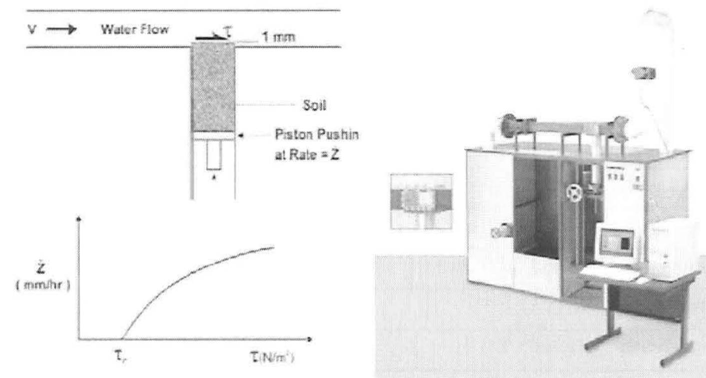

Figure 2 – Erosion Function Apparatus (Briaud et al, 2001a)

Figure 3 presents the results of the EFA tests. These are compared with the estimated erosion rates based on the theoretical models and parameters described above in Table 1, showing excellent agreement for the silt and clay materials tested.

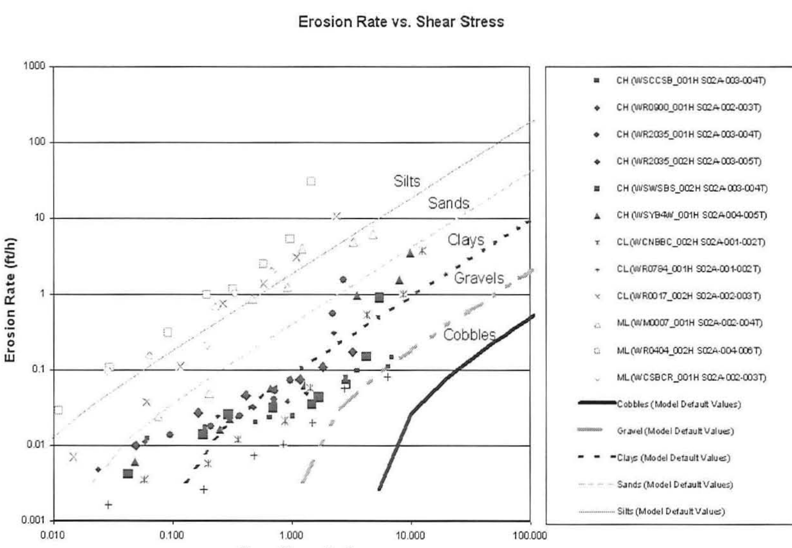

Figure 3 – EFA Testing Results

EXAMPLE CALCULATION

To demonstrate the application of the methodology, the following example calculation is provided. The river current and wind loading are summarized in Table 2 and levee conditions are summarized in Table 3.

Table 2 – River Current and Wind Wave Loading

Factor	Hydrograph Stage	
Water/Stream/River Current	1st	2nd
Water Surface Elevation, NAVD 88 (ft) =	15	10
Velocity, V (ft/sec) =	3.2	1
Duration for Velocity, d (hours) =	100	2000
Wind/Wave	1st	2nd
Wind Speed, U' (miles/hr) =	50	50
Duration of Wind (hrs) =	2	2
Maximum fetch length (ft), F =	60000	60000
Efficiency of wave breaking to erode sediments =	7.50%	7.50%

Table 3 – Levee Conditions (geometry, soils, armor and vegetation)

Geometry	
Channel bottom elevation, NAVD 88 (ft) =	0
Landside toe elevation, NAVD 88 (ft), LTE =	8
Levee slope (X Horizontal to 1 Vertical; Specify X) =	4
Effective levee width against erosion (ft)	40
Soil Type	
Levee and Foundation Soil Type	Sand - Erodible
Critical Shear Stress (psf), τ_c =	0.0136
Erodibility Coefficient (ft^3/lb-hr), k =	0.4093
Levee slope roughness (ft), K_L =	0.0197
Slope of Erosion Rate vs Velocity line, $m_{log\text{-}log}$ =	6.9
Velocity for which Erosion Rate is 1ft/h (ft/s), V_1 =	4.6
Armor /Vegetation	No/Yes
Velocity at which vegetation protection is lost (ft/s) =	3
Wave height at which vegetation protection is lost (ft) =	5

The loading and estimated erosion for current and wind for the first and second stages is presented on Figure 4.

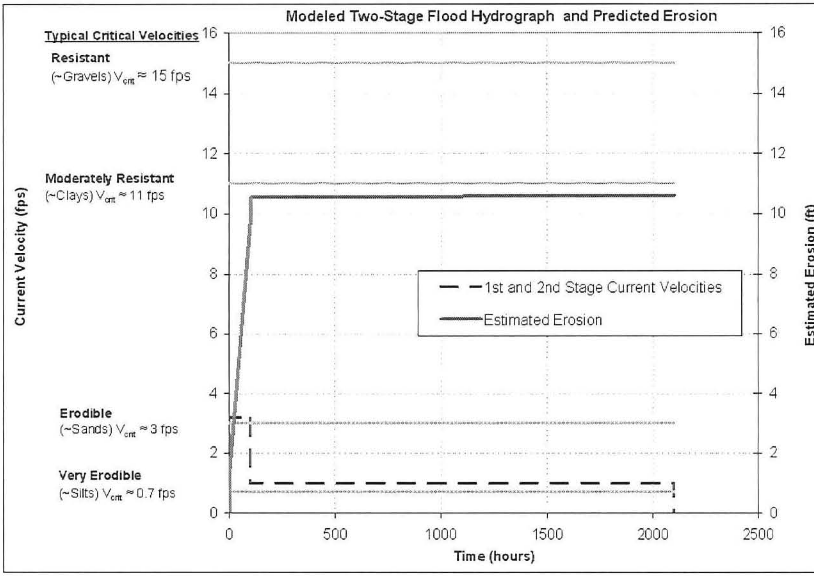

Figure 4 – Typical Erosion Evaluation Results for Two Stage Hydrograph

Wave erosion for stage 1 and stage 2 is estimated at 1.5 and 0.9 feet, respectively. Because estimated wave heights during stage 1 were greater than the wave heights that the vegetation could withstand, vegetation was lost during the beginning of stage 1 and provided no protection for the levee and foundation slopes during wind or current loadings for stage 1 or stage 2. Current erosion for stage 1 and stage 2 are estimated at 8.2 and <0.1 feet respectively. Current erosion for stage 2 is low because the current velocity is less than the critical velocity for the levee and foundation materials. Total erosion is estimated to be 10.6 feet, which is less than the levee width (40 feet), but it is substantial, nevertheless. In this study, if estimated erosion is greater than 25% of the foundation or embankment width, then the site is considered to have High erosion potential.

CONCLUSION

Using theoretical models combined with soils testing results, a model to predict erosion on the waterside slopes has been developed and is being used to assess the erosion potential of the waterside slopes as part of a three tiered screening process for over 350 miles of levees in California. The results of these analyses will be used to help assess levee erosion vulnerability and potential mitigation prioritization.

REFERENCES

Briaud, J.-L., Ting F., Chen, H.C., Cao Y., Han S. -W., Kwak K. 2001. *Erosion Function Apparatus for Scour Rate Predictions*. Journal of Geotechnical and Geoenvironmental Engineering. ASCE, Vol. 127, N. 2, pp. 105-113.

Briaud, J.-L., Chen, H.C., Li Y., Nurtjahyo, P., Wang, J. 2003. *Complex Pier Scour and Contraction Scour in Cohesive Soils*. National Cooperative Highway Research Program Report.

Danish Hydraulic Institute (DHI). 2007. *Mike 21 Flow Model*. Mud Transport Module, Scientific Background. DHI, Denmark.

Hanson, G.J., Simon, A. 2001. *Erodibility of Cohesive Streambeds in the Loess Area of the Midwestern USA*. Hydrological Processes. Vol. 15 No 1. pp. 23-38.

Hanson, G.H., Temple, D.M. 2001. *Performance of Bare-Earth and Vegetated Steep Channels Under Long-Duration Flows*. Presented at the 2001 ASAE Annual Meeting. ASAE Paper No. 012157.

Hanson, G.J., Cook, KR. 2004. *Apparatus, Test Procedures, and Analytical Methods to Measure Soil Erodibility in Situ*. Applied Engineering in Agriculture. American Society of Agricultural Engineers, Vol. 20, No. 4, pp. 455-462.

Larson, M., Kraus, N. 2000. *Enhancements of the Numerical Model of the Longshore Current NMLONG to Include Interaction Between Currents and Waves (NMLong-CW)*. United States Army Corps of Engineers. ERDC/CHL CETN-IV-25.

Swart, D.H. 1974. *Offshore Sediment Transport and Equilibrium Beach Profiles*. Delft Hydraulic Lab. Publication 131. Delft University. Delft. 302 pp.

United States Army Corps of Engineers. 1994. *Hydraulic Design of Flood Control Channels*. EM 1110-2-1601. June 30.

United States Army Corps of Engineers. 1984. *Shore Protection Manual, 4th Ed., 2 vol.* United States Army Corps of Engineers Waterways Experiment Station. U.S. Government Printing Office. Washington DC.

United States Army Corps of Engineers. 2006. *Coastal Engineering Manual (CEM)*. United States Army Corps of Engineers. Waterways Experiment Station. EM 1110-2-1100.

URS. 2007. *Erosion Toolbox: Levee Risk Assessment Methodology: Users Manual.* Report prepared for the United States Army Corps of Engineers. December.

Levee Erosion Screening Process

Wilbur Huang[1], Richard Millet[1], Scott Shewbridge[1], Juan Perri[1], Juan Vargas[1] Mike Inamine[2], and Steve Mahnke[2]

[1]URS Corporation, 2870 Gateway Oaks Drive, Suite 150, Sacramento, CA 95833; PH (916) 679-2260; email: wilbur_huang@urscorp.com
[2]Department of Water Resources, P. O. Box 942836, Sacramento, CA 94236

ABSTRACT

The California Department of Water Resources' Urban Levee Geotechnical Evaluations Program is evaluating urban levees in the Sacramento and San Joaquin river systems. A three-tiered Erosion Screening Process (ESP) has been developed to qualitatively assess the current risk of erosion failure on a levee's waterside slope. Erosion is caused mainly by a weakened geometric levee cross section or poor initial construction coupled with high flow velocity and/or wave action. Levees are evaluated through this three-tiered screening process until the erosion risk potential is determined. Each of the tiers progressively increases in detail. Tier one assesses overall geometry, fetch length, and historical performance. In the second tier, assessments are performed to evaluate the levee's surface resistance to velocity and wave shear stress. Also, field reconnaissance verifies expected levee performance and look for signs of erosion or unstable conditions. In the third tier, the ESP analyzes levee geometry, river geometry, soil and vegetation types, wind-wave impacts and river velocity impacts to categorize levee reaches into a high, medium, or low erosion risk.

INTRODUCTION

Purpose

The objective of this erosion screening process is to make a qualitative assessment of the potential for erosion failure on a levee's waterside slope. This paper presents the methodology that will be used to assess erosion potential in specific locations of the Sacramento and San Joaquin levee systems, which are being evaluated by the California Department of Water Resources' (DWR) Urban Levee Geotechnical Evaluations (ULE) Program.

Scope and Background

This qualitative analysis builds upon knowledge gained from both previous and concurrent erosion studies conducted by Ayres Associates, the United States Army Corps of Engineers (USACE), and others. However, it differs from those studies in that it provides additional data and an approach customized to DWR's needs. Light detection and ranging (LiDAR) and bathymetry surveys completed as a part of the ULE Program allow previously unknown erosion sites (like those fully beneath a low-water surface) to be included in DWR's mitigation prioritization activities. In addition, factors like wind and vegetation are reflected in the URS Erosion Screening Process (ESP) spreadsheet for this work.

A levee site with erosion risk is defined as a site where failure is likely to occur without intervention. Erosion risks are increased by a number of factors, which may include:

- Compromised levee prism geometry
- Geomorphologic trends, as indicated by historical damage
- River flow velocity and shear
- Wind-wave shear stress
- Construction from erodible materials
- Presence of detrimental vegetation
- Absence of beneficial vegetation or other slope protection

The erosion potential assessment is conducted using six pieces of information:

- Levee geometry
- Water current characteristics
- Wind characteristics
- Armor characteristics
- Vegetation characteristics
- Soil type

Erosion risks to riverine levees will most likely be due to a weakened levee cross section or poor initial construction coupled with high flow velocity and/or wave action. In large, open bodies of water like a bypass, wind-wave damage is expected to be a dominant cause of erosion. Erosion caused by factors like surface runoff, boat wakes, and embankment overtopping during a flood were not considered for ESP.

The risk potential is quantified by the ratio of the calculated total erosion (TE) and levee width (LW) at the pertinent water surface elevation (WSE) or levee effective width. Levee sites that meet threshold criteria for any risk factors are ranked to establish one of three risk levels:

1. High Erosion Risk. If the calculated TE is greater than the 25 percent of the effective width of the levee, the levee site is at immediate risk of an erosional failure during either a flood or a normal flow condition (TE/LW > 25%).
2. Medium Erosion Risk. If the calculated TE is in between 25 percent to 5 percent of the effective width of the levee, the levee site is at risk for failure due to weaknesses, but no immediate threat is apparent (5% < TE/LW < 25%).
3. Low Erosion Risk. If the calculated TE is less than the 5 percent of the effective width of the levee, the levee site does not show evidence of erosion potential that is cause for concern. There is either little threat from wind-wave impact and insignificant evidence of geometric deficiency or historical erosion problems, or the levee's surface material adequately resists predicted velocity and wave shear stress during a given flood event (TE/LW < 5%).

Current ULE Program ESP will use the program's LiDAR topography and bathymetry survey data to compare actual levee geometry with the USACE standard levee prism. Velocity, wind-wave shear stress, and erosion fragility during a given event will be compared to the strength of existing levee materials. Specific criteria and procedures for identifying sites at risk for erosion failure are described in the next section.

EVALUATION METHODOLOGY

ESP will be performed on program levees in 15 ULE Program study areas. Figure 1 illustrates the logic and three-tiered process for ESP.

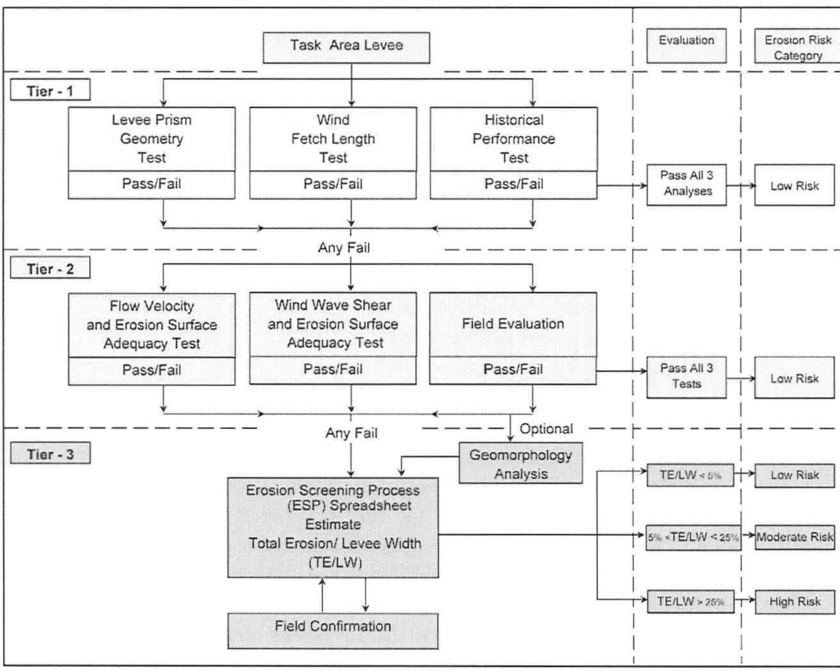

Figure 1. Erosion Screening Process Logic Diagram

Key:
ESP - Erosion Screening Process
TE - Total Erosion
LW - Levee Width

All program levees will be analyzed for the risk factors of tier one: geometry, fetch length, and historical performance. If a levee site passes all three tests in the first tier, it will be labeled as a low erosion risk site. If a levee site fails any of the three tests in the first tier, or if its historical performance is deemed questionable, the site will be advanced to the second tier for further study.

In the second tier, tests will be performed to evaluate the levee's surface resistance to velocity and wave shear stress. Field reconnaissance will verify expected levee performance and look for any signs of erosion or unstable conditions. If a levee site passes all three tests in the second tier, it will be labeled as a low erosion risk site, due to the fact that the compromised embankment has sufficient protection from velocity and wind shear stress. If a levee site fails any of the three tests in the second tier, it will be advanced to the third tier for further study.

In the third tier, ESP spreadsheet evaluation will be conducted on levee sites failing second tier tests. The ESP spreadsheet analyzes levee geometry, river geometry, soil and vegetation types, wind-wave impacts and velocity impacts to categorize tier three sites into high, medium, or low erosion risk sites.

Levee Prism Geometry Test

Specifications for a standard levee prism cross section on the Sacramento River Flood Control Project (SRFCP) are set forth in a Memorandum of Understanding (MOU) between USACE and the State of California dated November 30, 1953 (USACE and State of California, 1953). This MOU calls for a standard levee section to be constructed and maintained within the limits of the flood control system.

The MOU provides guidelines and specifications for:

- Infrastructure projects comprising the SRFCP
- Levee construction standards
- Cost of the SRFCP completion
- Responsibilities of the United States and the State of California with regard to completion of construction and operation of the SRFCP

Levee construction standards presented in the MOU also specify how levees will be maintained after construction within the limits of the flood control system. The MOU applies to levees authorized by the Flood Control Act of 1944. Not all existing levees in California have been constructed to this standard. For example, some levees constructed prior to 1944 may not meet the standard levee prism as specified in the MOU. Additionally, San Joaquin River Basin levees are not subject to MOU provisions. However, for consistency, this standard is considered for all tasks under ULE Program ESP.

To highlight deficiencies, ESP compares levees in the Sacramento River and San Joaquin River Basins to one of two standard levee prisms: one for river levees and one for bypass levees. Standard levee prism geometries are defined in Table 1.

Table 1. USACE Standard Levee Prism Geometry

Levee Locations	Crown Width (feet)	Riverside Slope (feet/feet)	Landside Slope (feet/feet)	Freeboard (feet)
River and Tributary Levees	20	3H:1V	2H:1V	3
Bypass Levees	20	4H:1V	3H:1V	6

To compare a standard levee prism to a given levee cross section, this test matches the top of the prism's landside to the levee's landside intersection with a given water surface elevation. This elevation is defined by the 200-year water surface, plus 3 feet. In any situation where the top of the levee is less than the given water surface elevation, an erosion evaluation was not performed. The standard levee prism is 20 feet in width at the crown with a slope of 3 horizontal to I vertical ratio (3H:1V) on the waterside. This comparison is one component of the first tier of the ESP.

Figure 2 illustrates geometric test at a typical levee erosion site. At any area on the waterside where the standard levee prism exceeds the existing levee section, the levee's integrity is considered compromised. Areas with extensive erosion may be subject to significant risk of erosion failure.

If an eroded area does not meet the standard levee prism geometry, but maintains a berm width of 35 feet or more (Ayres, 2007), that section will not be considered critical. Berm width is the horizontal segment of the bank that extends from the levee toe to the top of the riverbank.

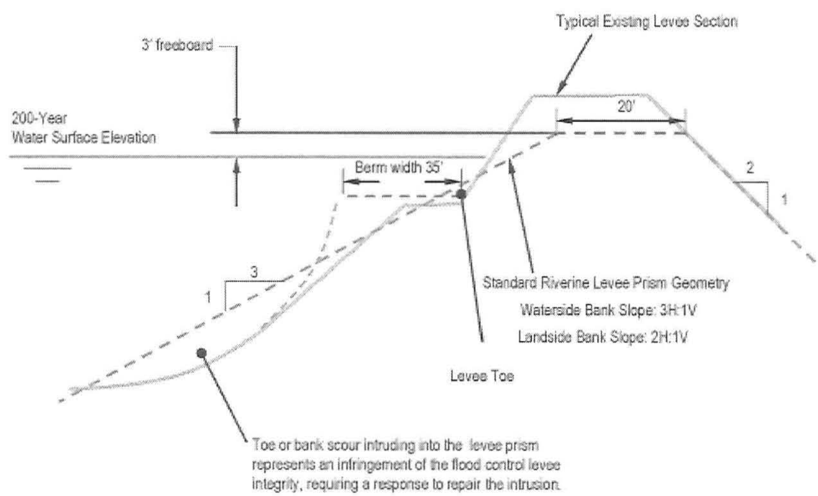

Figure 2. Placement of Standard Levee Prism Geometry within a Riverine Levee Section

Topographic data including land survey data on the levees and bathymetry data in the channel of perennial rivers are needed to generate existing levee cross sections to compare with the standard levee prism. Since the ULE Program began in 2007, land survey data have been collected using LiDAR survey technology. Bathymetry data collection began in 2008. In areas where recent survey data are not available, the 1997

USACE Comp Study (USACE, 2002) can provide supplementary data adequate for this analysis. Table 2 lists survey data types and their availability.

Table 2. Availability and Types of Topographic Data

Data Type	Availability	Horizontal Datum	Vertical Datum	Land Survey	Bathymetry Survey	Points	Contours
2007 DWR/URS LIDAR Data	Yes	UTM NAD1983	NAVD 1988	Yes	–	Yes	–
2008 DWR/URS Bathymetry Data	Yes	State Plane NAD 1983	NAVD 1988	–	Yes	Yes	–
1997 USACE Comprehensive Study Survey Data	Yes	State Plane-NAD 1983	NGVD 1929	Yes	Yes	Yes	Yes

Wind Fetch Length Test

Concurrent with prism geometry test and, as part of the first tier tests, wind-wave effects, will be considered wherever applicable. Bypasses and large river confluence areas may be subject to wind exposure that allows wave generation and wave erosion. Areas with more than 1,000 feet of open water for wind to act upon are the most likely areas to suffer wind-generated wave erosion. For this test, fetch length is measured as the maximum open water distance at a 45 degree angle to the levee's waterside slope (USACE, 1989).

In some instances, such as where the fetch is measured on a sharp bend, test by these methods may result in a fetch length greater than 1,000 feet, even within a narrow riverine channel where wind is much less likely to have a serious impact. As a result, an additional criteria requires that the local width of the channel be greater than 700 feet for the fetch length test to be performed. Wherever overall channel width is less than 700 feet, or the fetch length is less than 1,000 feet, little risk of wind-wave damage is presumed.

Historical Performance Test

As a final component of the first-tier test, available historical erosion data will be evaluated for any long-term erosion trends. Data will come from existing information provided by DWR and USACE, or from other consultants like Ayres and William Lettis & Associates. As the information is available, recent observations and repairs will be plotted for each study area to evaluate geomorphologic trends. Based on historical performance test, sites showing significant changes to their channel or bank will be added to the list of sites for be further evaluation under second tier tests.

Flow Velocity and Erosion Surface Adequacy Test

For erosion sites that fail first tier tests, peak flow and local velocity will be obtained from the USACE Comp Study or other available studies. Where existing data are not available, the USACE Alpha method described in USACE Engineering Manual (EM) 1110-2-1601 (USACE, 1991) will be used to estimate local peak velocities in the cross section. These data will be compared to the levee's waterside slope strength, as determined from recent ULE Program geotechnical boring logs and from field verification.

Riverine erosion occurs most commonly when levee material cannot resist the scouring forces of high-velocity flow. EM 1110-2-1601 recommends a set of permissible mean channel velocities for use as a guide to design non-scouring flood control channels. As part of second tier testing, ESP will apply the recommended velocity set listed in Table 3 to potentially problematic levee embankments to determine whether the embankment can withstand scour.

Table 3. Maximum Design Velocities Recommended by the USACE for Flood Control Channels

Levee Material	Maximum Design Velocity (feet per second)	
	Mean Channel Velocity at Straight Channel	Depth-Averaged Velocity at Channel Bend
Fine Sand, Sandy Silt	2.0	
Silt Clay, Soft Shale	3.5	
Coarse Sand, Fine Gravel, Clay	6.0	
Vegetation-lined Earth	8.0	
Poor Rock (Soft Sandstone, Non-uniform Revetment)	10.0	
Good Rock[1] (Riprap, Uniform Revetment)	15.0	

To account for the velocity increase on the outside of channel bends, EM 1110-2-1601 recommends an adjustment to the mean channel velocity. This adjustment factor reflects the depth-averaged velocity at a point 20 percent of the slope length from the toe of slope, where velocities are presumed highest for the embankment. The recommended USACE velocity adjustments in EM 1110-2-1601 on page 3-5 and in Plate B-33 are shown below (see Figure 3). The adjustment factor ranges from 1.0 to 1.6 and depends on the bend's centerline radius divided by the

[1] Reference from EM 1110-2-1601, Page 2-16: EM 1110-2-1601 suggests 20 fps for Good Rock. The velocity number has been adjusted for ESP based on prior DWR levee repair project experience in the Sacramento and San Joaquin River Basins.

channel's surface width, as well as the bend's angle and aspect ratio (bottom width/depth). This recommended adjustment does not apply to the side slopes of straight channels.

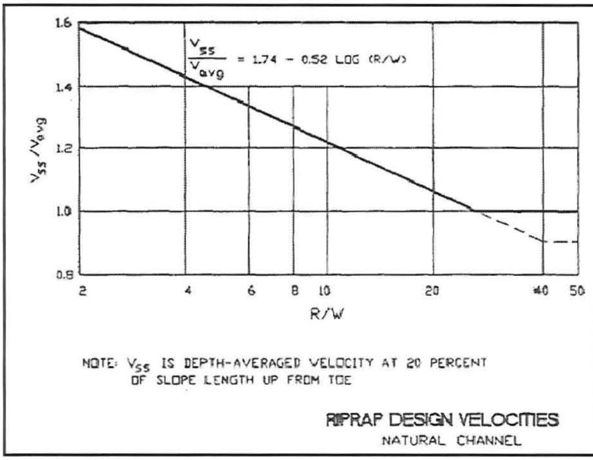

Figure 3. Plate 33, USACE Engineering Manual 1110-2-1601.

Key:
R - Center-line radius of the bend
W - Water Surface width

A two-dimensional hydraulic model will predicts the local velocities in a river more accurately, but this information is not available for ULE Program study areas. Because of this lack of information, the following simplified velocity adjustments will be applied for the ESP.

- For inside river bends, velocity will be reduced by up to 20 percent of the channel mean velocity.
- For outside river bends, velocity will be increased by up to 20 percent of the channel mean velocity.
- For levee reaches with a large overbank area, levee toe velocity will be reduced up to 50 percent of the channel mean velocity or 2 fps, whichever is higher.

Wind Wave Shear and Erosion Surface Adequacy Test

For areas that fail the first-tier test, the computed wave action shear stress will be compared with levee material strength to determine whether the waterside slope is likely to erode.

The statistical probability of a 200-year flood event occurring simultaneously with a maximum wind event is low. For that reason, the wind speed of a 50-year wind event will be used to compute wave height and stress on the levee during a 100-year flood WSE.

Wind-generated wave shear stress will be computed using USACE guidance, such as the Shore Protection Manual and the Coastal Engineering Manual (USACE, 1984, 2002).

Critical shear stress is the bed shear stress (i.e., tractive force caused by the flow of water over the riverbed) at which the grains or aggregates (i.e., bed material) start to move. Table 4 summarizes the critical shear stress for five types of levee material. These critical shear stress values were derived from URS' ESP User Manual which is, in turn, based on experimental field testing reported by Briaud et al. (2001; 2003) and Hanson and Simon (2001).

Table 4. Critical Shear Stress

Levee Material	Critical Shear Stress (psf, or pounds per square foot)
Silt (ML)	0.003
Sand (SP, SM and mixtures)	0.014
Clay (CL, CH, SC, GC)	0.094
Gravel (GP-GW)	1.058
Boulder and Cobbles	4.869

Field Evaluation

For levee sites under consideration in the second tier of ESP, field evaluation will be conducted to verify the levee's current condition and examine the levee for any sign of active erosion. If a geometry evaluation or field evaluation reveal signs of erosion, select field parameters will be collected to perform velocity, wind-wave, and ESP spreadsheet calculations. These parameters will include the levee's geometry, presence or absence of slope protection and vegetation, and slope soil type.

Levee material at each potential erosion site will be compared to the maximum estimated velocity and to wind wave shear stress. Levee material used for comparison will be determined from this field evaluation and recent ULE Program geotechnical boring logs.

ESP Spreadsheet

If a levee erosion site fails any of the second tier tests, the site will be further analyzed by reviewing existing geomorphology studies, if available, and then by applying URS' ESP spreadsheet (URS, 2009). The ESP spreadsheet was customized for this program from an earlier URS Erosion Toolbox, developed for the USACE as part of the Nationwide Levee Risk Assessment Methodology project (URS, 2007).

The ESP spreadsheet is a risk analysis tool for screening-level assessments of levee erosion failure risk. Based on the input parameters of levee geometry, material type, wind-wave and flow velocities, the ESP spreadsheet determines whether a levee can withstand combined erosive forces. Field confirmation will be performed for sites where the ESP spreadsheet indicates a borderline medium or high erosion risk, to confirm the final classification for these sites are correct.

To validate the categorizations provided by the ESP spreadsheet, 50 soil samples were collected throughout the ULE Program study areas; gradation and Atterberg limit tests were performed on the samples. Twelve soil samples were selected for its geographic locations and erosion rate tests were performed for these twelve soil samples using an Erosion Function Apparatus (EFA). These EFA results, along with the conclusions of an independent erosion advisory panel (IEAP, 2009), confirm the applicability of using the ESP spreadsheet and this ESP methodology in ULE Program study areas.

ESP RESULTS

The ESP spreadsheet calculates the total expected erosion of a site, which is the sum of erosion due to wave bottom currents and wave breaking, and the erosion due to current velocity. As discussed earlier, levee sites are ranked using the three-tiered process into one of three levels of erosion risk by comparing total expected erosion with the width of the levee at the pertinent water surface elevations, or a levee effective width. The final risk categories are determined as follows:

- High Erosion Risk. TE/LW > 25%
- Medium Erosion Risk.. 5% < TE/LW < 25%
- Low Erosion Risk. TE/LW < 5%

Detailed ESP and ranking results will be documented and included as a part of each study area's Geotechnical Evaluation Report (GER).

REFERENCES

Ayres Associates, (2007). 2006 Field Reconnaissance Report of Bank Erosion Sites and Site Priority Ranking – Sacramento River Flood Control Levees, Tributaries and Distributaries, Sacramento River Bank Protection Project, USACE. June.

Briaud, J., Chen, H., Li, Y. Li et al. (2003). Complex Pier Scour and Contraction Scour.

Briaud, J., Ting, F., Chen, C. et al. 2001. "Erosion Function Apparatus for Scour Rate Predictions," Journal of Geotechnical and Geoenvironmental Engineering. ASCE, Vol. 127, N. 2, pp. 105-113.

Hanson, G., Simon, A. (2001). "Erodibility of Cohesive Streambeds in the Loess Area of the Midwestern USA," Hydrological Processes. Vol. 15 No 1. pp. 23-38.

IEAP, 2009, An Independent Erosion Advisory Panel was formed in 2009 to provide independent review for the ESP. The IEAP included Jean-Louis Briaud, Tom Smith and Ronald Copeland.

URS. (2007). User's Manual, Erosion Toolbox: Levee Risk Assessment Methodology, USACE Nation Wide Levee Assessment. December.

URS. (2009). User's Manual, Erosion Screening Process Spreadsheet, Urban Levee Geotechnical Evaluation Program. April.

USACE and State of California. 1953. Memorandum of Understanding (MOU), Respecting the Sacramento River Flood Control Project, November 6.

USACE. (1984). Shore Protection Manual (SPM).

USACE. (1989). EM 1110-2-1414, Water Levels and Wave Heights for Coastal Engineering Design.

USACE. (1991). Engineering Manual (EM) 1110-2-1601, Hydraulic Design of Flood Control Channels. July 1, 1991 Version with revisions dated June 30, 1994.

USACE. (2002). EM 1110-2-1100, Coastal Engineering Manual (CEM), Part II. April 30.

USACE. (2002). Sacramento and San Joaquin River Basins, California, Comprehensive Study, Interim Report. December.

Study of Transient Flow Caused by Rapid Filling and Drawdown in Protection Levees

N. P. López-Acosta[1], G. Auvinet[2] and J. L. Lezama[3]

[1,2,3]Instituto de Ingeniería, Coordinación de Geotecnia, Universidad Nacional Autónoma de México, Ciudad Universitaria, Apdo. Postal 70-472, Coyoacan, 04510, D. F., México; PH (52 55) 5623-3500 Ext. 1121; e-mails: [1]nlopeza@iingen.unam.mx, [2]gauvinetg@iingen.unam.mx, [3]jlezamac@iingen.unam.mx

ABSTRACT

The aim of this paper is to study the transient flow caused by rapid filling and drawdown in levees constructed in order to protect urban areas exposed to flooding. In particular, the behavior of typical protection levees constructed in Villahermosa City in Tabasco Mexico affected by intense rainfalls at the end of 2007 is assessed. The analyses are performed by numerical modeling based on finite element method. The emphasis is on the study of time variation of flow velocities and hydraulic gradients in several points of interest within these structures. Results of parametric analyses varying magnitude and velocities of filling or drawdown are also given. Besides, the changing configuration of *saturation* and *desaturation lines* at different times of the transient flow is illustrated. Finally, general conclusions concerning these types of analyses are provided.

INTRODUCTION

The levees built near rivers, lakes and channel slopes are frequently subjected to sudden changes of water level (increments or decrements), which modify flow conditions inside the soil mass. Flow velocities, hydraulic gradients and seepage forces are developed that, in extreme conditions, can cause the total failure of the structure. These phenomena, known as *rapid filling* and *rapid drawdown*, are complex problems in which magnitude and velocity of filling or drawdown, hydraulic conductivity and porosity of materials constituting the levee, and also geometry of slope and initial boundary conditions of flow are involved. Damages and landslides observed in the *Grijalva* River margins in Villahermosa (Tabasco, Mexico) during floods of 2007 are largely attributed to these phenomena. This paper focuses on studying the transient flow, particularly the variation with time of flow velocities and hydraulic gradients which are generated within the levees protecting Villahermosa City against flooding as water levels increase and decrease because of the rain cycles and dams discharge in the region.

TRANSIENT FLOW ANALYSIS

Approach and basic equation

The transient flow in an isotropic and homogeneous soil domain is governed by the following partial differential equation:

$$div\left[k grad\left(h\right)\right]+c\frac{\partial h}{\partial t}=Q \qquad (1)$$

Where k is hydraulic conductivity of soil, h is hydraulic potential (also named hydraulic head), c is specific capacity of soil, t is elapsed time and Q is a discharge quantity corresponding to a possible source within the medium.

Equation (1) combines Darcy's law and continuity of flow. It can easily be generalized to the case of heterogeneous and anisotropic soils. In the case of partially saturated soils, specific capacity depends on porosity and degree of saturation. Deformability of soil skeleton is commonly ignored. At the same time, degree of saturation and permeability depend on local pressure (Van Genuchten 1980).

In the analyses performed in this study it is accepted that initially the water surface in contact with slope is at a certain elevation (lower or higher level) and that because of any natural or artificial cause, it rapidly ascends or descends to a higher or lower level. These oscillations in water level generate a transient flow by rapid filling and drawdown within the levee as illustrated in Figures 1a and b, respectively.

In what follows, it will also be accepted that a steady-state condition initially exists within the levee.

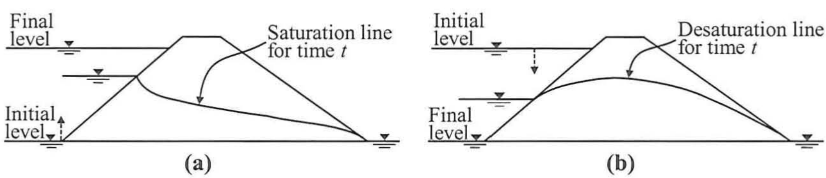

Figure 1. Schematic representation of (a) rapid filling and, (b) rapid drawdown phenomena.

General methods of solution

The methods that can be used for evaluating transient flow conditions due to rapid filling or drawdown phenomenon include:

- Analytical solution of partial differential equations (Alberro 2006).
- Approximate graphical method named *transient flow nets* (Cedergren 1989).
- Numerical techniques such as *finite element method* (e.g. *Plaxflow*, Delft University of Technology 2007), or *finite differences* (e.g. *Flac3D*, ITASCA Consulting Group Inc. 2009).

Numerical methods are the most common. They have been applied by different authors (Freeze 1971; Lam and Fredlund 1984; Lam et al. 1987; Ng and Shi 1998; Auvinet and López-Acosta 2001; Huang and Jia 2009; Auvinet and López-Acosta 2010; among others). The present study focuses on the finite element technique, which is discussed briefly below.

Finite element method (FEM)

Finite element method is a numerical technique which provides approximate solutions of partial differential equations for certain problems. Numerical techniques are preferred with increasing frequency due to their capability for solving complex problems in which equation (1) can be generalized to non homogeneous and/or anisotropic materials (Lam et al. 1987; Auvinet and López-Acosta 2010). In this study the FEM, using the *Plaxflow* algorithm (Delft University of Technology, 2007), is applied to solve transient flow problems by means of the approximate solution of equation (1). This algorithm utilizes the previously mentioned Van Genuchten model to represent flow in unsaturated soils and allows carrying out transient flow analyses in two different ways: (a) *Step-wise conditions* and, (b) *Time-dependent conditions*. This last situation is assumed in this paper. It explicitly considers the continuous time variation of water surface level, which is represented by particular data of water level introduced by tables. The *Plaxflow* algorithm provides hydraulic potential field, flow velocity field, pore pressure, degree of saturation field, among others, as exposed below.

APPLICATION TO A PROTECTION LEVEE

Problems of levees in Villahermosa Tabasco, Mexico

The *Grijalva* basin in Tabasco State Mexico is constituted by a complex system of rivers, which converge mostly in two rivers crossing Villahermosa City: *Carrizal* and *Grijalva* (Auvinet et al. 2008). In order to protect this city and other towns of the state from floods, two types of levees or dikes have been constructed: (a) Protection levees built on the margins of the rivers, and (b) Protection levees built around exposed urban areas (Fig. 2). Flooding in the *Grijalva* watershed occurring in 2007, exhibited the vulnerability of these structures. In many instances, the problems were classified as geotechnical, and they were related to rapid filling and drawdown conditions due to the oscillations of river water levels and to the seepage forces generated by rain infiltration at the crown of the levees. It has been observed (Auvinet et al. 2008) that problems in banks of rivers commonly begin with erosion, which in some parts (depending on the type of soil) is originated by *piping* and can result in landslides (Fig. 3). These eroded sections are generally protected with levees of clay material. Elements more resistant to erosive attack of water of river such as rockfill, *bolsacreto* or *colchacreto* system (concrete bags), breakwaters, sheet pile walls, etc. are also used. The banks of the river or the levees fail when the weight of these structures exceeds the bearing capacity of soil (Fig. 3). Generally, failure occurs in low shear strength strata, such as very compressible clays and peats which are erratically found in the banks of Villahermosa Rivers. It has been also detected that factors such as scour of the river bed, over-elevation of levees or overloading caused by weight of additional protection such as bags of sand, cause instability of levees. In addition, as said above, intense rainfalls in the region originate large and quick variations of the water surface of rivers and lagoons of the area.

(a) Levee on a river bank **(b) Levee in urban areas**

Figure 2. Types of protection levees constructed in Villahermosa, Mexico.

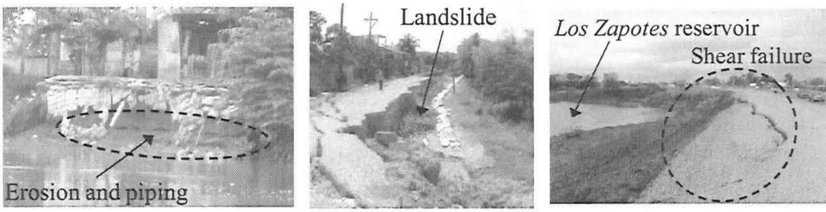

Figure 3. Evidences of instability in river banks and protection levees induced by rapid filling and drawdown.

Modeling of transient flow caused by rapid filling and drawdown

The transient flow caused by rapid filling and drawdown phenomena in a typical protection levee in Villahermosa City is assessed. Analyses are performed by means of the finite element method, using the *Plaxflow* algorithm (Delft University of Technology 2007). Simplified geometry of studied domain including soil foundation of levee is illustrated in Figure 4. The numbers of material layers are shown in the same figure. Properties of these materials are given in Table 1 (Auvinet et al. 2008).

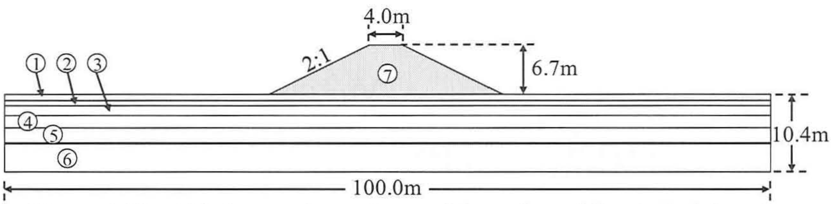

Figure 4. Simplified geometry and material number of the studied domain.

Table 1. Properties of material layers.

N°	Material	Hydraulic conductivity, *k*	Void ratio, *e*
1	Clay sand (SC)	0.0864 m/d (1×10^{-6} m/s)	0.43
2	Sandy clay of low plasticity (CL)	0.0864 m/d (1×10^{-6} m/s)	0.50
3	Organic sandy-clay silt of high plasticity (OH)	0.00864 m/d (1×10^{-7} m/s)	0.90
4	Clay sand (SC)	0.0864 m/d (1×10^{-6} m/s)	0.43
5	Silty sand (SM)	0.0864 m/d (1×10^{-6} m/s)	0.43
6	Organic clay of high plasticity (OH)	0.00864 m/d (1×10^{-7} m/s)	0.90
7	Clay levee	0.00864 m/d (1×10^{-7} m/s)	0.70

Data from the *Gaviotas* pluviometric station were taken into account for analyses of transient flow corresponding to a period of intense rainfalls from October

16 to November 29, 2007 (National Water Commission CONAGUA 2009). Based on these data, boundary conditions assumed for analyses are as follows:

- *For filling*: water surface ascends from initial level of 13.7m up to maximum level of 16.4m, in a period of 17 days (variation is illustrated in Figure 5a).
- *For drawdown*: water surface descends from maximum level of 16.4m up to final level of 11.3m, in a period of 27 days (variation is shown in Figure 5b).

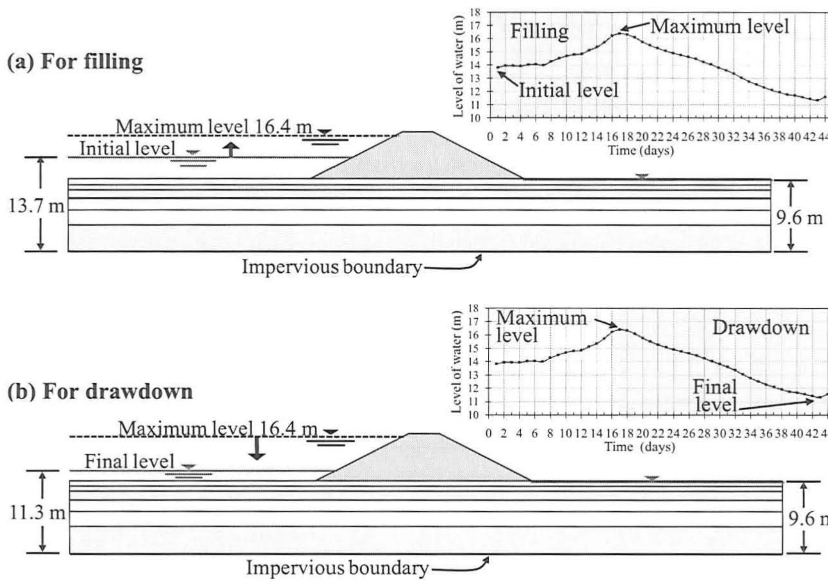

Figure 5. Boundary conditions assumed for analyses.

Results of analyses

Initial steady-state condition

An initial steady-state flow condition with the water level as indicated in Figure 5a is assumed. Results obtained in this case are shown in Figures 6a-d, concerning to pore pressure, hydraulic potential, hydraulic gradient and flow velocities, respectively. The two last figures reveal that highest values of gradient (i_{max}≈1) and velocity (V_{max}=1.2×10^{-2} m/d) occur at the toe of downstream slope of levee. This hydraulic gradient is practically equal to the so-called *critical hydraulic gradient*, i_{cr}, which refers to effective stresses being zero (no contact stress between soil particles), causing in the soil the phenomenon known as *piping*. The critical hydraulic gradient varies between 0.9 and 1.1, with an average close to 1 for most sandy soils (Braja 2004). The prior result shows that the levees built without internal drainage (e.g. lack of a toe drainage blanket) can be affected by erosion due to *piping* in their normal operating conditions.

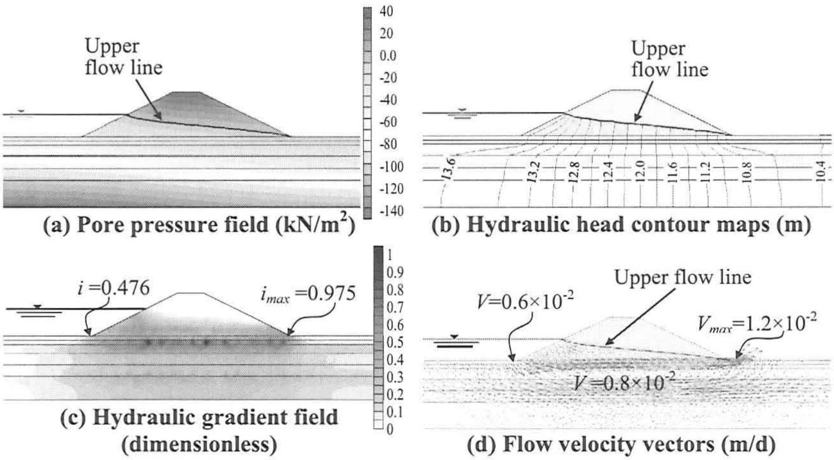

Figure 6. Results for initial steady-state flow condition.

Transient conditions

Figures 7a y b represent degree of saturation in the studied domain for two typical times during rapid filling and drawdown (17 and 44 days, respectively). In these figures can also be observed how the position of the water surface changes within the levee during rapid filling and drawdown. These free surface lines which separate unsaturated material (upper part) from saturated material are named *saturation lines* (for filling) and *desaturation lines* (for drawdown). Other authors prefer to call them *phreatic lines* (Lam and Fredlund 1984; Lam et al. 1987; Huang and Jia 2009). Some of these lines obtained at several times during both rapid filling and drawdown phenomena are illustrated in Figures 8 and 9, respectively. These lines exhibit the following characteristics:

- They are at atmospheric pressure.
- They are neither flow lines nor equipotential lines.
- At those points where they are intersected by equipotential lines, they satisfy the property: h=z (hydraulic head=position).

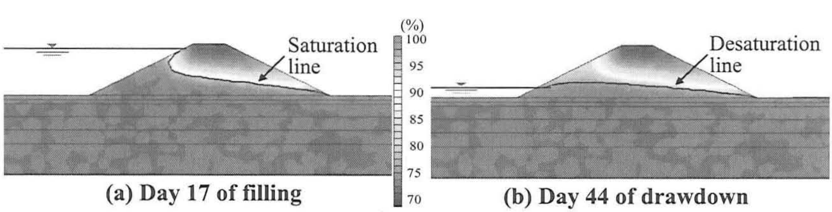

Figure 7. Degree of saturation (%) at different times during the transient flow.

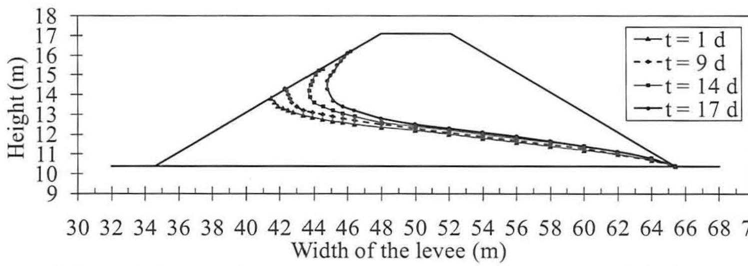

Figure 8. Saturation lines during filling (day 1 to 17, see Fig. 5a).

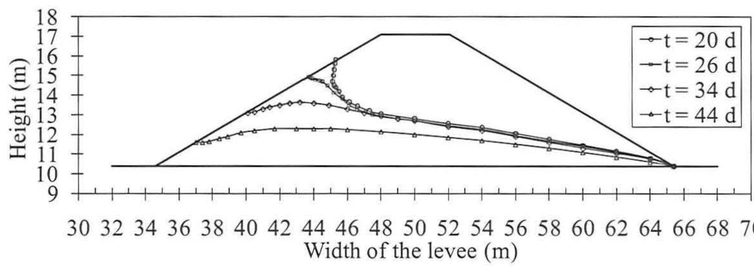

Figure 9. Desaturation lines during drawdown (day 20 to 44, see Fig. 5b).

In the same way, it is interesting to note that during transient flow certain regions of higher hydraulic gradients and flow velocities are generated, as appreciated in Figures 10 and 11, respectively. Predominantly the highest values of hydraulic gradients and velocities take place at the toe of downstream slope of levee. Specifically, the gradient values of those areas greater than the so-called critical gradient (>1) could facilitate *global piping* through the body of levee or through the foundation soil (Figure 10). These above mentioned highest values occur when maximum level of water surface is achieved. Additionally, Figure 11a shows that during rapid filling velocity vectors are directed towards downstream and during rapid drawdown the direction of some of these vectors changes towards upstream (Figure 11b). Particularly, during rapid drawdown it can be observed that velocities and gradients generated near the upstream slope as water level descends are not negligible; in extreme conditions they could facilitate *local erosion* of material in those zones. It should be again pointed out that the *desaturation line* is not rigorously a *flow line* since velocity vectors cross it (Figure 11b). Finally, from Figures 10 and 11, it can also be observed that in general the highest values of flow velocity occur in the more pervious materials of the studied domain. In contrast, the highest values of hydraulic gradient arise in the less pervious materials of this domain. This is a suggestion that instability problems of levees could not be solved by constructing them with more impervious material, but rather building them with more pervious material or even placing drains in strategic areas of the body of levees. Some authors have indeed concluded that soils with a low permeability such as clayey and silty soils are more prone to slope failure than granular materials (Pradel and Raad 1993).

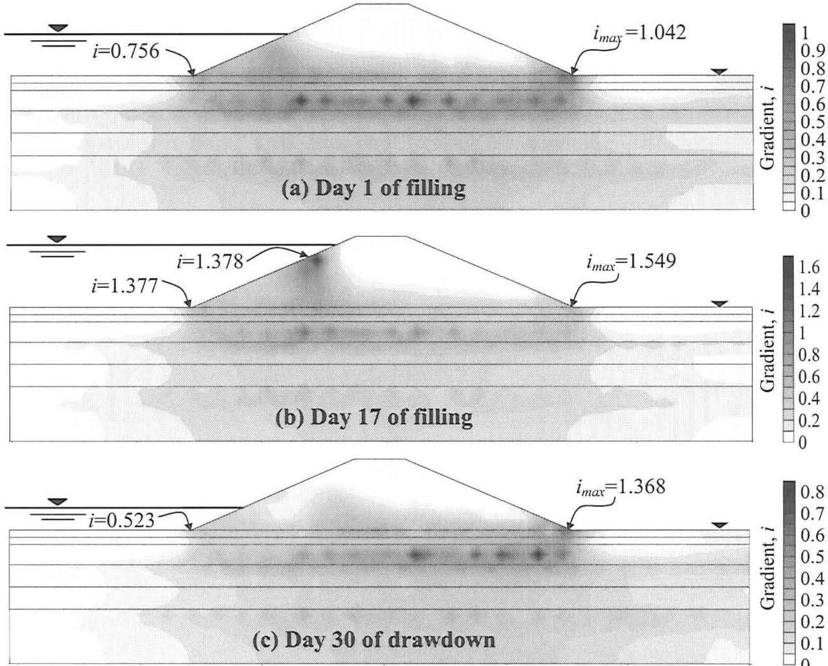

Figure 10. Hydraulic gradients (magnitude) for three different times during rapid filling and drawdown.

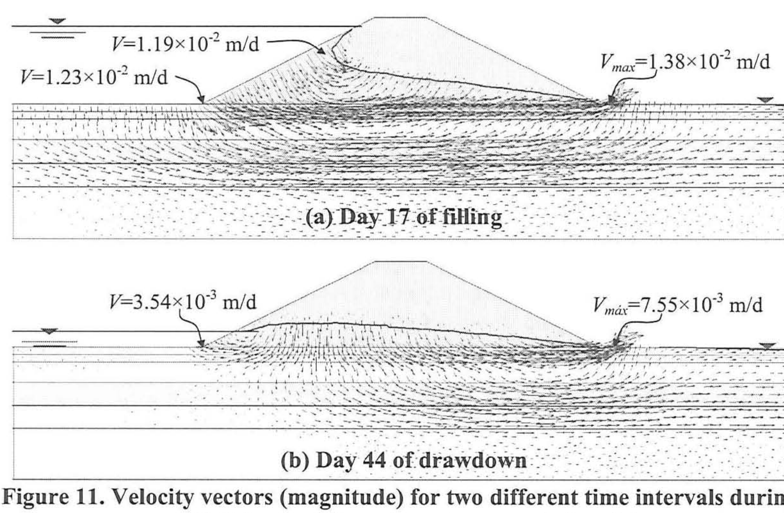

Figure 11. Velocity vectors (magnitude) for two different time intervals during rapid filling and drawdown (exaggerated scale).

In addition, parametric calculations were carried out varying filling and drawdown rate of original data from the *Gaviotas* pluviometric station (National Water Commission CONAGUA 2009). The summary of these results is provided in Figures 12 and 13. These figures lead to the following comments: (a) for higher filling rate, the maximum values of flow velocities occur at the toe of upstream slope of levee (Fig. 12); (b) in contrast, for lower filling rate, the maximum values of flow velocities occur at the toe of downstream slope of levee (Fig. 13).

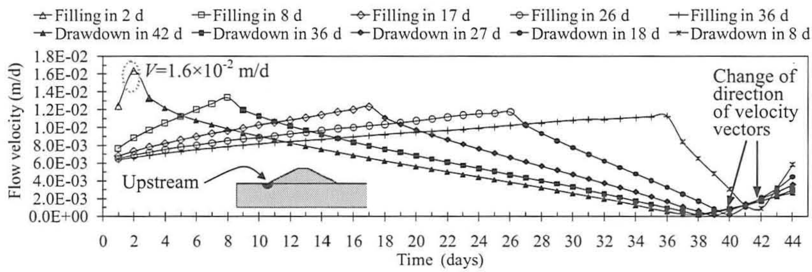

Figure 12. Flow velocity as a function of time for different filling and drawdown rates (at the toe of upstream slope of levee).

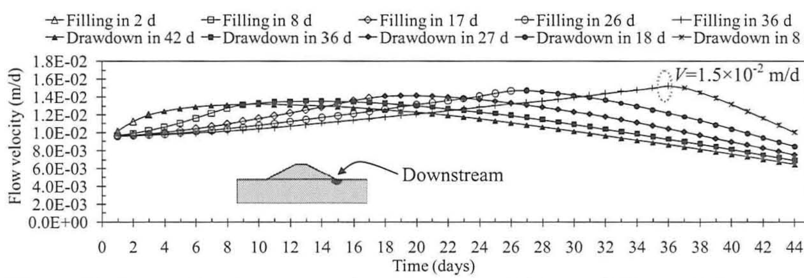

Figure 13. Flow velocity as a function of time for different filling and drawdown rates (at the toe of downstream slope of levee).

CONCLUSIONS

The transient flow caused by rapid filling and drawdown in typical levees of Villahermosa City in Tabasco Mexico, constructed to protect the population against flooding, was studied. Analyses were performed by numerical modeling using finite element method. Data from intense rainfalls occurred at the end of 2007 were considered in calculations. From results of analyses, some general conclusions can be drawn: (a) in both rapid filling and drawdown conditions, the highest values of flow velocities and hydraulic gradients occur at the toe of downstream slope of levee. The hydraulic gradient values of those areas greater than the so-called *critical gradient* could facilitate *global piping* through the body of levee or through the foundation soil; (b) during drawdown the flow velocities and hydraulic gradients generated near the upstream slope as water level descends are not negligible; in extreme conditions (e.g. steady intense rain for some time), they could facilitate *local erosion* of material in those areas and jeopardize slope stability. Currently, stability of slopes in this type of levees subjected to unsaturated transient flow considering the suggestions of recent researches (Griffiths 1994; Huang and Jia 2009) is also being assessed.

REFERENCES

Alberro, J. (2006). "Effect of transient flows on the behavior of earth structures." *8th Nabor Carrillo Lecture*, Mexican Society of Geotechnical Engineering SMIG, Tuxtla Gutierrez, Chiapas Mexico (in Spanish).

Auvinet, G. and López-Acosta, N. P. (2001). "Uncertainty in analyses of rapid drawdown of reservoirs." *Proc. 15th Intl. Conference on Soil Mechanics and Geotech. Engrg.*, Istanbul Turkey: 1065(6).

Auvinet, G., López-Acosta, N.P. and Pineda, A. R. (2008). "Final report of Integral Hydraulic Project of Tabasco (PHIT)." *Research Report of Geotech. Department*, Institute of Engineering UNAM, Mexico (in Spanish).

Auvinet, G. and López-Acosta, N.P. (2010). "Rapid drawdown condition in immersed slopes." *Special Publication Tribute to Ing. Jesús Alberro Aramburu*, Edited by Institute of Engineering UNAM and SMIG, Mexico: 167-189 (in Spanish).

Braja, M. D. (2004). "Principles of foundation engineering." 5^{th} ed., Cengage Learning Brooks Cole.

Cedergren, H. R. (1989). "Seepage, drainage and flow nets." 3^{rd} ed., John Wiley and Sons, New York, N. Y.

Flac3D V4.0 (2009). Option Dynamic. ITASCA International Inc. USA.

Freeze, R. A. (1971). "Influence of the unsaturated flow domain on seepage through earth dams." *Water Resour. Res.* 7(4): 929-941.

Griffiths, D.V. and Lane, P.A. (1999). "Slope stability analysis by finite elements." *Géotechnique* 49(3): 387-403.

Huang, M. and Jia C-Q. (2009). "Strength reduction FEM in stability analysis of soil slopes subjected to transient unsaturated seepage." *Computers and Geotechnics* 36: 93-101.

Lam, L. and Fredlund, D.G. (1984). "Saturated-unsaturated transient finite element seepage model for geotechnical engineering." *Adv Water Resources* 7: 132-136.

Lam, L., Fredlund, D.G. and Barbour, S. L. (1987). "Transient seepage model for saturated-unsaturated soil systems: a geotechnical engineering approach." *Canadian Geotech. J.* 24: 565-580.

National Water Commission, CONAGUA. (2009). http://www.conagua.gob.mx/ (accessed July 7, 2009).

Ng, C. W. W. and Shi, Q. (1998). "A numerical investigation of the stability of unsaturated soil slopes subjected to transient seepage." *Computers and Geotechnics* 22(1): 1-28.

Plaxflow Version 1.6 (2007). "Scientific Manual", Edited by R.B.J. Brinkgreve, Delft University of Technology and Plaxis, The Netherlands.

Pradel, D. and Raad, G. (1993). "Effect of permeability on surficial stability of homogeneous slopes." *J. Geotech. Engng*, ASCE, 119(2): 315-332.

Van Genuchten M. Th. (1980). "A closed form equation for predicting the hydraulic conductivity of unsaturated soils." *J. Soil Sci. Soc. Am.* 44(5): 892-898.

Simulating Levee Erosion with Physical Modeling Validation

Jared A. Gross, A.M.ASCE[1]; Christopher S. Stuetzle[2]; Zhongxian Chen[3]; Barbara Cutler[4]; W. Randolph Franklin[5]; and Thomas F. Zimmie, P.E., M.ASCE[6]

[1] Graduate Research Assistant, Dept. of Civil & Environmental Engineering, Rensselaer Polytechnic Institute, 110 8th Street, Troy, NY 12180. E-mail: grossj3@rpi.edu
[2] Ph.D. Candidate, Computer Science Dept., Rensselaer Polytechnic Institute, 110 8th Street, Troy, NY 12180. E-mail: stuetc@cs.rpi.edu
[3] Ph.D. Candidate, Computer Science Dept., Rensselaer Polytechnic Institute, 110 8th Street, Troy, NY 12180. E-mail: chenz5@rpi.edu
[4] Assistant Professor, Computer Science Dept., Rensselaer Polytechnic Institute, 110 8th Street, Troy, NY 12180. E-mail: cutler@cs.rpi.edu
[5] Professor, Electrical, Computer, and Systems Engineering Dept., Rensselaer Polytechnic Institute, 110 8th Street, Troy, NY 12180. E-mail: frankwr@rpi.edu
[6] Professor, Dept. of Civil & Environmental Engineering, Rensselaer Polytechnic Institute, 110 8th Street, Troy, NY 12180. E-mail: zimmit@rpi.edu

ABSTRACT: This paper studies rill and gully initiation and propagation on levees, dams, and general earth embankments. It specifically studies where these erosion features occur, and how long a particular embankment can sustain overtopping before breaching and catastrophic failure. This contrasts to previous levee erosion analysis, which has primarily concerned the final effects of erosion, such as soil loss, depth of scour and breach width. This paper describes the construction of scaled-down physical models of levees composed of different homogeneous sands, as well as sand-clay mixtures, and their laboratory testing. A 3-D laser range scanner captured the surface features of the physical model, before and after erosion. The resulting data is utilized in developing digital simulations of the rill erosion process. Those simulations combine 3-D Navier-Stokes fluid simulations and a segmented height field data structure to produce an accurate portrayal of the erosive processes, which will be validated by physical modeling.

INTRODUCTION

Levee failures that have occurred as a result of storm surges and flooding events have been primarily due to overtopping, although failure from seepage is also a possible failure mechanism. In either instance, the erosive processes can eventually lead to breaching of the levee and catastrophic damage on the adjacent floodplain. There have been many cases of earth embankment failures, for example, Hurricane Katrina in 2005, where breaching occurred and devastated the surrounding population. Levee failures are preventable, and a better understanding of the ways in which these embankments are designed and fail, so as protect against future failures, is a goal of this research.

The erosion processes described in this paper refer to hydraulic erosion. Small-scale erosion on earthen embankments is being studied, modeled and eventually simulated, with respect to the formation of rills and gullies. Validation of the simulation is a primary focus in this research, so scaled-down model levees are used to perform erosion experiments at 1 *g* and later at higher levels of *g* in a geotechnical centrifuge.

The results of experiments to date, are presented in this paper. Completed testing has been performed at 1 *g* using a homogeneous laboratory sand and Nevada sand – kaolin clay mixes. The physical models serve as the basis for developing accurate, digital simulations of the embankment erosion processes. Eventually, different types of soils and soil mixtures will be tested and complex geometries and boundary conditions utilized to quantitatively assess the effects of differing conditions.

RELATED RESEARCH

There is a considerable amount of information pertaining to erosion on earth structures such as levees, dams and embankments both from a civil engineering as well as a computer graphics perspective. Current research on the topic of erosion in the field of civil engineering is primarily associated with developing models that predict final erosive measures (i.e. scour depth, final breach width, total soil loss, etc.). In the computer graphics field, multiple attempts have been made to simulate hydraulic erosion, chiefly to generate realistic-looking terrain and surface deformation animations as a result of fluid flow. While the research in both fields is beneficial and relevant, neither model the erosion, sediment transport or deposition processes with real physical accuracy capable of predicting the extent of erosion or possible water inundation as a result of breaching.

Erodibility

The erodibility of a soil relates the velocity of the water flowing over the soil to the corresponding erosion rate experienced by the soil. A soil's erodibility was defined as a way to describe the behavior of a soil under erosion conditions. Wan and Fell (2004) describe the development of two erosion rate tests, the Hole Erosion Test (HET) and Soil Erosion Test (SET), which measure a soil's erodibility. Using an Erosion Function Apparatus (EFA), Briaud and his colleagues investigated the erodibility of several different types of soil. The soils were classified into different categories of erodibility based on degree of compaction, erosion rate, water velocity and hydraulic shear stress (Briaud, et al. 2008). Xu and Zhang (2009) found that in addition to soil type, the degree of compaction plays an important role in erodibility on embankments. The erosion resistance increases with compaction effort, particularly with fine soils.

Briaud et al. (2008) deviate slightly from the broad definition of soil erodibility in order to produce a more technically correct definition of the parameter. Since the velocity of the water at the soil-water interface is zero, yet soil is still eroded, soil erodibility is actually based on the hydraulic shear stress. The shear stress changes with water velocity so that it can be defined along the soil-water boundary, incorporating the soil features as well as the water properties along the flow field. This model is ideal for small scale erosion simulation, as it allows for a parameter to be applied to the soil as a field over the entire embankment.

Rill Initiation

Multiple factors influence erosion on an embankment including embankment configuration, flow velocity, slope discontinuities, presence of tailwater, and flow concentration at low points (Powledge, et al. 1989). These factors, if present, can impact the formation of rills and gullies on a slope, as well as the shape and speed in which the rill or gully propagates. On a slope, the overland flow first arrives as "sheet" erosion, then causes rill erosion with increasing flux (An and Liu 2009). Bryan and Rockwell (1998) studied agricultural sites near Toronto, Canada and found that significant rill incision typically occurred in early spring, immediately following snowmelt. This relates to the study of levees or earth dams that are adjacent to water bodies. They are saturated or can become nearly saturated rapidly, thereby creating rill initiation conditions.

Rills and gullies will form in areas of depression, or in areas where the soil does not have enough cohesion or shear strength to resist the hydraulic stresses from the flowing water. Factors affecting rill characteristics include the stress caused by the flow, roughness of the soil surface, slope gradient and soil erodibility (Mancilla, et al 2005). It was concluded that the most critical determinant of rill development is not threshold hydraulic conditions associated with intense runoff on steep slopes, or areas of depression, but impermeable subsoils that allow surface soils to become saturated (Bryan and Rockwell 1998).

Rill Propagation

After a rill has been initiated in an embankment slope, the initial rill will transport the majority of water and sediment. Occasional tributary rills may form temporarily that supply the main rill with water and sediment, but will taper off as the erosion process continues in the initial main rill (Mancilla, et al 2005). Erodibility within a rill may vary with depth, which can decrease the erosion process in granular soils, as a result of a reduced slope gradient. If a more erodible soil underlies the surface soil, however, the erosion rate in a rill or gully will actually be accelerated (Govers, et al. 2007).

Briaud et al. (2008) performed several tests that indicated that the rill erosion occurs first on the land side of the overtopped levee and progressively recedes, leading to eventual breaching. The quantity of soil eroded rapidly increases with the slope gradient, then decreases suggesting a critical slope gradient. If the slope of an embankment has not exceeded the critical gradient, interrill erosion occurs and transports sediment between rills or gullies. The majority of sediment carried by interrill erosion concentrates around rill heads, leading to an increased erosion rate and wider rill width in that area of the rill. Although the incidence of interrill erosion is larger than that of rill erosion, rill erosion is the dominant process on embankment slopes because it is significantly more intense (An and Liu 2009).

Performance Differences Amongst Various Soils

Post Hurricane Katrina field surveys showed that in general, rolled compacted clay fill levees performed well with minor erosion occurring when overtopped, whereas hydraulic filled levees with significant amounts of silt and sand performed poorly. Using good clayey material often required long haul distances that slowed construction progress. So nearby granular material was used instead (Sills, et al. 2008). In cohesive embankments, breaching occurs as a result of headcutting, whereas in granular embankments, surface slips occur rapidly due to seepage on the downstream slope (Xu and Zhang 2009).

Threshold hydraulic stress values tend to be higher on freely drained material. After formation of the water table, however, this value drops, thereby making freely draining granular soil much more erodible (Bryan and Rockwell 1998). Dealing with waste embankments, research by Thornton and Abt (2009) showed that lower clay contents correlated with greater potential susceptibility to the gully erosive process.

Cohesive soils are more resistant to erosion due to high clay content. However, care must be taken when specifying and inspecting the type of clay used. Dispersive clays are an exception because the clay particles spontaneously detach from one another under saturated conditions (Torres 2008). Rockfill and clay embankments are considered to have medium to low erodibility, while silt and sand are considered to have high to medium erodibility according to Briaud's erodibility classification (Xu and Zhang 2009).

Physically-Based Erosion Simulation

Hydraulic erosion has been accepted as the single most important process in the shaping and development of terrain. Because of this, hydraulic erosion research in computer graphics has focused mainly on terrain generation and animation. The height field erosion simulation performed by Musgrave et al. (1989) and the sedimentation process in the work by Chiba et al. (1998) are examples of terrain generation in computer graphics. In each example, an erosion process is simulated on a terrain to morph and mold it to be more realistic-looking.

Erosion simulations require efficient algorithms that can be run on dynamic data structures in order to capture the small-scale complexity of the process. There are three primary data structures that are often used for erosion simulation: height fields, voxel grids, and layered height fields. Stuetzle, et al. (2010) presented an extension to the layered height field, called a Segmented Height Field (SHF).

Although much work has been done to simulate erosion, very little of it has presented validation of results. Validation of our computer simulation by laboratory experimentation is a primary objective of this research. To our knowledge, validation of computer simulations has not yet been accomplished, though it has been attempted with some success by the Soil Degradation Assessment (SoDA) project (Valette et al. 2006).

PROCEDURES

Physical Modeling

Initial overtopping tests were conducted on a half-levee model within an open aluminum box of dimensions 0.356m x 0.61m x 0.914m (14" x 24" x 36"). A piece of plywood, 0.013m (½") in thickness, was cut to the dimensions 0.152m x 0.61m (6" x 24") and sealed in the aluminum box using silicone, which partitioned the space within the box into two distinct zones. The smaller zone measured 0.152m x 0.61m x 0.216m (6" x 24" x 8 ½") and was used as a reservoir for the water to rise in and eventually overtop the model levee, which was constructed in the second, larger zone using a moist, medium-well graded laboratory sand having a dry unit weight of 100 pcf and an internal friction angle, $\varphi = 39.6°$.

Constructed in lifts and compacted using a 0.102m x 0.102m (4" x 4") wooden hand tamp, a level base layer 0.076m (3") thick was placed first, followed by the half-levee with a 0.127m (5") wide crown and 5H:1V slope. This slope inclination as per the U.S. Army Corps of Engineers (USACE) Levee Design Manual to prevent damage from seepage exiting the slope on the land side for sand levees (USACE 2000). The elevation of the crown was 0.152m (6"), the same as the elevation of the plywood partition. The final configuration of the model levee in the box left a 0.127m x 0.61m (5" x 24") area, in plan, at the toe of the levee slope that acted as a floodplain. Figure 1 shows the physical experiment setup. A small aquarium pump was placed 0.013m (½") above the floodplain at the farthest point downstream in the box to pump out flood water and allow the overtopping to continue for a longer duration. In both (a) and (b), the water source is located on the left side of the box, and the pump to remove excess flood water is represented as the black object on the right side of the box.

Overtopping tests were also conducted on a full-levee model in the same aluminum box described above, using the same laboratory sand as well as sand-clay mixes. The sand-clay mixes had a dry unit weight of 96 pcf. The 0.152m x 0.61m (6" x 24") plywood was replaced with a 0.076m x 0.61m (3" x 24") piece of plywood that was sealed in the box with silicone, partitioning the box into halves for the laboratory sand testing only. A core was not used during the sand-clay mixture tests, as the levee slopes were flat enough and the soil had sufficient cohesion to prevent seepage failures. The role of the plywood in this setup was to serve as a low-permeability core for the levee. A base layer 0.038m (1 ½") thick was constructed in lifts and compacted with the hand tamp on each side of the partition. The full-levee was constructed with a 0.203 m (8") wide crown and 5H:1V slopes, so that the elevation of the crown was 0.013m (½") above the elevation of the plywood core, allowing for some breaching to occur. The pump was placed at the most downstream point, 0.013m (½") above the floodplain, and water was allowed to overtop the levee for tests with flow rates

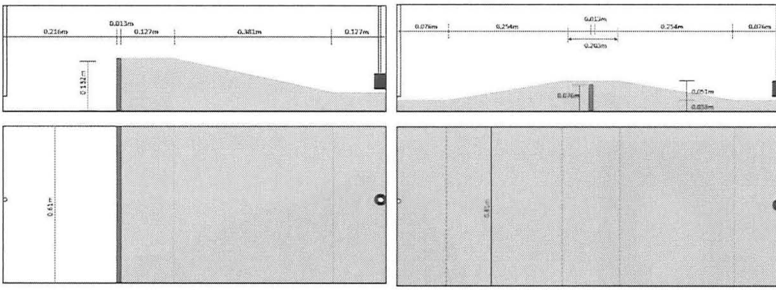

(a) (b)

Figure 1. Schematic view of both the initial (a) and current (b) experimental test setup. The upper images are section views, while the lower images are the setup in plan.

ranging from 0.0063 L/sec to tests with flow rates of 0.040 L/sec. The majority of tests conducted have used a constant flow rate between 0.010 L/sec and 0.015 L/sec, however, more extreme cases (very slow flow rate and very rapid flow rate) were investigated to observe the influence of flow rate. In each test, evidence of rill erosion was carefully monitored.

Data Collection

3-D scans were taken before erosion simulation began and immediately following erosion of the levee model. Each scan represented a different terrain elevation of the levee. The scans were taken using a 3-D laser range scanner (Fig. 2a), which provided a point cloud (Fig. 3c and 3d) with color information for each data point. This data was then processed to ready it for adaptation to the Segmented Height Field (SHF). To minimize holes in the data from occlusion, two scans were made of each elevation and registered using keypoints on the rigid aluminum box (Smith, et al. 2008). Once each scan for a single elevation was aligned to the same coordinate system, points were then discretized by superimposing a 2-D horizontal grid over the point cloud and snapping each point to its nearest grid space. The data in each grid space was then averaged to create a single height value per grid space, creating a height field. Grid cells not assigned a height value from the scan are interpolated using ODETLAP (Stookey, et al. 2008). This procedure was repeated for each layer, and used to create a single SHF from the layers of height fields, shown in Figure 2.

The renderings in Figures 2b, 3c and 3d were created using the program *Mathematica* and are colored according to elevation. The relatively equal spacing of the elevation contours in Figure 3c compared to the displaced and irregular elevation contours in Figure 3d illustrate the movement of sediment and the presence of a rill on the slope after water had overtopped the model levee. A slight curve in the elevation contours in Figure 3c is seen on the landside slope. The rill formed in that area where the elevation changed slightly, as expected according to previously published findings. Figures 2b and 3d show the rill regression on the levee crown stopping half way across the crown. The receding channel stops at this location because the plywood core had been reached from displacement of sediment and illustrates the effectiveness of a core in at least slowing down the process of a full breach occurring.

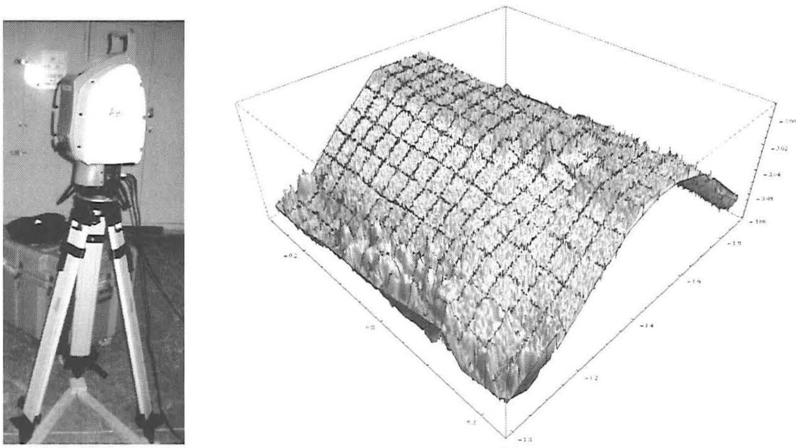

(a) (b)

Figure 2. (a) 3-D laser range scanner (b) 3-D rendering of a post-erosion simulation using laboratory sand scan data.

Interpolation and Visualization

In order to perform an erosion simulation, a surface must be extracted from the data structure. To do this, the data is converted into a tetrahedral mesh, allowing surface information to be extracted, such as slope, as well as generate surface normals for visualization. These not only improve the quality of the resulting visualization, but also yield more accurate physical simulations by allowing water to flow smoothly down the levee's slopes and through channels cut within the soil.

RESULTS

Half-Levee Setup

Water began to overtop the reservoir and flow through the soil (groundwater, seepage, etc.), thereby saturating the soil, and slowly flowed over the crown of the embankment on the surface. Surface tension was evident, as the water on the surface of the crown had boundaries (i.e. the water did not come over the top in one big sheet of water). Once the water had crossed the crown on the surface, rill initiation at the top of the embankment was observed, beginning at the crest of the slope (the intersection of the crown edge and edge of the slope) and eroding its way to the toe of the slope. This formed the primary rill on the slope and the time required for this rill to form was defined as "T_{rill}". Secondary, or tributary, rills formed and contributed to the main rill, but the water tended to continue to erode the initial rill, rather than form a new main rill. Once rilling had begun on the slope, the water began eroding a channel that receded across the crown from the crest of the slope towards the plywood. The rill on the slope went one direction and the channel on the crown went in the opposite direction, but in line with the rill on the embankment slope.

Recorded times for rill initiation to occur on the levee slope for this setup are shown in Table 1. For this setup, the levee slope was 0.389m (15.3") in length. The data for this setup yielded unique results. It was the expectation that a high flow rate would erode the slope more rapidly. This relationship may be true for embankments that are already saturated, however, in this setup the plywood divider prevented the model from becoming saturated until overtopping began. So, as water was flowing on the surface, the model was also in the process of becoming saturated. The water at higher flow rates moved more rapidly over the surface of the soil than through the soil, essentially eroding less erodible unsaturated sand and producing larger values of T_{rill}. Because the water at lower flow rates did not move significantly faster over the soil surface compared to flowing through the soil, the model was able to become saturated and more erodible before the rilling process began and yielded smaller values of T_{rill}.

Table 1. Rill initiation times for the half-levee model.

Test No.	Flow Rate, Q, (mL/sec)	T_{rill} (sec)
HL – 01	25	55
HL – 02	12.5	12
HL – 03	11.1	16

Full-Levee Setup – Laboratory Sand

In addition to water eroding a channel on the slope, the rill process also involves the location of a specific area on the slope due to geometric or compositional variations, unique to each embankment. To ensure the experiments accurately simulated rill erosion processes, a full-levee model was constructed with a plywood core, so that the geometry of the wood would not be the determinant in the location of rill formation. The results of this setup are shown in Figure 3.

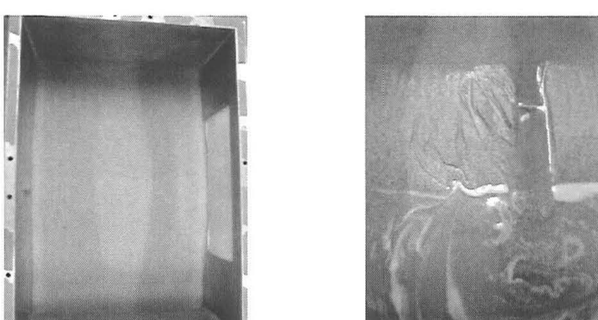

(a) (b)

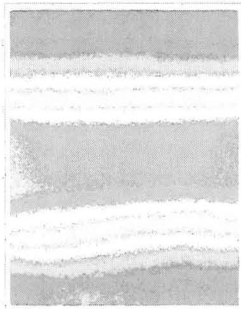

(c)

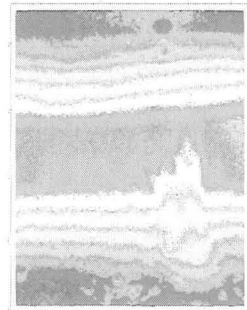

(d)

Figure 3. Laboratory testing: (a) current experimental setup (b) primary rill and tributary rills (c) visualization of the experimental setup using 3-D point cloud data (d) visualization of the setup post-erosion simulation using 3-D point cloud data.

Water was supplied to one side of the levee and the water level was allowed to slowly rise until overtopping began. The full-levee model also offered the benefit of more realistic saturation conditions, as the water could flow through the sand to the floodplain side of the levee. Once the water had crossed the levee crown, rill initiation began, at a location influenced by the levee itself, and a channel was eroded on the slope, as well as across the levee crown. Additionally, the use of a full-levee model allowed for a more complete rilling process, as the channel that receded across the levee crown had the opportunity to reach the water-side slope, thereby breaching the levee.

Recorded times for rill initiation and times for the water to cross the 0.203m (8") levee crown, as well as initial (w_i) and final (w_f) moisture contents of the levee soil are provided in Table 2. For this setup, each levee slope was 0.259m (10.2") in length.

Table 2. Rill initiation times for full-levee model.

Test No.	Flow Rate, Q, (mL/sec)	$T_{cross\ crown}$ (sec)	T_{rill} (sec)	w_i (%)	w_f (%)
FL – 01	12	44	15	N/A	N/A
FL – 02	7.41	69	14	7.72	N/A
FL – 03	6.25	86	21	N/A	N/A
FL – 04	14.29	38	40	8.01	24.79
FL – 05	11.1	12	16	9.13	23.62
FL – 06	40	40	22	9.78	23.33
FL – 07	9.1	154	27	14.58	23.66
FL – 08	11.1	114	29	10.45	22.60

Full-Levee Setup – Nevada Sand – Kaolin Clay Mix

The full-levee testing of the sand-clay mix followed the same procedure as the full-levee testing with the laboratory sand. However, the preparation of the model varied slightly. The sand-clay levee model did not incorporate a low-permeability core of any kind during the testing. The Nevada sand and kaolin clay also were carefully measured in predetermined proportions based on the sand versus clay content (100-0, 90-10, 85-15) for the particular experiment. Specific volumes of water were measured in order to be mixed thoroughly in the mixer at the desired initial moisture content of 7.5%.

The observed macroscopic erosion processes in the sand-clay mixes were very similar to the erosion processes observed in the laboratory sand experiments. The water began to saturate the soil while the water level rose on the waterside of the levee, then progressed over the crown of the levee and eventually formed a rill on the landside slope and began to recede across the crown, as in the sand experiments. The microscopic erosion processes showed larger clumps of soil (approximately 1.59mm ($^1/_{16}$") to 3.18mm ($^1/_8$") in diameter) being removed from the levee crown and a type of undercutting taking place, resulting in a faster breach time. The breach time was defined as the time from the beginning of the rill initiation to the time when a channel had completely receded length of the levee's crown. Figure 4 shows the time required for the initial rill ("T_rill") to form on the landside slope of the levee and for full breaching ("T_breach") to occur as a function of kaolin clay content.

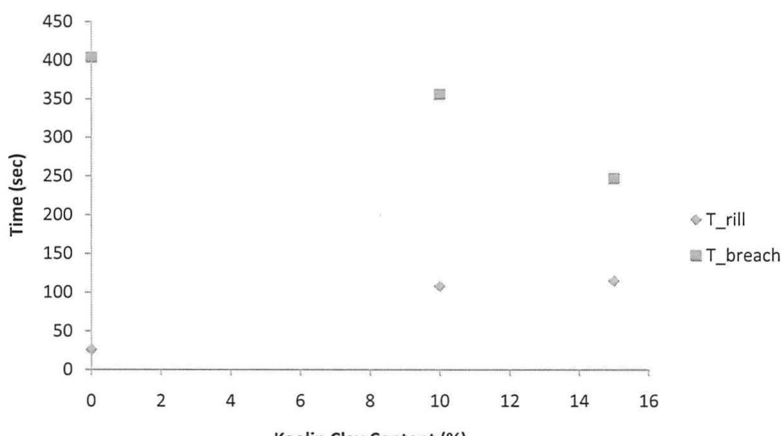

Figure 4. Time required for the initial rill and for full breaching to occur in sand-clay levees.

As depicted in Figure 4, the faster breach times occur with increasing clay content of the levee and increased size of sediment being eroded from the levee's crown. Conceptually, the data shown in Figure 4 seem counterintuitive as increasingly cohesive levees should require more time for erosion to occur, due to the lower permeability of the material. Physically, the data shown are reasonable if the sediment clumping is considered. Larger and therefore heavier particles were removed from the levee when the rilling process commenced. The flowing water could not carry the mass and deposited the clump of soil farther up on the levee slope, so the clumps of soil accumulated at the leading end of the rill thereby creating a large amount of soil to be eroded down the slope and resulting in longer initial rill formation times. As the channel receded across the levee crown, large clumps of soil were eroded and carried a short distance while suspended in the water before reaching the bottom of the channel when rolling could occur. Because the direction of the erosion occurring on the levee's crown is opposite the direction of flow, deposition of sediment did not impede the erosion process, resulting in more rapid breach times as clay content, and clump size, increased Also, because the water travels at a greater velocity on the surface than through the clayey levee, more surface erosion is observed in a shorter period of time. Further testing is required to determine if this trend will continue as the levee becomes dominated by clayey soils.

CONCLUSIONS AND FUTURE CONSIDERATIONS

The model levees eroded more rapidly when fully or nearly fully saturated. A low-permeability core in the center of a levee prevented failure from seepage, and extended the time required for a full breach of the model to occur. A critical clay content in the levees composed of sand-clay mixtures existed at approximately 15-20% kaolin clay content. A requirement for a core at the center of the levee could be imposed for soils of this composition.

The physical modeling capabilities allow for layered models, such as the inclusion of soil cores, and complex geometries with different crown widths and slope inclinations. Using a geotechnical centrifuge, erosion tests will be performed that will allow simulation and understanding of structures that will be subjected to stresses and forces encountered in earth embankments in the field. Measurement of flow velocity and hydraulic shear stress will be incorporated in future testing. Change detection software will be utilized to gather and process data for multiple layers of soil, allowing for simulation of more complex soil models in the software.

REFERENCES

An, Y., and Liu, Q. Q. (2009). "Two-Dimensional Hillslope Scale Soil Erosion Model." *Journal of Hydrologic Engineering*, 14(7), 690-697.

Briaud, J.-L., Chen, H.-C., Govindasamy, A. V., and Storesund, R. (2008). "Levee Erosion by Overtopping in New Orleans during the Hurricane Katrina." *Journal of Geotechnical and Geoenvironmental Engineering*, 134(5), 618-632.

Bryan, R. B., and Rockwell, D. L. (1998). "Water Table Control on Rill Initiation and Implications for Erosional Response." *Geomorphology*, 23, 151-169.

Chiba, N., Muraoka, K., and Fujita, K. (1998). "An Erosion Model Based on Velocity Fields for the Visual Simulation of Mountain Scenery." *The Journal of Visualization and Computer Animation*, 9(4), 185–194.

Govers, G., Gimenez, R., and Van Oost, K. (2007). "Rill Erosion: Exploring the Relationship Between Experiments, Modelling and Field Observations." *Earth-Science Reviews*, 84, 87-102.

Mancilla, G. A., Chen, S., and McCool, D. K. (2005). "Rill Density Prediction and Flow Velocity Distributions on Agricultural Areas in the Pacific Northwest." *Soil & Tillage Research*, 84, 54-66.

Musgrave, F. K., Kolb, C. E., and Mace, R. S. (1989).. "The Synthesis and Rendering of Eroded Fractal Terrains." *The Proceedings of the 16th Annual Conference on Computer Graphics and Interactive Techniques*. 41–50.

Powledge, G. R., Ralston, D. C., Miller, P., Chen, Y. H., Clopper, P. E., and Temple, D. M. (1989). "Mechanics of Overflow Erosion on Embankments. II: Hydraulic and Design Considerations." *Journal of Hydraulic Engineering*, 115(8), 1056-1075.

Sills, G. L., Vroman, N. D., Wahl, R. E., and Shwanz, N. T. (2008). "Overview of New Orleans Levee Failures: Lessons Learned and Their Impact on National Levee Design and Assessment." *Journal of Geotechnical and Geoenvironmental Engineering*, 134(5), 556-565.

Smith, E. R., King, B. J., Stewart, C. V., and Radke, R. J. (2008). "Registration of Combined Range-Intensity Scans: Initialization Through Verification." *Computer Vision and Image Understanding*, 110(2), 226-244.

Stookey, J., Xie, Z., Cutler, B., Franklin, W. R., Tracy, D., and Andrade, M. V. A. (2008). "Parallel ODETLAP for Terrain Compression and Reconstruction." *Proc., The 16th ACM SIGSPATIAL International Conference on Advances in Geographic Information Systems*, Nov. 5-7, 2008, Irvine, CA.

Stuetzle, C. S., Chen, Z., Cutler, B., Franklin, W. R., Gross, J., Perez, K., and Zimmie, T. (2010). "Computer Simulations and Physical Modelling of Erosion." To Appear In: *Proc., The 7th International Conference on Physical Modelling in Geotechnics*, June 28-30, 2010, Zurich, Switzerland.

Thornton, C. I., and Abt, S. R. (2008). "Gully Intrusion into Reclaimed Slopes: Long-Term Time-Averaged Calculation Procedure." *Journal of Energy Engineering*, 134(1), 15-23.

Torres, R. L. (2008) "Considerations for Detection of Internal Erosion in Embankment Dams." *Proc., Biennial Geotechnical Seminar Conference*. ASCE, 2008. 82-98.

U.S. Army Corps of Engineers (USACE). (2000). Design and Construction of Levees. Engineer Manual. Washington D.C.: Department of the Army.

Valette, G., Prevost, S., Lucas, L., and Leonard. (2006). "SoDA project: A Simulation of Soil Surface Degradation by Rainfall." *Computers & Graphics*, 30(4), 494–506.

Wan, C. F., and Fell, R. (2004). "Investigation of Rate of Rate of Erosion of Soils in Embankment Dams." *Journal of Geotechnical and Geoenvironmental Engineering*, 130(4), 373-380.

Xu, Y., and Zhang, L. M. (2009). "Breaching Parameters for Earth and Rockfill Dams." *Journal of Geotechnical and Geoenvironmental Engineering*, 135(12), 1957-1970.

Testing and Analysis of Erodibility of Hongshihe Landslide Dam

D. S. Chang[1,4], Limin Zhang[2,4], M. ASCE, and Yao Xu[3]

[1]Ph.D. Candidate, Department of Civil and Environmental Engineering, The Hong Kong University of Science and Technology, Hong Kong, China; email: cechangd@ust.hk
[2]Associate Professor, Department of Civil and Environmental Engineering, The Hong Kong University of Science and Technology, Hong Kong, China; email: cezhangl@ust.hk
[3]Research Associate, Department of Civil and Environmental Engineering, The Hong Kong University of Science and Technology, Hong Kong, China; email: xuyao@ust.hk
[4]Affiliated Researcher, State Key Laboratory of Geohazard Prevention and Geoenvironment Protection, Chengdu University of Technology, Sichuan, China.

ABSTRACT: The Great Wenchuan Earthquake of Ms 8.0 in Richter scale on 12 May 2008 caused the formation of 34 large and numerous smaller landslide dams. Hongshihe Landslide Dam is one of the large-scale dams. The erodibility of fresh landslide deposits plays an important role in evaluating the breaching process of such landslide dams due to overtopping. A landslide dam typically comprises freshly deposited mass of heterogeneous, unconsolidated or poorly consolidated earth materials and is vulnerable to overtopping failure. The landslide deposits are usually broadly graded with particle sizes ranging from clay to boulders. Moreover, their grain size distributions are highly heterogeneous along depth and along the run-out direction of landslide debris. Due to the variation of soil properties, the soil erodibility also varies significantly along the run-out direction and depth. This paper describes a series of field jet index tests conducted at two landslide dams shortly after the earthquake to investigate the erodibility of freshly deposited landslide soils. The basic soil parameters (i.e., grain-size distribution, bulk density, water content, and Atterberg limits), as well as the coefficient of erodibility and critical erosive shear stress at different locations were also measured to examine the variation of soil erodibility of Hongshihe Landslide Dam along the run-out direction, depth, and the water-flow direction. The results show that the coefficient of erodibility increases significantly along the run-out direction but decreases slightly with depth and along the water-flow direction, whereas the changes in critical erosive shear stress are limited along the run-out direction, depth, and the water-flow direction.

INTRODUCTION

On 12 May 2008, a strong earthquake of magnitude 8 in Richter scale occurred in Sichuan Province, China. Approximately 30,000 landslides were triggered by the earthquake. Some of these landslides blocked rivers and formed 34 large and numerous smaller landslide dams (Cui et al. 2009; Zhang 2009). Hongshihe Landslide Dam is one of the large-scale dams. All the 34 large-scale landslide dams failed by overtopping, with the assistance of blasting or division channels in some cases. The erodibility of fresh landslide deposits plays an important role in evaluating the overtopping failure of such landslide dams. The landslide deposits are usually broadly graded with particle sizes ranging from clay to gravels or even boulders (Costa and Schuster 1988; Casagli et al. 2003). Moreover, the grain-size distributions are highly heterogeneous along depth and along the run-out direction of landslide debris (Dunning 2006; Crosta et al. 2007; Chang et al. 2009a). A landslide dam comprising freshly deposited mass of heterogeneous, unconsolidated or poorly consolidated earth materials is vulnerable to breaching due to overtopping. Because of the variations of soil properties, the soil erodibility varies significantly along depth and the run-out direction. It has been highlighted the breaching process of a landslide dam is influenced by the variations in soil erodibility along depth, especially for the breach initiation time (Chang and Zhang 2010). Moreover, the evolution of breach width during the overtopping process can be affected by the variations in soil erodibility along the run-out direction. It is therefore important to quantitatively study the erosion resistance of such landslide dams in different directions.

The objective of this paper is to study the variations in the soil erodibility at Hongshihe Landslide Dam along the run-out direction, depth and the water-flow direction based on results of field erodibility tests and measured basic soil parameters. In this work, jet index field tests were carried out on two landslide dams triggered by the Wenchuan earthquake. The basic soil parameters (i.e., grain-size distribution, bulk density, and water content) along the run-out direction and on the breach side slope were also measured. The variations in the erosion resistance of the landslide deposits along the run-out direction, depth, and the water-flow direction are analyzed.

FIELD TESTING OF ERODIBILITY USING JET INDEX METHOD

The erosion resistance of soils can be represented by the coefficient of erodibility, K_d, and the critical erosive shear stress, τ_c through the following equation:

$$E = K_d\left(\tau_e - \tau_c\right) \tag{1}$$

where E is the erosion rate; τ_e is the effective stress at the soil/water interface. K_d reflects how fast the soil erodes; while τ_c reflects the ease of initiation of erosion in the soil. To investigate the erodibility of freshly deposited landslide dams, field soil erodibility tests were conducted on two landslide dams (Hongshihe Landslide Dam and Libaisi Landslide Dam) triggered by the 12 May 2008 Wenchuan earthquake. The jet index method was used, which was developed by Hanson (1991) and is adopted as ASTM standard D5852-00 (ASTM 2000). The tests were carried out under natural compaction conditions with relative compactions ranging from 0.69 to 0.89 and under different controlled compaction conditions with relative compactions ranging from 0.59 to 0.97. It is found that the critical erosive shear stress varies in a relatively narrow range from 0.4 Pa to 6.8 Pa, whereas the coefficient of erodibility differs by two orders of magnitude as shown in Table 1. The basic soil parameters (i.e., bulk density, water content, grain-size distribution, Atterberg limits, and specific gravity) at each location were also measured. A multi-variable nonlinear regression analysis is performed based on the field test results and the basic soil properties. It is found that the void ratio, e, and the coefficient of uniformity, C_u, have strong correlations with K_d and that the fines content (< 0.063mm), P, the plasticity index, PI, and the void ratio, e, have strong correlations with τ_c. Finally, two empirical equations are obtained through regression analysis to quantitatively describe the soil erodibility parameters (Chang et al. 2009b):

$$K_d = 20075e^{4.77}C_u^{-0.76} \tag{2}$$

$$\tau_c = 6.8(PI)^{1.68} P^{-1.73}e^{-0.97} \tag{3}$$

VARIATIONS IN ERODIBILITY OF HONGSHIHE LANDSLIDE DAM

Due to the 2008 Wenchuan earthquake, a large landslide, i.e. the Donghekou landslide, blocked Hongshihe River and formed the Hongshihe landslide dam. The location of the landslide dam is shown in Figure 1. The Hongshihe landslide dam was approximately 50 m in height, 250 m in length across the river, 500 m in length along the river, and 4×10^6 m^3 in reservoir volume (Ren and Dang 2008). With the rising of the lake water level, water started to overtop the lowest crest on 16 May 2008 and a breach finally formed by overtopping.

Table 1. Field measured erodibility parameters for landslide deposits on two landslide dams under different soil conditions

Locations	H1	H2	H3	H4	H5	H6	H7	H8	H9	H10	H11	H12	H13	H14
K_d (mm^3/N-s)	37	35	44	52	44	40	100	126	30	3	7	192	3	8
τ_c (Pa)	6.8	6.5	6.3	6.0	5.9	6.3	5.4	2.8	1.5	3.7	2.5	5.6	4.4	1.5
Soil conditions	IC	IC	IC	IC	IC	IC	IC	IC	IC	CC	CC	IC	CC	CC

Locations	H15	H16	H17	H18	H19	L1	L2	L3	L4	L5	L6	L7	L8
K_d (mm^3/N-s)	5	112	147	828	6	54	28	8	65	4	861	1085	76
τ_c (Pa)	3.1	3.2	2.2	2.2	2.2	1.2	0.6	1.9	2.4	1.5	0.4	1.0	2.1
Soil conditions	IC	IC	IC	LC	IC	IC	IC	CC	IC	CC	LC	LC	CC

Note: IC = In-situ condition; CC = Compacted condition; LC = Loosened condition; H = Hongshihe Landslide Dam; and L = Libaisi Landslide Dam.

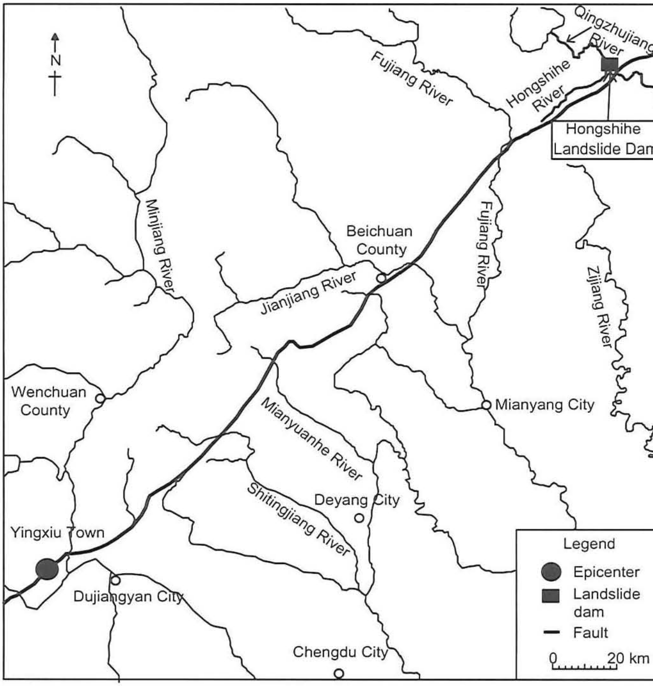

Figure 1. Location of the Hongshihe landslide dam

To investigate the variations in the erodibility of the landslide deposits of Hongshihe Landslide Dam along the run-out direction, depth, and the water-flow direction, totally 8 soil samples along the run-out direction and 5 soil samples along the side slope of the breach were taken as shown in Figure 2. The basic soil parameters (i.e., bulk density, water content, grain size distribution, Atterberg limits, and specific gravity) were measured in-situ and in the laboratory for each sample. The grain-size distributions for the deposits at the erosion testing locations are shown in Figure 3. It shows that the landslide deposits are broadly-graded ranging from clay to stone [clay (< 0.002 mm), silt (0.002 mm–0.075 mm), sand (0.075 mm–2 mm), gravel (2 mm–75 mm), stone (75 mm–2000 mm), rock (> 2000 mm)], and the fines content ranges from 9.4% to 36%. The definitions of particle sizes follow Kulhawy and Chen (2009). Other soil parameters are summarized in Table 2.

Variations in erodibility along the run-out direction

The sampling distance was 25 m for most soil samples along the run-out direction, other than the distances between H23 and H24 and between H24 and H25, which were 5 m and 45 m respectively as shown in Figure 2. Figure 4(a) shows the variations in the mean particle size, d_{50}, along the run-out direction. The values of d_{50} are in the range of 3-20 mm and exhibit a weakly increasing trend in the run-out direction. This coincides with the conventional observation that large particles move to the front in a landslide (Crosta et al. 2001). The fluctuations of d_{50} become progressively smaller in the run-out direction. The variations in soil dry density, ρ_d, along the run-out direction are shown in Figure 4(b). ρ_d ranges from 1239 to 1839 kg/m^3. There is a clear trend of decreasing dry density along the run-out direction. This is because the fines (clay and silt) and sand contents decrease along the run-out direction, which cannot fully fill the pores formed by gravel and stones, causing the void ratio to increase along the run-out direction. Another reason may be that the deposits in the front of the landslide have less chance to be compacted during the landslide process.

The coefficient of erodibility, K_d, and the critical erosive shear stress, τ_c of the landslide deposits along the run-out direction can be obtained using Eqs. (2) and (3) according to the measured basic soil parameters. Figure 4(c) shows the variations in the coefficient of erodibility along the run-out direction. K_d increases along the run-out direction ranging from nearly 1 to 750 mm^3/N-s. This is mainly due to the increase of void ratio and decrease of coefficient of uniformity along the run-out direction. Both factors make it more difficult for the deposits to form a stable structure. Note that a stable structure means that the pores formed by the coarse particles are nearly completely filled by the fine particles.

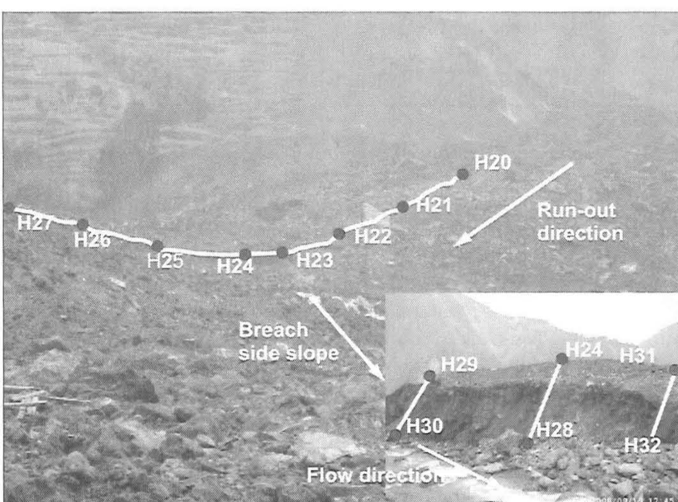

Figure 2. Sampling locations at Hongshihe Landslide Dam along the run-out direction and the side slope of the breach

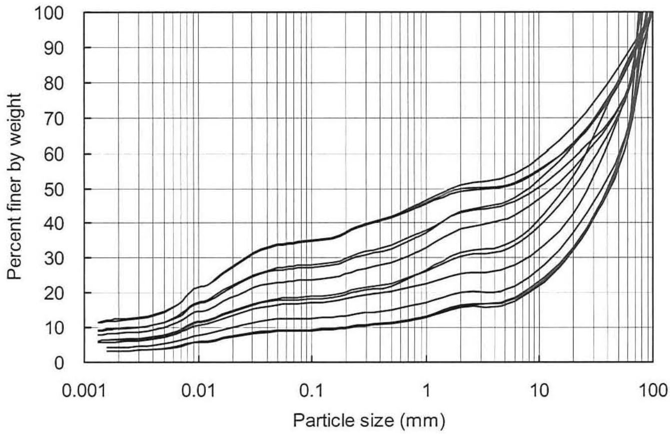

Figure 3. Gain size distributions of landslide deposits at 13 sampling locations

Table 2. Summary of soil properties at 13 locations along the run-out direction and the side slope of the breach

Locations	Dry density ρ_d (kg/m^3)	Void ratio e	d_{50} (mm)	C_u	PI (%)	Fines content P (%)	Specific gravity G_s
H20	1839	0.46	4.1	3200	20	24.5	2.69
H21	1790	0.50	3.0	4375	22	28.7	2.70
H22	1809	0.48	19.2	4267	15	19.4	2.67
H23	1553	0.73	12.5	120	8	9.4	2.68
H24	1352	0.98	5.0	1620	12	18.8	2.68
H25	1445	0.85	13.0	211	13	9.6	2.67
H26	1338	1.00	11.0	1133	16	13.0	2.67
H27	1239	1.16	13.5	195	12	9.8	2.68
H28	1478	0.81	8.5	2233	12	17.6	2.68
H29	1290	1.08	2.5	3250	20	28.1	2.68
H30	1443	0.86	1.5	5000	22	35.1	2.69
H31	1340	1.00	0.9	3400	22	35.9	2.68
H32	1485	0.81	1.2	4500	22	36.0	2.70

The variations in the critical erosive shear, τ_c, along the run-out direction are shown in Figure 4(d). The values of τ_c are mostly in the range of 3 to 12 Pa and exhibit a weakly increasing trend along the run-out direction. One reason is due to the decrease of the fines content along the run-out direction. Thoman and Niezgoda (2008) found similar results from field tests that the critical erosive shear stress increases with decreasing fines content for cohesive soils. According to Hanson and Simon's classification (Hanson and Simon 2001), the erodibility of the deposits along the run-out direction falls into the moderately resistant or resistant category. It can be observed that the initiation of erosion becomes slightly harder but the erosion rate becomes larger along the run-out direction under the same flow conditions once erosion is initiated. The erosion resistance of the landslide deposits in general becomes weakened along the run-out direction.

Variations in erodibility along depth

Soil samples were taken at three different profiles at a 25-m sampling distance. Two locations were chosen along depth at each profile as shown in Figure 2. The sampling distances between H29 and H30, H24 and H28, H31 and H32 were 4, 7, and 6 m, respectively. K_d and τ_c can be calculated based on the measured basic soil parameters using Eqs. (2) and (3).

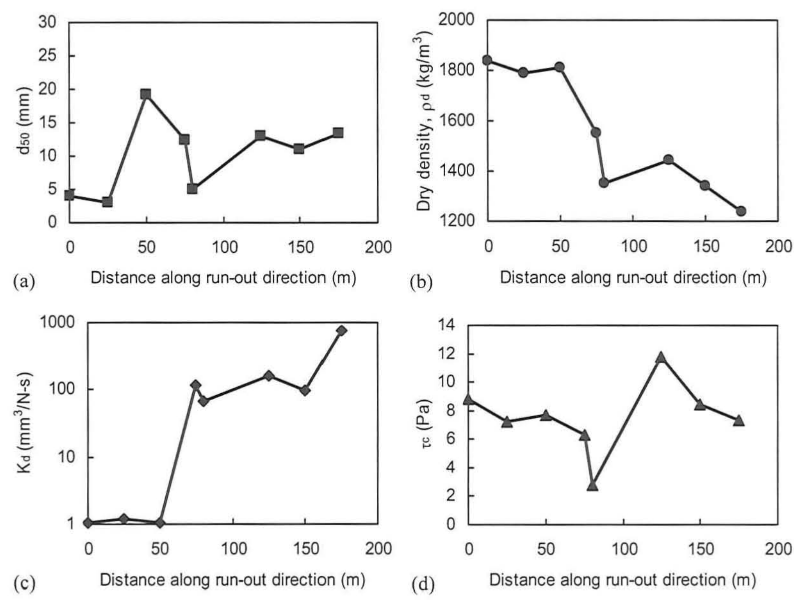

Figure 4. Variations in soil properties along the run-out direction at Hongshihe Landslide Dam: (a) mean particle size; (b) dry density; (c) coefficient of erodibility; and (d) critical erosive shear stress

Figure 5 shows the variations in soil erodibility, dry density and mean particle size along depth in each profile. The values of K_d are in the range of 10 to 80 mm^3/N-s and exhibit a decreasing trend along depth, whereas the values of τ_c are in a narrow range of 2 to 4 Pa and show a slightly increasing trend along depth. A general observation is the erosion resistance of the deposits increases along depth. This is mainly due to that the deposits at greater depths were compacted more by the self-weight of the falling materials during the process of landslide. The increment of dry density over a depth difference of 5 m is approximately 10% as shown in Figure 5. The variations in mean particle size with depth are not conclusive in Figure 5. In an ideal landslide slide, small particles usually accumulate at the bottom layer (Crosta et al. 2001).

Variations in erodibility along the water-flow direction

Sampling locations H29, H24, H31, and H30, H28, H32 were located at the top and bottom of the breach side slope and arrayed along the water-flow direction as shown in Figure 2. Figure 6 shows the variations in soil erodibility along the water-flow direction. Both the coefficient of erodibility and the critical erosive shear stress are in a narrow range along the water-flow direction. Thus, the erosion resistance could be treated as the same along the water-flow direction when simulating the erosion process of such landslide dams. The total length of the dam along the water-flow direction was about 500 m, while only three profiles along the water-flow direction were studied in this paper. Therefore, the trend of the variations in erodibility along the water-flow direction needs to be further investigated.

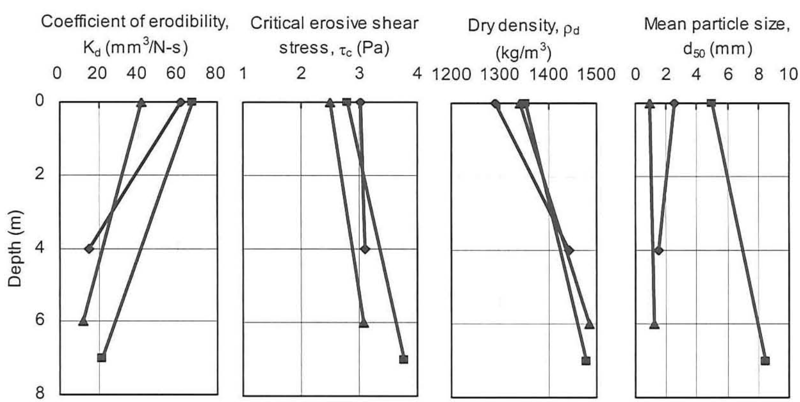

Figure 5. Variations in soil erodibility and mean particle size along depth at Hongshihe Landslide Dam

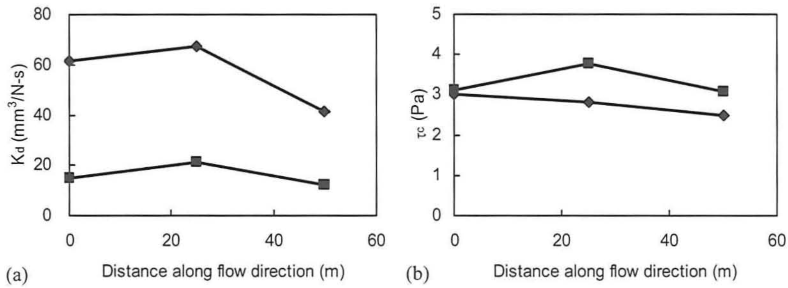

Figure 6. Variations in soil erodibility along the water-flow direction at Hongshihe Landslide Dam: (a) coefficient of erodibility; (b) critical erosive shear stress

SUMMARY AND CONCLUSIONS

Field jet index tests were conducted at two landslide dams induced by the 12 May 2008 Wenchuan earthquake to investigate the erodibility of landslide dams. The basic soil parameters of the landslide deposit along the run-out direction, depth and water-flow direction were measured in-situ and in the laboratory. The landslide deposits show broadly-graded and highly heterogeneous features and fall into moderately resistant to resistant category according to Hanson and Simon's erodibility classification.

The variations in the soil erodibility of Hongshihe Landslide Dam along the run-out direction, depth, and water-flow direction are studied based on the basic soil parameters using the empirical equations. The coefficient of erodibility decreases slightly with depth and along the water-flow direction but increases by nearly two orders of magnitude along the run-out direction. The changes in the critical erosive shear stress are limited along the run-out direction, depth, and the water-flow direction. Hence the scour rate in the deposits may decrease as overtopping erosion proceeds to larger depths under the same water depth. Moreover, the breach could enlarge more easily in the frontal part of the landslide since the coefficient of erodibility is high in the frontal area. The findings obtained in this paper are mainly applicable to large landslides with long sliding distances. For small landslides, the soil erodibility along the depth may also show the similar trend as that of a large landslide. However, the soil erodibility may not show clear trend along the run-out direction.

ACKNOWLEDGEMENTS

The research was substantially supported by the Research Grants Council of the Hong Kong SAR (No. 622207) and the State Key Laboratory of Geohazard Prevention & Geoenvironment Protection (DZJK-0815). Special thanks are due to Prof. Qun Chen and Prof. Bixiong Li of Sichuan University, and Prof. Runqiu Huang of Chengdu University of Technology for their kind assistance during the field tests in the Wenchuan earthquake zone.

REFERENCES

ASTM. (2000). "Standard test method for erodibility determination of soil in the field or in the laboratory by the jet index method." *D5852-00*, Philadelphia, Pa.

Chang, D.S. and Zhang, L.M. (2010). "Simulation of the erosion process of landslide dams due to overtopping considering variations in soil erodibility along depth." *Nat. Hazards Earth Syst. Sci.*, 10: 933–946.

Chang, D.S., Zhang, L.M., Xu, Y., and Huang, R.Q. (2009a). "Analysis of overtopping failure of Hongshihe Landslide Dam after Wenchuan Earthquake." *J. Eng. Geol.*, 17(1): 50-55. (in Chinese)

Chang, D.S., Zhang, L.M., Xu, Y., and Huang, R.Q. (2009b). "Field testing of erodibility of two landslide dams triggered by the 12 May Wenchuan earthquake." Submited to *Landslides*.

Casagli, N., Ermini, L., and Rosati, G. (2003). "Determining grain size distribution of the material composing landslide dams in the Northern Apennines: sampling and processing methods." *Eng. Geol.*, 69: 83–97.

Costa, J.E. and Schuster, R.L. (1988). "The formation and failure of natural dams." *Geol. Soc. Am. Bull.*, 100: 1054-1068.

Crosta, G.B., Calvetti, F., Imposimato, S., Roddeman, D., Frattini, P., and Agliardi, F. (2001). Granular flows and numerical modelling of landslides. Report of DAMOCLES project, August 2001, 73 pp.

Crosta, G.B., Frattini, P., and Fusi, N. (2007). "Fragmentation in the Val Pola rock avalanche, Italian Alps." *J. Geophys. Res.*, 112(F01006).

Cui, P., Zhu, Y.Y., Han, Y.S., Chen, X.Q., and Zhuang, J.Q. (2009). "The 12 May Wenchuan earthquake-induced landslide lakes: distribution and preliminary risk evaluation." *Landslides*, 6: 209-223.

Dunning, S.A., Rosser, N.J., Petley., D.N., and Massey, C.R. (2006). "Formation and failure of the Tsatichhu landslide dam, Bhutan." *Landslides*, 3: 107-113.

Hanson, G.J. (1991). "Development of a jet index to characterize erosion resistance of soils in earthen spillways." *Transactions of the ASAE*, 34(5): 2015-2020.

Hanson, G.J. and Simon, A. (2001). "Erodibility of cohesive streambeds in the loess area of the midwestern USA." *Hydrol. Process.*, 15: 23-38.

Kulhawy, F.H. and Chen, J.R. (2009). "Identification and decription of soils containing very coarse fractions." *J. Geotech. Geoenviron. Engrg.*, 135(5): 635-646.

Ren, X. and Dang, Y.P. (2008). "Construction organization and construction management for emergency risk-elimination of landslide dams in Qingchuan Country." *J. Water Resour. Hydropower Eng.*, 39(8): 27-30. (in Chinese)

Thoman, R.W. and Niezgoda, S.L. (2008). "Determining erodibility, critical shear stress, and allowable discharge estimates for cohesive channels: case study in the Power River Basin of Wyoming." *J. Hydraul. Eng.*, 134(12): 1677-1687.

Zhang, L.M. (2009). "Challenges in multi-hazard risk assessment and management: Geohazard chain in Beichuan Town caused by Great Wenchuan Earthquake." *Geotechnical Risk and Safety*, Taylor and Francis Group, London, 237-244.

Earth Dam Failure by Erosion, A Case History

Scott Newhouse[1], P.E., M.ASCE

[1]Senior Engineer; Bechtel Power Corporation, 5275 Westview Drive, Frederick, MD 21703

ABSTRACT

In January, 1998 the Archusa Creek Dam failed by breaching through its emergency spillway. The dam is a low earth dam, 7.6 m (25 ft) tall, and 1370 m (4,500 ft) crest length. It is located in southeast Mississippi, in Clarke County, near the town of Quitman. At the time of its failure, the dam had a concrete ogee weir for a principal spillway, and a vegetated earth emergency spillway. (Spillway configuration has been modified since the failure.) The impounded lake is a state-owned water park, used solely for recreation. Fortunately, the dam is a low hazard structure. The Chickasawhay River is less than 0.4 km (¼ mi) downstream of the dam. The dam is in the flood plain of the river; accordingly, there is little development downstream. Consequences of failure were mostly limited to the loss of the water park.

The dam failed during a rain storm corresponding to approximately a 5 year return period. The failure was triggered by intense rainfall of near 10.8 cm (4.25 in.) falling in just a few hours over the watershed. The watershed is very large compared to the size of the reservoir; the ratio of watershed area to lake surface area exceeds 50:1. Consequently, such a storm event results in very high inflow to the reservoir. Runoff generated by the storm caused a rapid rise in lake level to elevation above the flood pool, resulting in flow over both the principal and the emergency spillways. A breach formed through the emergency spillway due to erosion. The failure mechanism is an established, well known one, of progressive erosion and head-cutting due to excessive water flow velocity.

By modern design standards, the dam should have sustained this storm event without incident. Modifications to the dam made in 1994 set the stage for failure. The paper evaluates these modifications, along with the dam's design and specific features and factors that led to failure.

INTRODUCTION

Archusa Creek Dam was built in 1971. Figure 1 illustrates the location of the dam, near Quitman, Mississippi. A state agency owns the lake and dam; it is used exclusively for recreation (operation of a water park). The lake is shallow, with typical depth of about 1.2 m (4 ft), and generally ranging from 1.2 to 2.4 m (4 to 8 ft).

The lake is about 172 ha (425 ac). Size of the lake's watershed is about 15,800 ha (39,000 ac), resulting in significant in-flow to the lake during storm events. There is little storage volume available in the lake compared to in-flow; consequently, the dam must pass nearly all in-flow.

The lake is in the flood-plain of Chickasawhay River. A high river stage produces tail-water below the dam that often exceeds the lake elevation.

DAM DETAILS

The dam is built of compacted earth fill with a maximum height of 7.6 m (25 ft) and a length of about 1370 m (4,500 ft). The dam is homogenous, with no internal seepage control and no foundation cut-off. Fill material for the dam is generally fine silty sand, as this soil was locally available for construction.

In the 1980s the principal spillway was fitted with an inflatable gate; this configuration was modified in 1994 due to ongoing problems with maintenance and vandalism. In 1994 the spillway was modified with an ogee crest and series of sluice gates through the ogee. The crest and the gate inlets were all fitted with fish retaining screens.

For passing in-flow exceeding the principal spillway capacity, the dam was designed with an uncontrolled emergency spillway, with vegetated earth surface/lining. During the 1994 modification, the emergency spillway was widened from 120 m (400 ft) to 300 m (1000 ft). It was again modified shortly before the 1998 failure with the excavation of a drainage ditch within the spillway to facilitate rapid drainage of flood water from lake-side residential yards. This later modification contributed to the dam breach by initiating erosion in the emergency spillway. Notably, the fish retaining screens clogged with debris during the failure storm and contributed to breaching by restricting spillway capacity.

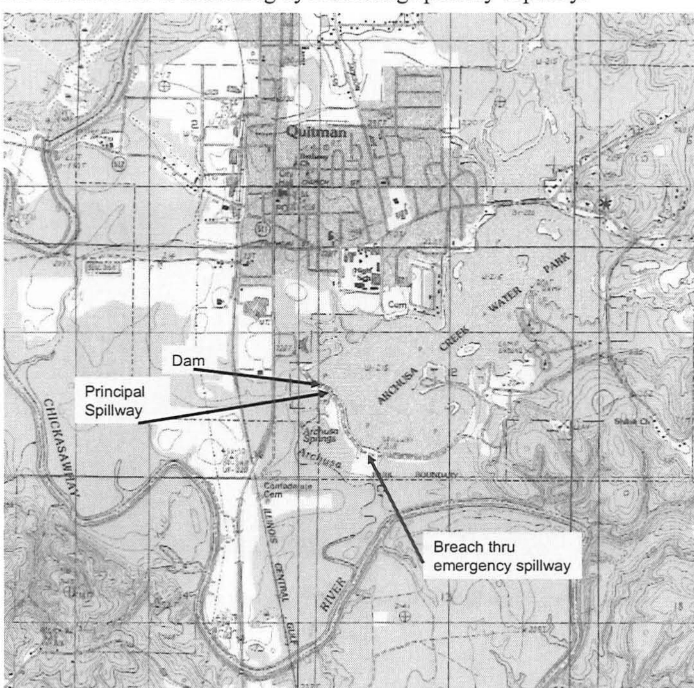

Figure 1. Location map (source map USGS Quitman, Miss. Quadrangle, 1983).

DETAILS OF DAM BREACH FAILURE

The breach formed by erosion of soil within the vegetated earth emergency spillway due to high discharge velocity which the spillway surface could not sustain. Figures 2 and 3 illustrate the position of the breach within the dam. The storm causing the failure was an event corresponding to a 5 year return period. Rainfall from this storm was nearly 16.5 cm (6.5 in.) in a 3 day period. However, the dam's failure was preceded by intense rainfall of 10.8 cm (4.25 in.) over a period of only a few hours.

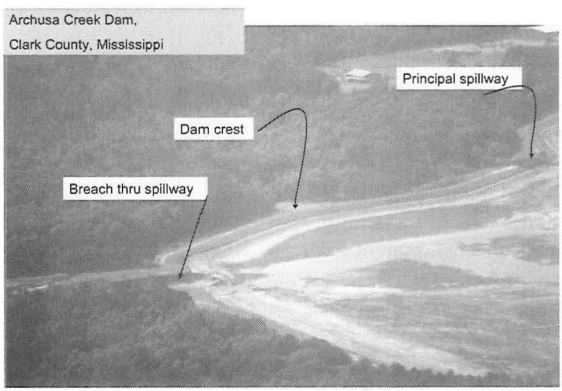

Figure 2. Breach through emergency spillway.

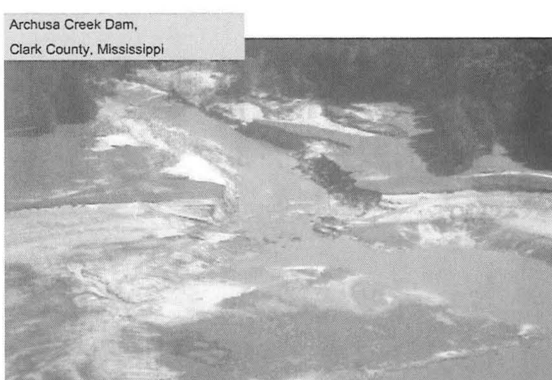

Figure 3. Close-up view of breach.

Figure 4. Breach through emergency spillway showing grass surface.

Figure 5. Photo illustrating principal spillway and typical depth of lake.

Emergency Spillway Operation

Analysis shows that the emergency spillway would activate with a storm corresponding to a 2 year return period. Consequently, the emergency spillway was subjected to frequent flow. Hydraulic analysis indicates that flow in the emergency spillway in the 1998 failure storm was 200 m^3/s (7,000 cu ft/s), with a velocity exceeding 1.5 m/s (5 ft/s).

Erosion Mechanism

NRCS and USACE design references establish a range of velocity that a vegetated earth spillway can sustain. Federal Energy Regulatory Commission (FERC) (2003) tabulates sustainable velocity listed in applicable NRCS and USACE design guide documents, as excerpted below, in Figure 6. The NRCS document establishes a typical sustainable velocity in the range of 0.6 to 1.5 m/s (2 to 5 ft/s), depending on the base soil and the grass type. Maximum sustainable velocity (atypical) is about 2.4 m/s (8 ft/s) for a non-erodible soil and specific Bermuda species of grass.

Table III-3
Maximum Channel Velocities
(US Army Corps of Engineers, EM 1110-2-1601, 1991)

Channel Material	Mean Channel Velocity (ft/sec)
Fine Sand	2.0
Coarse Sand	4.0
Fine Gravel	6.0
Earth - Sandy Silt	2.0
Grass-lined Earth (slopes less than 5%)	
Bermuda Grass on Sandy Silt	6.0
Kentucky Blue Grass on Sandy Silt	5.0

The US Natural Resource Conservation Service (NRCS) (formerly the US Soil Conservation Service) provides maximum permissible velocities for channels lined with grass. The NRCS maximum permissible velocities for the relevant slope range are summarized on Table III-4 below.

Table III-4
Maximum Permissible Velocities for Grass Lined Channels
(US Natural Resource Conservation Service, Source: SCS 1985, Table 7-1)

Type of Cover	Slope Range (percent)	Permissible Velocity (ft/sec)	
		Erosion-resistant soils	Easily eroded soils
Bermuda Grass	0-5	8	6
Buffalo grass, Kentucky bluegrass	0-5	7	5
Sod-forming grass mixtures	0-5	5	4
Other grasses	0-5	3.5	2.5
Remarks: The values apply to average, uniform stands of each type of cover. Use velocities exceeding 5 ft/sec only where good covers and proper maintenance can be obtained			

Figure 6. Range of sustainable Velocity on Vegetated Earth Surface (from FERC (2003)).

The fine silty sand soil used as fill in the emergency spillway has a low resistance to erosion. According to the criteria in Figure 6, maximum sustainable velocity on the Archusa Creek Dam's emergency spillway is 0.8 m/s (2.5 ft/s). Based on calculated velocity during the 1998 failure storm near 1.5 m/s (5 ft/s), erosion through the spillway material would have been expected. The calculated velocity is based on the broad flat spillway; the ditch excavated into the emergency spillway would have resulted in velocity exceeding 1.5 m/s (5 ft/s).

The specific erosion mechanism is illustrated and explained by Seed et al (2006). This group extensively studied the soil erosion process in levee over-topping after the Hurricane Katrina disaster in New Orleans. The work by Seed et al is not specifically applicable to vegetated earth spillways. But the erosion principle for soils is the same in the levee study and in the case of the dam spillway. Results of the New Orleans levee study match with the specific events on the dam spillway, the erosion of a fine sand soil. The levee study parameters for velocity and critical shear stress apply to a bare soil without vegetation. For the dam spillway, once the vegetation was lost during the breach event, the resulting bare soil was then similar to the study condition.

Figure 7 illustrates that fine silty sand soil within the dam's emergency spillway is generally the most easily eroded soil category, and that erosion will result in this soil at a shear stress of about 0.1 N/m^2, the minimum for all soil types.

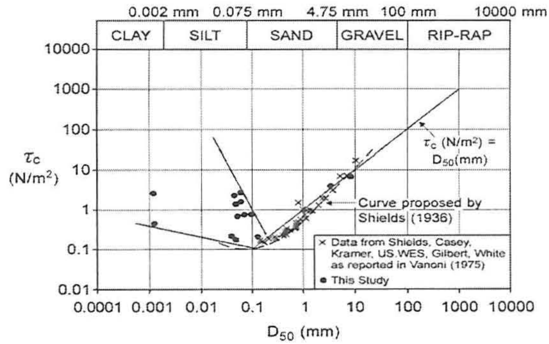

Figure 7. Quantified measure of erodibility- Critical shear stress versus mean soil grain size (From Seed et al (2006)).

Figure 8 shows that for shear stress above the threshold value for fine sand, 0.1 N/m^2, a significant scour rate results. For the water velocity imparted to the spillway during the failure storm, exceeding 1.0 m/s, Figure 8 indicates that fine sand in the spillway would erode at a rate exceeding 1000 mm/hr. These values apply to a bare soil not protected by vegetation. Accordingly, the values do not establish specific parameters for velocity and erosion rate applicable to the dam spillway. However, Figure 8 does provide a quantifiable indication that erosion would take place within the dam spillway during the breach storm event.

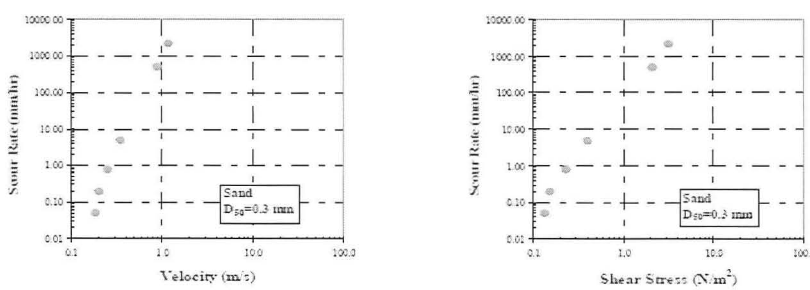

Figure 8. Erodibility function for a sand (from Seed, et. al. (2006)).

With the expected scour rate over 1000 mm/hr, and velocity imparted to the spillway exceeding 1 m/s, Figure 9 illustrates that the spillway would be highly erodible and prone to failure by overtopping. The levee study results depicted in Figures 7 through 9, combined with the sustainable velocity range portrayed in Figure 6, explain why erosion resulted in the spillway during the breach storm event.

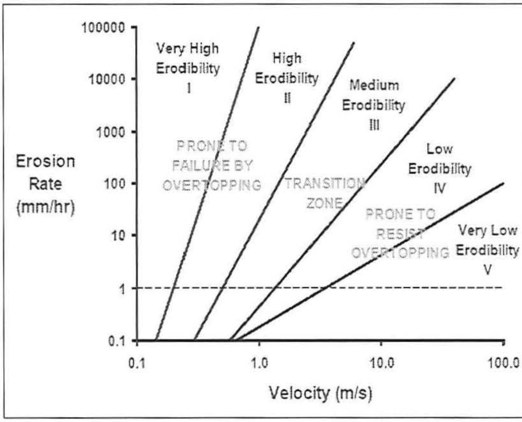

Figure 9. Proposed guidelines for levee overtopping (from Seed et. al. (2006)).

Overtopping is essentially the same erosion process that takes place in a vegetated earth spillway. This conclusion is especially true for the Archusa Creek Dam, as addressed in the DISCUSSION portion of the paper.

NRCS (1997) defines the specific process of erosion in dam earthen spillways. They describe a 3 phase process:

- The failure of the vegetal cover protection (if any) and the development of concentrated flow
- The downward and downstream erosion associated with the concentrated flow that leads to formation of a vertical or near-vertical head-cut in the vicinity of initial failure
- The upstream advance and deepening of the head-cut resulting from flow over the vertical or near vertical face

Figure 10 illustrates the process of over-topping failure in earth dams. The figure illustrates the 3 phase mechanism NRCS describes. Failure is initiated by erosion of the soil particles due to excess velocity. A near vertical face is formed, which travels progressively toward the reservoir during the erosion process (head-cutting). Finally the head-cutting process effects complete breach of the dam.

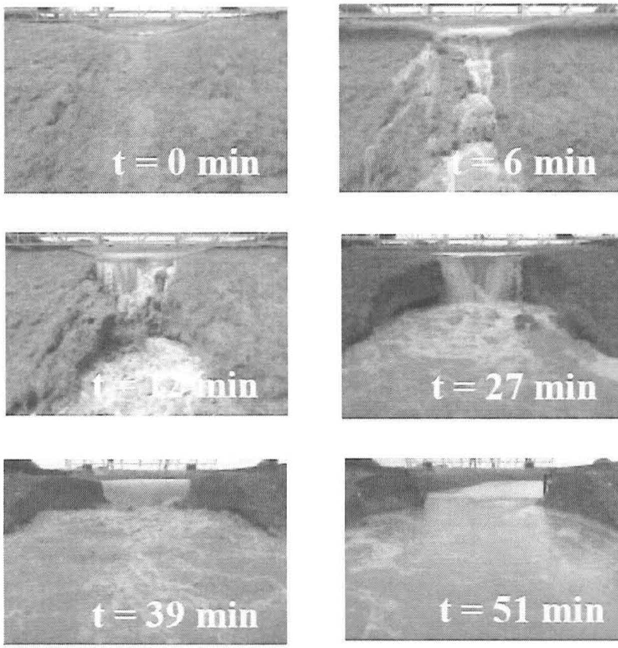

Figure 10. Illustration of dam breach by overtopping- embankment breach test of a homogeneous non-plastic sandy soil conducted at the ARS Hydraulic Laboratory, Stillwater, OK (from FEMA (2001)).

DISCUSSION

Earth Spillway Design

Established design methods call for earth spillways to be located at abutments, and founded in cut. The criterion to place the spillway in cut is to prevent erosion of fill soil. The NRCS design guide has extensive guidance for location, alignment, and grade for an emergency spillway so that erosion will not cause a breach failure, summarized below. Figure 11 illustrates design guidance for these criteria.

- Location- The most important element of location is to place the spillway where erosion and breach does not result in dam failure. As discussed above, this criterion is met by locating the spillway at an abutment, cut into native soil (alternatively the spillway can be cut through a saddle in terrain on the lake perimeter). Preferred location for the spillway is where it can discharge downstream without flow onto the toe of the dam. For sites where this alignment is impractical, training dikes can be used to keep flow off of the dam toe. But this configuration is not preferable.
- Alignment and grade- The spillway control section is designed to reduce velocity over the spillway to a sustainable level. Alignment and slope on the

spillway are set so that velocity stays within the sustainable range for the length of the spillway.

Earthen emergency spillway design for the Archusa Creek Dam did not conform to these criteria. The spillway was not located at an abutment in cut. Rather it is located in the middle of the dam, with its bottom in fill. The spillway did not have a control section sufficient to lower velocity to a sustainable level. Further, the drainage ditch excavated into the spillway concentrated flow and increased velocity, initiating erosion during the failure storm.

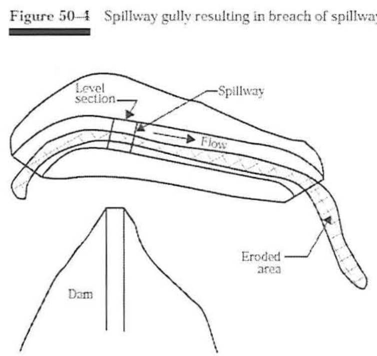

Figure11. Diagram illustrating proper emergency spillway layout (From NRCS (1997)).

With the emergency spillway not in conformance with these guidelines, erosion was a threat to dam safety. The choice of an emergency spillway lining of grass was inappropriate. Some armored lining, e.g. rip-rap would be required for the emergency spillway geometry in order to prevent erosion that could result in dam breach.

Hydraulic Design

NRCS design guides, and most state regulations, require reservoir storage and principal spillway capacity such that flow over an emergency spillway commences at a storm return period of 100 years. The 1998 configuration of the Archusa Creek Dam emergency spillway resulted in flow on near 2 year frequency.

CONCLUSIONS

For the 1998 dam configuration, the earth emergency spillway had an activation frequency of every 2 years, where this frequency by current design standards should be near 100 years. Consequently the emergency spillway was used frequently, as opposed to use on an emergency basis. For this frequency of use, the spillway should have been an armored auxiliary spillway. The Archusa Creek Dam was repaired by building a new auxiliary spillway. The main repair component was a concrete labyrinth weir spillway built within the breached area. This new concrete spillway is used as an auxiliary one, solving the problem of flow over an earthen emergency spillway at a 2 year frequency.

The dam breach was actually an over-topping failure. Because the earth emergency spillway is located in the interior of the dam (versus at an abutment), and built on fill (versus in cut), water flowing over this surface is essentially the same as flowing over the dam.

The case shows the merit of the NRCS design guidance for earth emergency spillways. The features identified that do not conform to the NRCS design guide were the major factors leading to failure:

- Location on the dam- not positioned at the abutment cut into native soil. The spillway was located near the center of the dam, in a position where erosion led to breach through the dam.
- Spillway surface- in fill versus cut into native soil. The use of erodible fill soil in the spillway established the speed limit for water flowing over it, roughly 0.8 m/s (2.5 ft/s). The 1998 storm produced flow with velocity much greater than this limit.
- Lack of control section- no means to control velocity at the spillway entrance.
- Unsuitable lining- grass would not sustain the discharge velocity and frequency

The final conclusion pertains to addition of fish retaining grates over the principal spillway crest and sluice gate openings. Generally these grates are put over dam outlet controls to keep fish from travelling out of the lake. During the failure storm these grates clogged with debris, restricting flow through the principal spillway. The capacity lost to grates clogged with flood debris may have never been considered in the dam's operation. Use of fish retaining grates has been implicated in failures and near failures of small dams, due to diminished spillway capacity. However, any demonstrable benefit of the grates is not clearly established.

REFERENCES

FERC. (2003). "Silver Lake Dam: Root Cause Report on the May 14th, 2003 Operation of the Fuse Plug Spillway and Subsequent Channel Erosion Resulting in the Uncontrolled Release of Silver Lake." FERC web-site.

FEMA. (2001). "ISSUES, RESOLUTIONS, AND RESEARCH NEEDS RELATED TO EMBANKMENT DAM FAILURE ANALYSIS." *PROC. FEMA WORKSHOP, JUNE 26-28, 2001, OKLAHOMA CITY, OK, FEMA PUBLICATION No. 541,* FEMA web-site.

NRCS. (1997). "Earth Spillway Design." Chapter 50, *Part 628 Dams, National Engineering Handbook,* NRCS web-site.

Seed et al. (2006). "Investigation of Performance of the New Orleans Flood Protection Systems in Hurricane Katrina on August 29, 2005." National Science Foundation, University of California web-site.

Effect of Seepage on River Bank Stability

Yee-Meng Chiew[1], Nandakumar Narasimhan[2] and Jian Chu[3]

[1]School of Civil and Environmental Engineering, Nanyang Technological University, Nanyang Avenue, Singapore 639798, PH: (+65) 6790-5256; e-mail: cymchiew@ntu.edu.sg
[2]School of Civil and Environmental Engineering, Nanyang Technological University, Nanyang Avenue, Singapore 639798
[3]School of Civil and Environmental Engineering, Nanyang Technological University, Nanyang Avenue, Singapore 639798, PH: (+65) 6790-4563; cjchu@ntu.edu.sg

ABSTRACT

The collapse of river banks around the world has caused widespread damages to land and property. In many instances, human lives are lost as a result of such failures. A better understanding of the mechanism leading to river bank failure is necessary before engineers can arrive at a cost-effective countermeasure to prevent such a disaster. To this end, an experimental study was conducted in a laboratory flume to investigate the correlation between river bank stability and seepage under a unidirectional current. The study examined the collapse of a bank slope consisting of non-cohesive sediment with the channel and ground water flow as the only variables. The experiments were carried out on two bank slopes = 27 and 20 degrees with the horizontal. While most studies hitherto have focused on the two variables independently (i.e., seepage and current effects separately), this study investigated their combined effect on failure of the bank slope. The dimensionless Reynolds number, which is a measure of shear stresses, is used as an indicator of erosion due to the main channel flow, while the critical hydraulic gradient is used to account for the onset of collapse. Moreover, the critical hydraulic gradient is also plotted as a function of the dimensionless seepage rate, which is the ratio of the applied shear velocity and the rate of drawdown, $u_*/(dh/dt)$. The results show that an increased in channel flow velocity (hence an increase in bed shear stresses) enhances slope failure, thereby causing it to collapse at a lower hydraulic gradient than that in a quiescent condition or with very low flow velocity. Additionally, the bank slope at 20 degrees requires a higher hydraulic gradient to initiatiate collapse as compared to its 27-degree counterpart with the same channel flow velocity. The study provides an improved understanding on slope failure in river channels, particularly for cases when there is a rapid drawdown of the flow stage during the recession period of the flood hydrograph.

INTRODUCTION

The collapse of river banks can cause widespread damages to land and property. This is particularly relevant to agrarian societies such as China and India. Figure 1(a) shows the collapse of a 6-m high bank along the Han River in China. Figure 1(b) shows the collapse of a bank along Yangtze River in Hubei Province (Xinhua News Agency, 2008), China while Fig. 1(c) shows how houses fell into the river as a result of failure of a bank along the Mekong River in Vietnam. All these examples reveal the importance in providing cost-effective engineering solutions to prevent a loss of lives and properties associated with river bank failures.

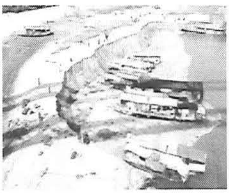

Figure 1(a): Collapse of a 6-m high river bank along Han River. Area affected >100 m x 20 m

Figure 1(b): Collapse of a river bank along Yangtse River, China, 2008.

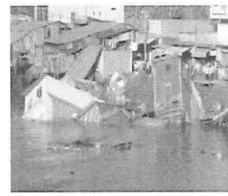

Figure 1(c): Collapse of a river bank along Mekong River, Vietnam

The movement of groundwater through porous river banks makes it an important parameter when analysing the stability of a channel. While groundwater flow alone sometimes may not significantly contribute to the displacement of sediments under certain conditions, it could become important when combined with flows in the river. To this end, experiments are performed to examine how the governing variables e.g., velocity of flow, hydraulic gradient etc. would affect river bank stability.

While fluvial erosion under seepage has been the subject of some studies, e.g., Cheng and Chiew (1999), Rao and Nagraj (1999), etc., few studies have been devoted to the study of river banks failure with seepage under a unidirectional flow. The bulk of available research focuses on the incipient motion or entrainment of sediments rather than the collapse of the entire bank. Geotechnical papers on slope stability, e.g., Hight et al. (1999), Hunt (2007), and Michalowski & Viratjandr (2006), do not account for channel flow hence fluvial erosion is neglected in these studies. In view of this limitation, the objective of this paper aims to investigate the combined effect of seepage and main flow velocity on river bank stability in order to provide an improved understanding on this topic.

EXPERIMENTAL SETUP AND METHODOLOGY

The experiments were conducted in a laboratory flume that was 7 m long, 1.6 m wide and 0.6m deep. The flume, which is shown in Fig. 2, had been modified to accommodate the river bank and the accompanied seepage unit to effect groundwater flow. The plan view of the modified flume together with the dimensions is shown in Fig. 2(a), while the test section is shown in Fig. 2(b). Water enters the flume through a perforated barrier so as to smoothen the flow in the channel. The flow depth is controlled by using a tail gate at the downstream end of the flume.

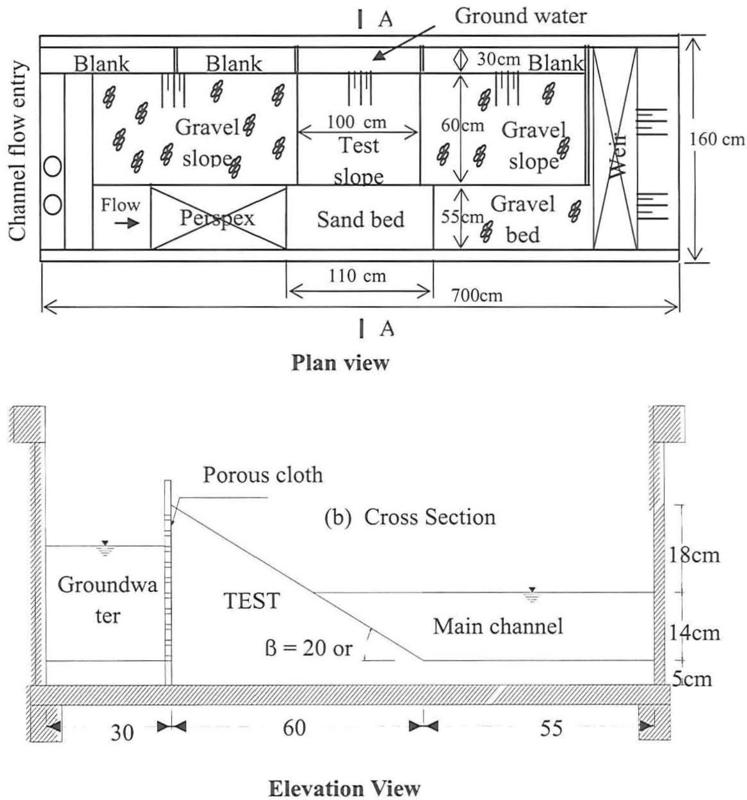

Figure 2: Experimental flume set-up (a) Plan view; (b) Elevation (A-A) View

The length of the test section is 1 m, in which uniformly distributed sand with a median grain size, d_{50} = 0.2 mm was placed. Two different bank slopes = 20° and 27° were tested in the study. The test section is located about 3 meters from the entrance to the flume. This is to allow for stabilisation before the flow reaches the test section. The portion of the flume upstream and downstream of the test section is lined with gravel so as to minimise disturbances often encountered when flowing water moves from one surface to another. Another transitional surface was introduced upstream of the sand bed. This consisted of a Perspex sheet with the same sand grains glued on its top (see Fig. 2a). The seepage section comprises a 1-m long perforated Perspex sheet with 2-cm diameter holes at 5 cm intervals throughout its length and up to a height of 30 cm. This sheet is covered with a cloth so as to ensure uniform seepage.

Experimental Procedure

Preliminary tests were conducted with the intention of getting certain basic properties of the bed sediment used in the study. This includes a constant head permeability test and sieve analysis to determine the coefficient of permeability and grain size distribution of the bed sediment, respectively. Moreover, the angle of repose of the sediment also was determined using the standard test whereby loose dry sand was dropped from a height of 20 cm. The resulting slump angle was calculated using simple trigonometric ratios from the measured dimensions of the sediment heap. Table 1 summarizes the basic properties of the bed sediment used in the study. The results so-obtained show that the bed sediment is a poorly-graded fine sand, with a median grain size of 0.2 mm.

Table 1. Property of sediment used in study

Median grain size, d_{50} (mm)	Uniformity Coefficient	Angle of repose	Coefficient of Permeability(m/s)
0.2	1.29	29.7	5.47×10^{-4}

The following tests procedure was adopted for all the tests in the study:

(a) Water is slowly pumped into the flume and the groundwater reservoir using 2 different hydraulic machines until the pre-determined steady state is reached, which is identified as the condition where the water levels in the main channel and groundwater reservoir are the same.
(b) Additional water is pumped into the groundwater reservoir at different rates to introduce a head difference, causing seepage through the test slope.
(c) The rate of increase of water level in the groundwater reservoir is quantified as dh/dt.
(d) The groundwater level is carefully monitored throughout the experiment, particularly to record the time taken for the river bank just to collapse. This constitutes the onset of critical failure of the slope.
(e) The experiment is repeated with different flow velocities in the main channel. For each undisturbed mean velocity, U_o, the experiment is repeated 5 times with the same dh /dt in order to ensure consistency.
(f) The hydraulic gradient at the onset of collapse is calculated using the flow net diagram as described in Harr (1962). This is the measured critical hydraulic gradient, i_c.
(g) Using the measured data, a correlation between the critical hydraulic gradient, i_c and the particle Reynolds number, Re_* ($= u_* d_{50}/\nu$) is prepared. The critical hydraulic gradient is also plotted against a dimensionless

seepage rate, $u_*/\{dh/dt\}$ in order to examine the effect of drawdown on the stability of the slope.

(h) The bed shear velocities of the tests were determined using the velocity profile obtained by measuring the flow velocities at various depths. The values for the shear velocity, u_* were calculate using the mean velocity equation for a rough bed.

$$\frac{U_o}{u_*} = 5.75\log\frac{y_o}{k_s} + 6 \tag{1}$$

where U_o = undisturbed mean velocity in the main channel; u_* = shear velocity; y_o = flow depth; and k_s = bed roughness height.

BANK SLOPE FAILURE MECHANISM

In order to examine how the threshold of bank slope failure is related to the applied shear stresses in the main channel and seepage flow through the bank, one needs to have a precise definition of what this constitutes. In general, bank slope failure is identified by the appearance of deformation on the surface of the test section. To this end, the entire failure process, which is documented in a series of photographs in Fig. 3, can be classified into three different stages. The first stage, which is the critical failure stage, constitutes the onset of collapse and the accompanying localized downward movement of the sand particles on the slope (Fig. 3b). Advanced failure, which leads to a larger mass of sand movement and a "slurry" of debris flow is shown in Figs. 3(c), (d) and (e). At this (second) stage, failure cracks begin to propagate sideways along the bank. With time, the cracks slowly propagate upward along the slope, causing further instability. The complete collapse of the slope is shown in Fig. 3(f). At this final stage no further observable movement of the slope occurs; the water levels in the groundwater reservoir and main channel are the same again.

Figure 4 shows the total collapsed bank slope after water is completely drained from both the main channel and groundwater reservoir. It also shows an enlarged view of a particular section of the failed slope. Moreover, a ruler is superimposed in the figure to provide the magnitude of the extent of the collapsed slope. While the onset of bank slope failure (Fig. 3b) could be sudden, the transition from the first to the third stage is gradual and uncertain.

In order to avoid ambiguity, the critical failure shown in Fig. 3(b) is used as the benchmark for all experiments for further analyses. This failure type is a flow slide which is typical of submerged sandy slopes and is similar to what has been described in Hight et al (1999).

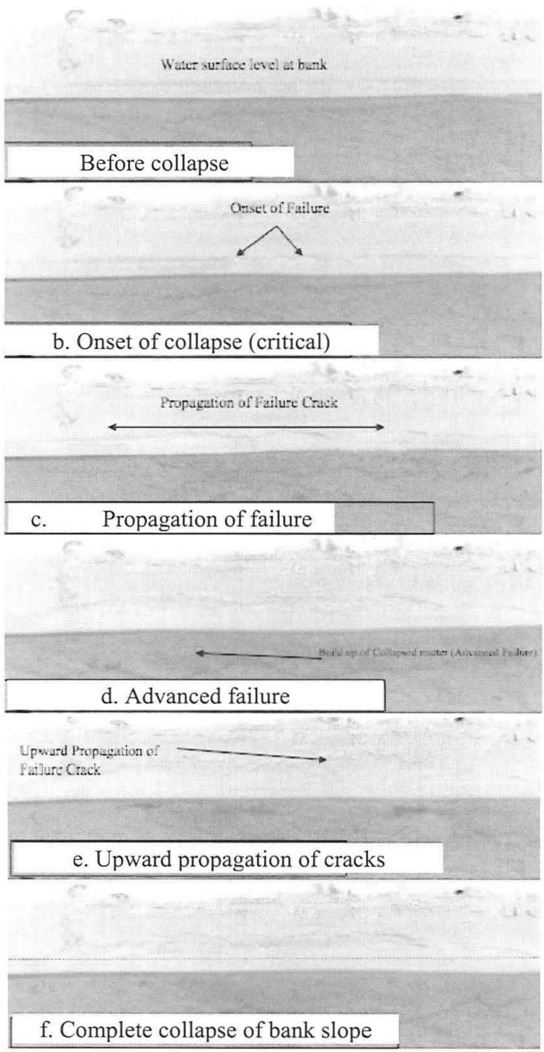

Figure 3: Failure process of experimental slope

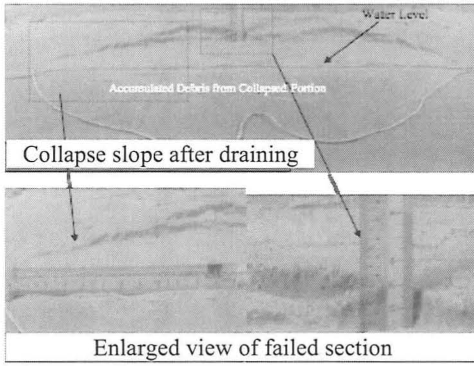

Figure 4 Collapsed portions of bank slope

RESULTS ANDS DISCUSSION

Figure 5 shows the plot of the measured critical hydraulic gradient, i_c as a function of the particle Reynolds number, Re_*. It reveals a marked difference in the critical hydraulic gradient for the onset of collapse of the two different bank slopes. While the 27-degree slope fails at a critical hydraulic gradient of 0.331 at $U_o = 0$, the 20-degree slope does so at a significantly higher value of 0.463. This can be attributed to the proximity to the angle of repose of the 1:2 slope (27 degrees), which causes the slope to become unstable, even at low hydraulic gradients.

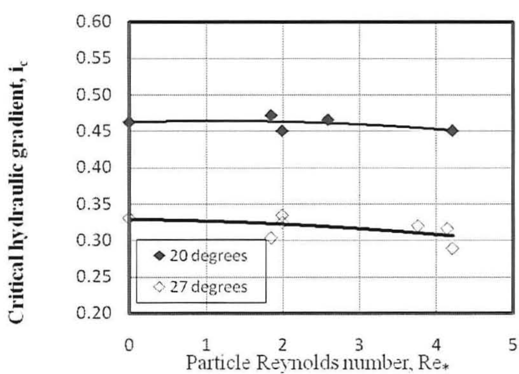

Figure 5. Effect of particle Reynolds number, Re_* on critical hydraulic gradient, i_c

At higher main channel flow velocities, the data show a small reduction in the hydraulic gradients required for the onset of collapse. This is due to the increased channel flow velocity that causes the sand on the surface of the slope to be eroded, thus facilitating the collapse. The fact that sediment particles on the bank is already in motion is supported by the computed bed shear velocity in that location, which is found to be well above the critical shear stress required for the initiation of motion calculated using the Shields diagram (Shields, 1936). Moreover, small sand dunes were observed at the base of the slope indicating that the sediment particles are already in motion.

An additional parameter, namely, the seepage rate, dh/dt is known to have an important effect on the pore water pressure distributions and thus hydraulic gradients in the soil in the slope. When dh/dt is higher, the pore water pressure builds up in the soil because of its inability to dissipate the pore pressure quickly enough. To examine how this may affect bank slope stability, a dimensionless seepage rate is proposed as a first approximation, and the measured data fitted to examine its effect on the critical hydraulic gradient, i_c. To this end, the plot of the measured critical hydraulic gradient as a function of the dimensionless seepage rate, $u_*/\{dh/dt\}$ is plotted in Fig. 6. Here, the dimensionless seepage parameter is used to quantify the relative magnitude of the applied shear stress on the bed and the rate at which pore water pressure is dissipated. The experimental data show that a higher dimensionless seepage rate leads to lower critical hydraulic gradient, i.e., that it is easier for a slope to fail for a higher $u_*/\{dh/dt\}$, even though the effect does not appear to be large. One may infer from the data to mean that an increased bed shear stress or a reduction in dh/dt will lead to a reduced critical hydraulic gradient. The results in this series of test support those summarized in Fig. 5 that the undisturbed applied shear stress on the main channel has an effect on the overall stability of the river bank.

As observed in the experiments and other case histories (Hight et al. 1999), slopes fail in a series of slides. It normally initiates from the toe and then propagates upward. Another effect of the river flow is the removal of debris of the first slide at the toe in the form of a scour. The debris plays a stabilizing effect on the slope. Once it is removed, it will cause the slope to be less stability and lead to the occurrence of subsequent slides, as demonstrated by Leong et al (2001), and to a certain extent, illustrated in Fig. 3. It may be surmised that the faster the river flow, the greater the ability for the debris to be removed and the faster the rate of removal. Therefore, the flow rate of the river and its turbulence will also affect the stability of slope.

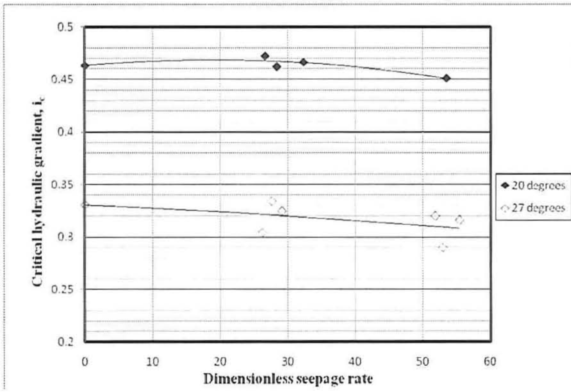

Figure 6. Effect of dimensionless seepage rate, u*/(dh/dt) on critical hydraulic gradient, i_c

CONCLUSIONS

The following conclusions are drawn based on the experiments of a 27- and 20-degree bank slope consisting of non-cohesive sediment with a uniform grain size distribution and median diameter of 0.2mm

1. The 27-degree bank slope undergoes failure at a significantly lower hydraulic gradient as compared to the 20-degree bank slope for the same undisturbed main flow velocities.
2. The hydraulic gradient needed to just initiate bank failure is not only related to the seepage flow through the bank, but also the particle Reynolds number.
3. The critical hydraulic gradient for a given bank slope is lower for a higher particle Reynolds number.
4. The critical hydraulic gradient for a given bank slope is lower for a higher dimensionless seepage rate.

ACKNOWLEGEMENT

The authors acknowledge the support from DHI-NTU Water & Environment Research Center and Education Hub.

REFERENCES

Cheng, N. S. and Chiew Y. M. (1999). "Incipient Motion with Upward Seepage", *J Hydraulic Research*, IAHR, 37(5): 665- 681.

Harr, M. E. (1962), Groundwater adn Seepage, Mcgraw Hill, New York.

Hight, D. W., Geogiannou, V. N., Martin, P. L., and Mundegar, A. K. (1999). "Flow slides in micaceous sands." Problematic Soils, Yanagisawa, Moroto, and Mitachi, eds. Balkema, Rotterdam, The Netherlands: 945–958.

Hunt, R. E. (2007). "Geotechnical Engineering Investigation Handbook: 2nd E dition", Taylor and Francis Group, CRC Publication.

Leong, W. K., Chu, J., and Hight, D. W. (2001). "Slip failures in granular slopes: some observations from model tests." *Proc. 14th Southeast Asian Geotechnical Conference*, 10-14 Dec, Vol. 1, Hong Kong: 819-824.

Michalowski. R. L. and Viratjandr, C. (2006), "Limit Analysis of Submerged Slopes Subjected to Water Drawdown" *Canadian Geotech. J.* 43(8): 802- 814.

Rao, R. A. and Nagraj, S. (1999), "Stability and Mobility of Sand Bed Channels affected by Seepage" *J. of Irrigation and Drainage Engrg.*, 125(6): 370- 379.

Sheilds, A., (1936), Anwendung der Aehnlichkeitsmechanik und der Turbulenzforschung auf die Geschiebebewegung, Mitt. Preuss. Versuchsanst. Wasserbau Schiffbau, (English translation by W. P. Ott and J. C. van Uchelen, 36 pp., U.S. Dep. of Agric. Soil Conser. Serv. Coop. Lab., Calif., Inst. of Technol., Pasadena, 1936).

Xinhua News Agency (2008), "Unstable Geology Triggers River Bank Collapse" Retrieved 13th September 2008 from China.org.cn. Website: http://www.china.org.cn/environment/news/2008-04/08/content_14512247.htm

Experimental Study of Internal Erosion of Fine Grained Soils

A. Benamar[1], A. Beaudoin[1], A. Bennabi[2], H. Wang[1]

[1]LOMC FRE CNRS 3102, University of Le Havre BP 540 - 76058 – France; email:benamar@univ-lehavre.fr; beaudoin@univ-lehavre.fr; huaqing.wang@univ-lehavre.fr
[2]GRG3, ESTP 28 Avenue Président Wilson 94234 Cachan – France ; email : abennabi@adm.estp.fr

ABSTRACT

Internal erosion has long been a major problem associated with earth structures. Laboratory experiments provide a potential insight into the processes involved. The design of dam embankments is usually based on hydraulic criteria. Some of the hydraulic criteria are based on sediment transport theory where the critical velocities are derived from the different approaches comparing the drag force of the particles and the hydraulic load. Many hydraulic criteria for suffusion are based on tests with consistent soil samples or on analytical descriptions of the particle and pore geometry derived from characteristic parameters. An experimental study of soil suffusion is performed on a laboratory column subjected to different flow conditions and soil parameters. The permeability variation along the soil column is controlled. The initiation and the kinetics of soil suffusion are investigated using a laboratory fine grained soil (mixed sand and clay) and a natural soil. Attempts are also made to assess the influence of the clay content and the type of fine particles. The results demonstrate that low hydraulic gradients can cause suffusion. The critical shear stresses for various soil tested differ slightly when the nature of grains and fines are varied. The hydraulic gradient affects the cumulative eroded mass upon a certain threshold value.

INTRODUCTION

Internal erosion takes place when water that seeps through the soil carries fines particles away from the embankment or foundation of dams. Internal erosion of soil particles is one of the most common causes for failure of the structures. This phenomenon is dangerous because it may not show external evidence that it is taking place. Natural clay in a dispersive state has been known as one of the fundamental factors that contribute to piping in earth dam and erosion of compacted soil of landfill clay liner. Internal erosion failures are often associated with penetrations of dams as outlet pipes buried in the embankment and concrete spillways that cross the embankment. Because of the embankment dams are constructed in zones of different materials, the deformations might also lead to cracks where internal erosion can be initiated. In the incidents of internal erosion, increased leakage was an evident problem. In several cases, sinkholes have formed in dams as a result of piping of well-graded core soils. These broadly-graded cores were glacial in origin with nearly linear gradations (Sherard, 1979). Filters have two basic functions, namely to prevent erosion and allow drainage of seepage water. The filtration of the silt-sized fraction is critical when soils are used for dam cores. In order to assess the stability of the broadly-graded soils, Sherard (1979) suggests splitting the gradation curve at the 1.0 mm particle size and analyzing it as two separate gradations. Vaughan and Soares (1982) suggest that permeability of the filter material should be the main measure for filter design. Kenney et al (1985) have carried out further investigations on pore size distribution of granular filters using either a theoretical or experimental approach. Sherard et al (1984) also carried out a series of experiments to evaluate the pore size of sand and gravel filters and concluded that pore sizes can be related to D_{15} size. Many studies regarding the design of filters have been done and currently Sherard and Dunnigan's (1989) results are widely used.

Before dispersion, eroded particles are significantly larger than the primary particles of the soil. This indicates that erosion occurs as aggregates of materials (Locke et al., 2000). The process of internal erosion is usually described by the initiation, continuation and progression phases. The identification of pipe development and the likely failure of the earth embankment lie in the understanding of the initiation mechanism of internal erosion. Suffusion is the process where the fine particles of the soil wash out or erode through the voids formed by coarser particles. As it takes place mainly due to the coarser particles, it can be prevented if the soil has well graded particle size distribution along with small voids. Lefebvre *et al.* (1986) investigated the influence of the natural structure of the undisturbed clay samples on the rate of erosion. They showed that the undisturbed structured clay provided much higher erosion resistance than the de-structured remoulded clay samples. Wan and Fell (2004a) used slot erosion and hole erosion tests to investigate the erosion resistance of the core material of fill dams. Both tests essentially adopted similar concepts, except that the slot erosion test possessed a longer flow channel. 14 different core materials were tested and an 'erosion rate index' was introduced to classify and grade the erosion resistance observed. A simplified approach was also proposed to assess the likelihood of internal erosion and piping in embankment dams. Wan and Fell (2004a, b) defined the variation of erosion rate assuming the erosion curves (i.e. erosion rate vs. shear stress) were linear with constant slopes. More recently, Wan and Fell (2004b) attempted multiple linear regressions to estimate the 'erosion rate index' based on the results of the hole erosion test and the slot erosion test. They proposed two equations for quantifying the rate of erosion, one for coarse-grained and the other for fine-grained soils. Sterpi (2003) performed laboratory tests and modelled the erosion and transport by combining the conservation of mass of moving particles with a suitable law of erosion, coupled with seepage equation. Gap grading in glacial deposits is a relatively common occurrence. These types of materials often have been used as construction materials for earthfill dams. Evidence between piping in dams and dykes and the presence of gap-graded materials within the structures and foundations was established (Fannin & Moffat, 2006). The gap grading does not always occur within the finest fractions of the gradation curves and is often found in the middle fractions. Often, the missing materials are the medium to coarse sands. Recent experiences with piping incidences in dams seem to correlate with the occurrence of gap-grading in glacially derived soils.

In this study we evaluate a criteria used for the soil stability against erosion. The term "suffusion" will be used to describe the mass movement of the fine fraction within the skeleton of potentially unstable soils. Suffusion tests were performed in the laboratory on reconstituted samples and embankment soil in order to assess the suitability of soil to erosion. Besides this experimental research, some attempts have been made to model the particle erosion and transport in a porous medium on the basis of numerical approach. A numerical model, based on advection-dispersion with a release term, is used to adjust the experimental results of the outlet concentration of removed fine particles.

EXPERIMENTAL PROCEDURE

The apparatus (figure 1) is typically a Plexiglas cylinder of 40 mm internal diameter and 120 mm length. The specimen rests on a lower mesh screen (80 μm opening size), supported on a perforated base plate and a large size opening mesh (1.2 mm) is used in the upper face. The specimen was reconstituted by mixing sand and clay in various proportions and deposited in the cylinder using a spoon and compacted (double compaction) at the fixed density of 1.53 g/cm^3. The fabric is believed best controlled than a natural compacted fill. Wet mixtures of graded sand and clay particles (kaolinite) in two proportions (3% and 5% by weight), whose grading is presented on figure 2, were used. The moulding water content at which the mixtures were prepared to achieve the fixed dry density was close to 6%. The prorosity of reconstituted material was close to 0,42 and the initial hydraulic conductivity was estimated from seepage tests $k=2.10^{-4}$ m/s for 5% mixture and $k=6.10^{-4}$ m/s for 3% mixture. The upward seepage flow is induced by the assigned value of the hydraulic head, which depends on the difference in elevation between the upper reservoir and the overflow valve (Fig. 3). The height of the soil sample was maintained at 12 cm in all the experiments and the column is kept vertical. Suffusion tests were performed where water height was applied rapidly in some experiments (mixture 5%) and gradually in others (mixture 3%) to study the effect of time rate of pressure application on particle mobilization. Hence, after the soil was saturated under standing water, the water height was increased until and beyond erosion starts. Upward flow through the sample is head-controlled using a laboratory supply of distilled water at about 20°C, which can be moved up in order to increase the water height. Differential pressure transducer mounted between the upstream and downstream of the soil sample establish the difference of water head, and hence the average hydraulic gradient along the specimen. Periodic measurement of volumetric discharge rate determines the corresponding hydraulic conductivity. The critical gradient obtained was 1,3 and 0,8 respectively for mixture 3% and 5%. Outlet concentrations were determined by using a turbidity meter, whose readings were correlated previously to clay concentrations in water. Particles that wash from the specimen are collected in a tank. Upon completion of testing, one specimen was extracted from the cylinder for grain size analysis (Multisizer Malvern). In order to assess the suitability to suffusion of the side dam soils, an embankment sample soil coming from an earthfill dam was tested in the same erosion apparatus. Three processes are presumed to occur simultaneously during particle transport:

Detachment of clay particles from the parent soil matrix; Transport of particles in pore water by convective-dispersive processes; Deposition of clay particles which may be trapped in some pores owing to local changes in pore flow velocities or variations in pore geometry. The removal of particles from the soil matrix into pore water suspension causes an increase in pore space, which in turn increases the permeability of the medium. If the soil sample is subjected to a constant external pressure gradient, then the flow velocity (both Darcian and seepage) increases, which in turn causes more particles to be removed. One may be led to believe that this process would continue indefinitely and wash out the sample entirely. However, the soil matrix is held together rigidly and the applied stresses can not remove more than a fraction of available fine particles.

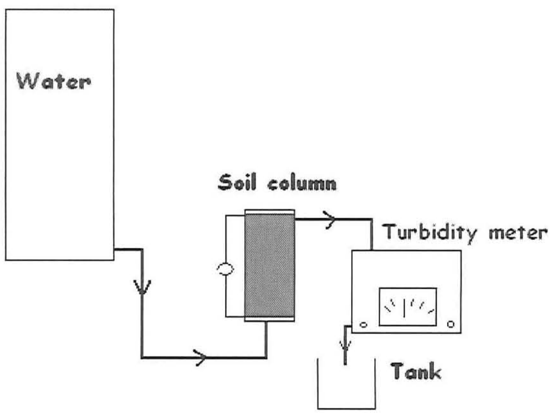

Figure 1. Drawing schema of the experimental set up

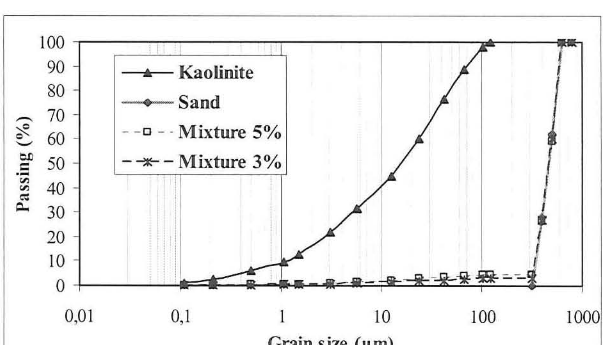

Figure 2. Gradation curves of materials and mixture

RESULTS AND DISCUSSION

Suffusion of laboratory mixed soil

In order to better understand the internal behaviour of gap-graded soils, tests were performed with different mixtures of sand and clay. Suffusion process occurs if fine particles are removed from the soil matrix and transported outlet the sample. The main objective of the test was to determine the steady-state gradients required to initiate fines migration in the soil. The erosion characteristics are typically described the critical shear stress, which represents the minimum shear stress when erosion starts. It is known (Wan and Fell, 2004) that coarse-grained, noncohesive soils erode more rapidly and have lower critical shear stresses than fine-grained soils. Knowledge of the erosion characteristics of the soil in the core of an embankment dam must help in the assessment of the likelihood of dam failure due to piping erosion.

The results of suffusion tests are analyzed using the outlet curves of measured concentration. Figure 3 below shows the concentration-time curves obtained for two mixtures (5% and 3%). The soil containing 3% of kaolinite presents earlier significant suffusion and the curve reaches rapidly a peak concentration before decreasing and then increasing to a second peak before falling to zero. The flow rate being more important (six times) in mixture 3%, the drag forces are able to mobilize in a second step more particles which remain attached in the mixture 5%. The mixture with 5% kaolinite seems to let the particles to be removed from the soil less rapidly but with more consistent duration of concentration effluent. The maximum concentration reached is close to that of 3% mixture. More residual concentration is observed over the time, showing a continuous suffusion even with a weak magnitude. This result indicates the effect of particle content in the soil on the susceptibility to suffusion and the cumulated particle removal. The 5% kaolinite curve shows an earlier slight suffusion due to an easy removal of particles in the vicinity of the outlet.

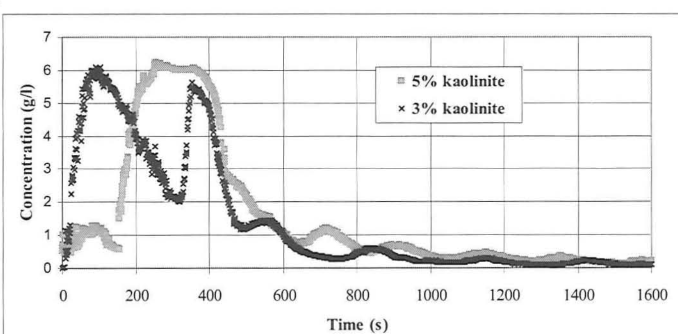

Figure 3. Concentration-time curves of two tested soil mixtures

The widely used process for determining internal instability of a soil against suffusion is that described by Kenney and Lau (1985). This method assesses the removal of the free fines under the velocity of flow. The free fines are considered here to be the kaolinite particles. Kenney and Lau suggest a method for predicting the material response based on the analysis of the "shape curve" of the material grading. This curve is drawn by plotting, for each value of grain size D, the percentage of mass having grain sizes between D and 4D (H value) versus the percentage of mass having a grain size smaller than D (F value). A shape curve lying below the suggested boundary line (H=F) indicates unstable grading. The Kenney-Lau plot of the soil with 5% of fines is shown on Figure 4. The plot indicates that the soil of mixture 5% is well below the H=F line when F is below 5 percent (fines content), indicating that this material should be internally unstable against movement of fines and vulnerable to suffusion. This material has a large gap in grain size curve (Fig. 2), yielding a $D_{15}/d_{85} = 6$ that is deemed unstable according to Sherard criteria.

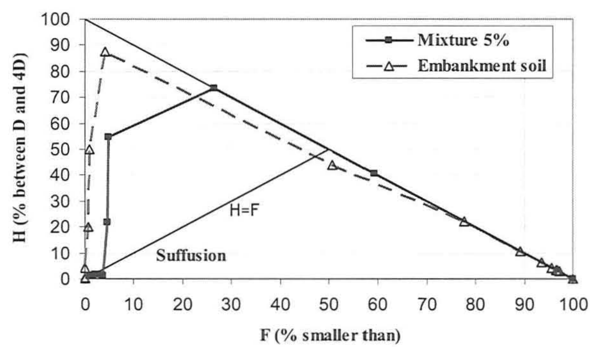

Figure 4. Plot of Kenney-Lau criteria for internal stability

Suffusion of embankment soil

In order to test a natural soil against suffusion, a sample embankment soil (a silty sand) is subjected to water flow. The hydraulic gradient was increased until the erosion was initiated (when the gradient was close to 7.5), and then the water head was maintained at steady-state and outlet concentration measured (using turbidity sensor device). Outlet flow samples are collected in order to analyse the size particles distribution using a laser multisizer (Malvern). Figure 5 shows the initial complete gradation of the soil and the gradations of the fines (<80 µm) before and after suffusion. The gradation curves of the fines show that the medium fraction of fines (sizes between 0.5 and 50 µm) was mainly removed from the soil.

The Kenney-Lau plot of the embankment soil is also presented on Figure 4. This material provide a curve which is above the line H=F, indicating that this material is internally stable against suffusion. This result is corroborated by the suffusion test where the removal of particles was started at a relatively high hydraulic gradient (i = 7,5). However, the plot indicates also that the soil is well above the H=F line when F is below 50 percent. This indicates that this material should be internally sometimes unstable against suffusion.

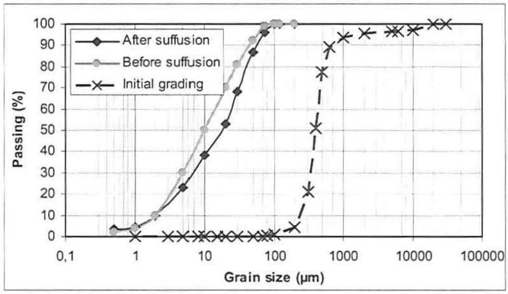

Figure 5. Gradation curves of embankment soil

MODELLING OF EROSION

The transport of suspended particles in porous media under saturated flow conditions is commonly described using the convection dispersion equation below:

$$\frac{\partial(w_c(t,x)C(t,x))}{\partial t}=\frac{\partial}{\partial x}\left(D_L(t,x)\frac{\partial(w_c(t,x)C(t,x))}{\partial x}\right)-\frac{\partial(U(t,x)w_c(t,x)C(t,x))}{\partial x}+\frac{\partial(\rho_p w_c(t,x))}{\partial t} \tag{1}$$

where w_c refers to the effective porosity, C the suspended particles concentration, $D_L=\alpha_L U$ the hydrodynamic dispersion, α_L the longitudinal dispersivity, U the pore flow velocity and ρ_p the bulk density of suspended particles. In order to take into account the processes of particle deposition and release, a kinetic of the first order is introduced:

$$\frac{\partial(\rho_p w_c(t,x))}{\partial t}=\rho_p K_{rel}(w_o-w_c(t,x))-K_{dep}w_c(t,x)C(t,x) \tag{2}$$

where w_o is the total porosity, K_{rel} and K_{dep} are the coefficients of release and deposition kinetics. The initial and boundary conditions are given by:

$$C(t=0,x)=0 \quad \text{and} \quad \frac{\partial C}{\partial x}(t,x)=0 \tag{3}$$

By introducing the new variables $S=\partial(\rho_p w_c)/\partial t$ and $C_T=w_cC$, Eq.1 can be written as:

$$\frac{\partial C_T(t,x)}{\partial t}=\frac{\partial}{\partial x}\left(D_L(t,x)\frac{\partial C_T(t,x)}{\partial x}\right)-\frac{\partial(U(t,x)C_T(t,x))}{\partial x}+S(t,x) \tag{4}$$

The particle methods are well adapted to solve the problems dominated by the advection process. By using the dispersion velocity method, the advection – dispersion equation (Eq. 4) is rewritten on the form of an advection equation (Lions *et al.*, 2001):

$$\frac{\partial C_T(t,x)}{\partial t}+\frac{\partial((U(t,x)+U_d(t,x))\cdot C_T(t,x))}{\partial x}=S(t,x) \tag{5}$$

where U_d is the dispersion velocity, obtained by identifying the previous equation with the equation (Eq. 1):

$$U_d(t,x)=-D_L(t,x)\frac{\partial(C_T(t,x))/\partial x}{C_T(t,x)} \tag{6}$$

To solve the equation (5), it has to be written in a Lagrangian framework yielding the discrete form:

$$\frac{dx_i}{dt}=U(t,x_i)+U_d(t,x_i) \text{ and } \frac{d\Omega i}{dt}=\int_{|Pi|}S(t)ds \tag{7}$$

As usual in the particle methods, the term C_T is discretized in a set of moving particles P_i defined by its location x_i and its weight Ω_i. The first equation (7) is an evaluation of characteristic lines, performed by using the explicit Euler scheme and the second equation (7) describes the temporal evolution of weight of particles, estimated by means of a simple Euler scheme. The particle methods offer the advantage to verify automatically the initial condition (Eq. 3) and the boundary conditions (Eq. 3) are satisfied by using the ghost particle method (Cleary *et al.*, 1999).

In suffusion, the processes of particle detachment, transport and deposition are assumed to occur simultaneously. In order to uncouple detachment and transport from deposition, the model is modified by making the deposition kinetics null in Eq. 2. In order to reduce the number of parameters to be adjusted, the present numerical model is arranged to model only the suffusion (release of particles). Dedicated test ("clean" suffusion) was then carried out using a thin soil sample (mixture of sand 0,8-1 mm and 2% silt) placed at the extremity of the column before a sand filter, making the flow rate homogeneous along the column. The suffusion tests with rapid pressure application (gradient close to 7) were performed on the soil with primary porosity close to 42%. The performance of the model by comparison with experimental results is discussed. The concentration-time curves and the results of cumulative mass removal are presented for model validation. The concentration-time curves indicate that the amount of removed particles is influenced by fines content significantly. Fig. 6(a) shows experimental and numerical results of concentration-time curve and Fig. 6(b) shows the cumulative amount of particle removed as a function of time. A good agreement is obtained, even if the numerical peak concentration being slightly greater than the measured one. Both the experimental and numerical curves (fig. 6a) show the initial steep rise in concentration resulting from the imposed hydraulic gradient rate and the abrupt drop in concentration once the pressure is maintained steady. Consequently, soil detachability is very high. The numerical and experimental curves of the cumulative particles removed from the soil sample (fig. 6b) show a fast initial removal which slows down once the pressure remains constant. The fast rise and fall of the concentration are well captured by the numerical curve. The results indicate that the rate of particle removal reaches a constant asymptotic value. The numerical cumulative particle removal overestimates slightly the experimental concentration. These results indicate that the model proposed shows promise for future development and application in particle transport at the laboratory scale.

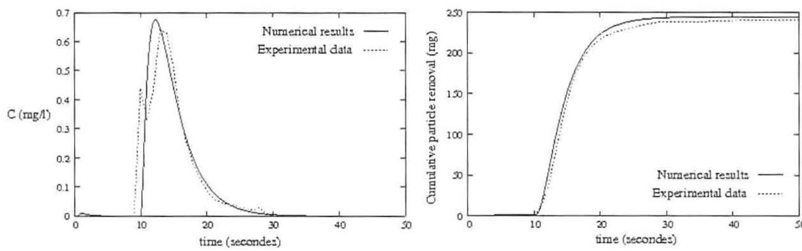

(a) (b)

Figure 6. Numerical and experimental concentration-time curves (a) and cumulative particle removal (b) for coarser soil sample with initially 2% silt subjected to rapid pressure application.

SUMMARY AND CONCLUSIONS

This paper dealt with the results of an experimental investigation of the suffusion of gap-graded soils and the development of a numerical model simulating particle removal in laboratory columns subjected to external gradients. This study shows that gap-graded materials often suffer internal erosion at relatively low hydraulic gradient. The process of suffusion can produce high gradient within internally unstable materials. The potential for instability is governed by the shape of the grain size distribution curve, which may be quantified using the split gradation method according to Sherard (1979) and evaluated with the ratio D_{15}/d_{85}. The mixed soil with this ratio close to 6 exhibited internal instability at relatively low gradient. The analysis of outlet concentration-time curves for soil mixtures with different clay content allows concluding about the influence of fines content on the erosion rate and the initiation of the process. The sample subjected to a rapid pressure application exhibited the initial steep rise in concentration and the abrupt drop, while the test performed with gradual pressure application shows a steady-state concentration at outlet before decreasing progressively.

Comparison of model and experimental results indicated a quite good agreement. These results indicate that the model proposed shows promise for future development and application in particle transport at the laboratory scale. However, this model is applicable to homogeneous soils at the laboratory column scale.

ACKNOWLEDGMENTS
This study is part of a French national research program ERINOH (ERosion Interne des Ouvrages Hydrauliques).

REFERENCES

Becker, D.E., Crooks, J.H.A., Been, K., and Jefferies, M.G. (1987). "Work as a criterion for determining in-situ and yield stresses in clays." *Canadian Geotech. J.* 24 (4): 549-564.

Cleary, P.W. and Monaghan, J.J. (1999). "Conduction modeling using smoothed particle hydrodynamics." *J. Computational Physics* 148: 227-264.

Cottet, G.H. and Koumoutsakos, P. (2000). "Vortex Methods Theory and Practice". Cambridge University Press.

Fannin, R.J., Moffat, R., (2006). "Observations on internal stability of cohesionless soils", *Geotechnique* 56 (7), 497-500.

Fell, R., Wan, C. F., Cyganiewicz, J. & Foster, M., (2003). "Time for development of internal erosion and piping in embankment dams." *J. Geotech. Geoenviron. Engrg.* 129(4), 307-314.

Kenney, T. C., Chahal, R., Chiu, E., Ofoegbu, G. I., Omange, G. N. & Ume, C. A., (1985). "Controlling constriction sizes of granular filters." *Canadian Geotech. J.* 22(1), 32-43.

Lefebvre, G., Rohan K., Douville S., (1985). « Erosivity of natural intact structured clay : Evaluation.» *Canadian Geotech. J.* 22, 508-517.

Lions, P.L and Mas-Gallic, S. ,(2001). "Une méthode particulaire déterministe pour des equations diffusives non linéaires." *C.R. Acad. Sci.* Paris 332 (série 1): 369-276.

Locke, M., Indraratna, B., Cummins, Philips, and Adikari, G., (2000). "Embankment Dam Rehabilitation", *ANCOLD 2000 Conference on Dams*.

Sherard, J. L., (1979). "Sinkholes in dams of coarse, broadly graded soils." *13th Int. Congress on Large Dams*, New Delhi, Q49, R2, 25-35. International Commission on Large Dams, Paris.

Sherard, J. L. & Dunnigan, L. P., (1989). "Critical filters for impervious soils." *J. Geotech. Engrg.* 115(7), 927-947.

Sherard, J. L., Dunnigan, L. P. & Talbot, J. R., (1984). "Basic properties of sand and gravel filters." *J. Geotech. Engrg.* 110(6), 684-700.

Sterpi, D., (2003). "Effects of the Erosion and Transport of Fine Particles due to Seepage flow", *Int. J. Geomechanics*, 3 (1), 111-122.

Vaughan, P.R., and Soares, H.F. (1982). "Design of filters for clay cores of dams." *J. Geotech. Engrg.* 108: 17-33.

Wan, C.F. and Fell, R. (2004a). "Investigation of rate of erosion of soils in embankment dams." *J. Geotech. and Geoenvir. Engrg.* 30 (4): 373-380.

Wan, C.F. and Fell, R. (2004b). "Laboratory tests on the rate of piping erosion of soils in embankments dams." *Geotech. Testing J.* 27 (3).

Effect of Suffusion on Mechanical Characteristics of Sand

Nathan Shwiyhat, P.E.[1] and Ming Xiao, Ph.D., P.E.[2]

[1] Project Engineer of BSK Associates and Graduate Student at California State University, Fresno, CA., USA. Email: nshwiyhat@bskinc.com.
[2]Assistant Professor, Department of Civil and Geomatics Engineering, California State University, Fresno, CA., USA. Email: mxiao@csufresno.edu. Phone: (559) 278-7588.

ABSTRACT

The mechanical characteristics of earth dams and levees, such as settlement, permeability, and strength, can be affected by internal erosion in the forms of piping and suffusion. This paper reports a preliminary experimental study on the changing mechanical characteristics (permeability, consolidation) with the progression of suffusion of a sandy soil. The internal erosion tests are conducted using a triaxial apparatus. The pedestal of the triaxial cell is modified to allow seepage and eroded soil particles to exit the specimen into an effluent tank. The seepage is induced in the specimen by controlled constant hydraulic gradient. The eroded soils are collected in the effluent tank so that the erosion rate and extent can be measured. Variations of the specimen's permeability and volume during the erosion are recorded. With approximately 5.5% fines in the sand, the test suggests that suffusion can occur and cause soil settlement. Suffusion of finer particles may also clog the downstream soil layer and results in permeability reduction. Suffusion and volume reduction gradually diminish relatively quickly to an un-measurable level after 4hr of seepage through the soil under a hydraulic gradient of approximately 20.

INTRODUCTION

Internal erosion can have devastating consequences to earthen, hydraulic structures. A survey of 11,192 dams revealed that 136 dams showed signs of damage and 46% of those damaged were related to internal erosion (Foster et al., 2000). During Hurricane Katrina, three levee breaches were possibly caused by underseepage-induced failure due to piping (Seed et al., 2008a, 2008b; Sills et al, 2008). Internal erosion can be divided into two main forms: piping and suffusion (if neglecting dispersion). Piping is a process of soil particles being mobilized and then transported downstream along a flow path by flowing water. The eroded soils result in a tubular pipe that progresses upstream in the soil matrix. The erosion could lead to the sudden collapse of the structure and consequently massive flooding and devastation in the downstream.

The other form of internal erosion is suffusion, which is the migration of fine soil particles within a coarser soil matrix, or soil skeleton. Suffusion usually occurs in soil matrices that are sufficiently coarse to permit the movement of fines in the constrictions formed between particle contact points. Wan and Fell (2008) reported that more porous soil structures allow more readily for suffusion. Additionally, they found that soils with plastic fines require larger hydraulic gradients for erosion to occur. The fines susceptible to transport are those entirely contained within the pores of the coarser structure and may not support effective stress, as the coarse structure carries external loads. In order for the coarse structure to behave as a load-supporting skeleton, the fine particles must be scarce enough in quantity so they do not fill the voids entirely within the coarse skeleton (Wan and Fell, 2008). Suffusion, though less catastrophic in terms of potential failure mechanisms, can be chronically destructive. Suffusion commonly results in the clogging of soil filters or drainage layers and lead to the presence of excess pore water pressure. Suffusion may also result in increased porosity, permeability, seepage, and accentuated consolidation of a soil layer or earthen structure. Experimental research by Wan and Fell (2004) found that "...50% of the finer fraction as defined by the point of inflection of broadly graded soils and the fine limit of the gap in gap-graded soils can be eroded" by suffusion in internally unstable soils. Suffusion and the subsequent void ratio increase could cause settlement. More research has been focused on when, where, and why internal erosion can occur but less on the lasting mechanical effects of internal erosion, particularly the effect of suffusion on the settlement potential of a soil stratum due to the loss of fine particles within the soil skeleton.

To model the in-situ stress conditions, triaxial tests can be used to study suffusion and piping. Sanchez et al. (1983) were the first researches to evaluate the erosion potential of embankment core materials using triaxial erosion tests. The recent experiments by Bendahmane et al. (2008) revealed the complex effects of confining pressure on suffusion. The true triaxial tests by Richards and Reddy (2008) preliminarily indicated the confining stress and pore pressure are critical to piping initiation. This research employs the similar experimental design of triaxial erosion tests and focuses on the effect of suffusion on the mechanical behaviors of a sandy soil.

MATERIALS AND METHODOLOGY

A poorly-graded sandy soil is tested. The sand was obtained from a local aggregate mining company operating on the San Joaquin River in Fresno, California. Kaolinite was added to, and evenly mixed in the sand at a ratio of 2.5% (by dry mass), so that the fine particles may be subjected to suffusion. The gradation is presented on Figure 1. The total fine content (passing U.S. #200 sieve) in the mixed soil is approximately 5.5%. Modified proctor test (ASTM D-1557) performed on the mixed sample found a maximum dry density of 1.867 g/cm^3 (or 116.5 lb/ft^3) at an optimum moisture content of 9.5%. Additional information pertaining to the river sand and the Kaolinite clay used in this experiment is contained in Table 1.

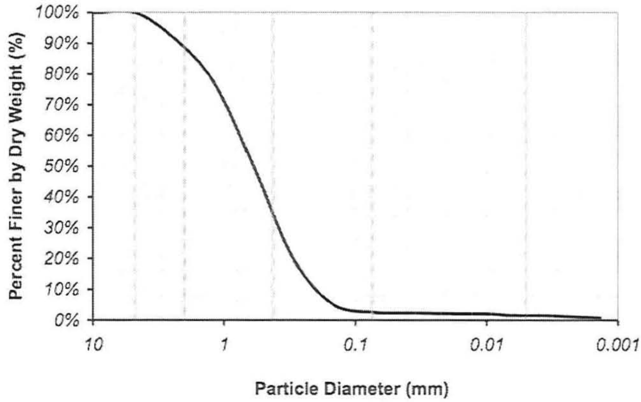

Figure 1 – Grain size distribution of the sandy soil with 2.5% Kaolinite

Table 1 – Soil properties

Soil Gradation	Poorly Graded Sand (SP)	Kaolin (CL)
% Coarse Sand Fraction	12	--
% Medium Sand Fraction	55	--
% Fine Sand Fraction	30	--
% Silt	1	24
% Clay (Clay Sized)	2	76
D_{10} (mm)	0.21	--
D_{30} (mm)	0.39	--
D_{60} (mm)	0.77	--
Coefficient of Uniformity, C_u	3.7	--
Coefficient of Gradation, C_c	0.94	--
Specific Gravity	2.69	2.61

The suffusion tests are conducted using a triaxial apparatus, which is modified to allow effluent water and eroded soil particles to exit the cell and be captured in an effluent tank. The effluent tank can be pressurized to simulate any reasonable downstream pressure. For this test the downstream pressure was maintained at atmospheric pressure. During the suffusion process, the change in total specimen volume is monitored by a Volume Change Transducer Unit (VCU) connected to the cell water supply. Figure 2 provides a photo diagram of the test setup and Figure 3 illustrates the details of the modifications to the triaxial cell base pedestal. The base pedestal is connected to the bottom of the triaxial cell and then to a large control valve that is located on the bottom of the base, outside of the cell. The top portion of

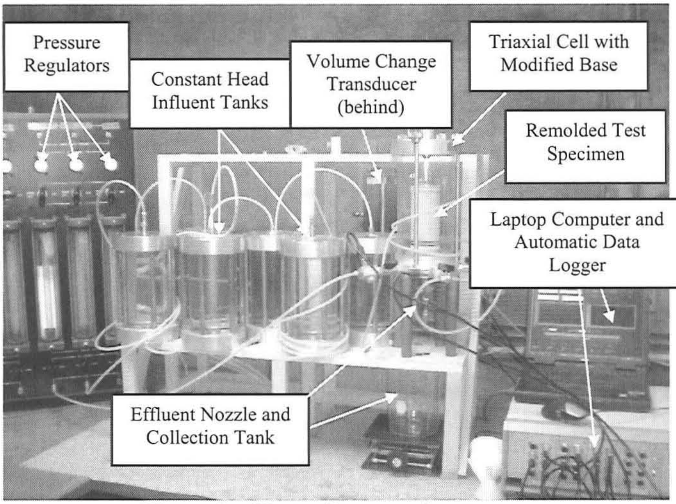

Figure 2 – Photo diagram of test setup

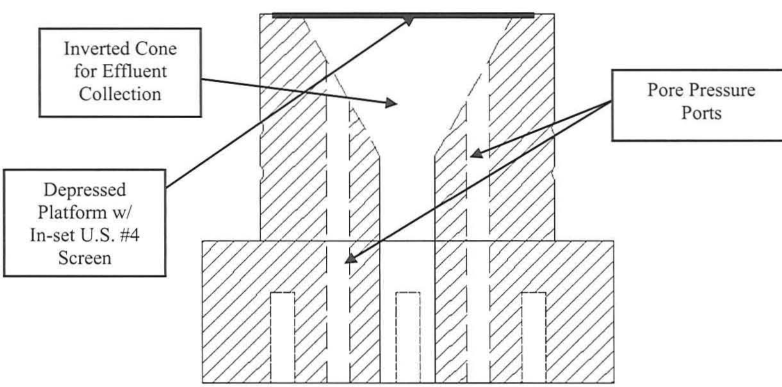

Figure 3 – Details of modifications to triaxial base pedestal

the pedestal is bored out in the shape of an inverted cone and funnels into a large port that connects to the control valve. A U.S. #4 screen (4.75mm) is set into a depressed platform on the top of the pedestal to support the remolded specimen while permitting unrestricted drainage. The screen is intended to support the specimen during the undrained compression test that follows the internal erosion test to examine the strength reduction due to suffusion. Due to the page limit of this paper, compression test results are not reported.

A specimen of 5.11 cm (or 2 inch) in diameter and 10.22 cm (or 4 inch) in height is remolded to 85% of the maximum dry density at the optimum moisture content. The specimen is saturated with de-aired, deionized water under pressure applied through a pneumatic bladder that pressurizes the de-aired water. The specimen is maintained at an effective stress of 13.8 kN/m^2 (or 2 psi) during the saturation process until a minimum "B" value of 0.95 is obtained. Bendahmane et al. (2008) found that for clay-sand mixtures, there first exists a critical gradient at which suffusion of the fine clay particles occurs and as the gradient is increased, there also exists a second critical gradient at which the sand structure is eroded by piping (backward erosion). Our previous tests found that at the critical gradient for piping, the sandy specimen typically collapsed upon the initiation of piping. The goal of this research sets out to quantify the sustained mechanical changes in soil due to suffusion, so the testing is carried out at a gradient less than that required for the initiation of piping of the sand matrix. After saturation is reached, the specimen is subjected to a constant downward hydraulic gradient of approximately 20.8. The effluent is continuously collected during the erosion process at predetermined volume intervals. The total volume change of the specimen is continuously monitored via the VCU. Permeability of the specimen is frequently measured with the collected effluent volume. The erosion is continued until the effluent water visually clears up. From each collected effluent with eroded soils, the volume of effluent is recorded and then the entire contents are oven dried and weighed to determine the mass of the eroded material to the nearest one-thousandth of a gram.

RESULTS AND DISCUSSION

The permeability, erosion behavior, and volumetric behavior of the specimen are monitored during the entire erosion test, which runs for 250min. The results are provided in the following sections.

Permeability Behavior

During the erosion test, the permeability of the specimen generally decreased as the suffusion continued (Figure 4). Approximately one order of magnitude in permeability reduction was observed. Several other researchers have reported similar permeability reductions in the presence of suffusion. The permeability reduction is due to the clogging of constrictions between soil solids by eroded fines. The decreased diameters of the pore throats result in a decreased porosity (perhaps across only a thin and limiting layer at the bottom of the specimen), reducing the overall permeability of the entire specimen.

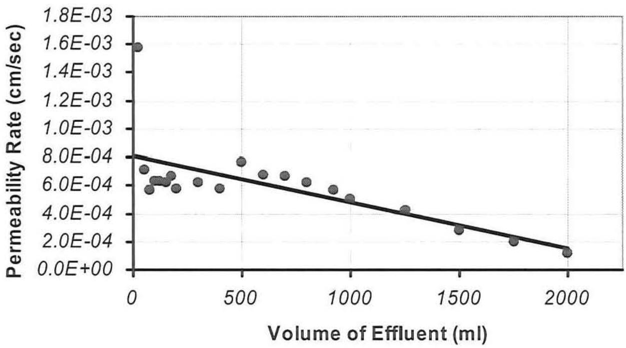

Figure 4 – Permeability variation with effluent volume

Suffusion Behavior

The suffusion rate also decreased as the test progressed. In total, 1.510 gram of soil solids were eroded during the testing. This is approximately 0.5% of the dry mass of the specimen. Figure 5 shows the total mass of eroded soils with respect to time and Figure 6 shows the concentration of the eroded solids in the effluent with respect to the total volume of effluent. Since the fine solids that are contained loosely within the pore structure of the coarse skeleton are more susceptible to suffusion, an asymptotic trend (shown in Figure 5) is expected — as the fines are gradually washed out, the coarse skeleton remains. Additionally, with decreasing size of pore throat constrictions due to the likely particle clogging at the downstream section of the specimen, suffusion gradually diminishes until no solids are washed out, as indicated in both Figures 5 and 6.

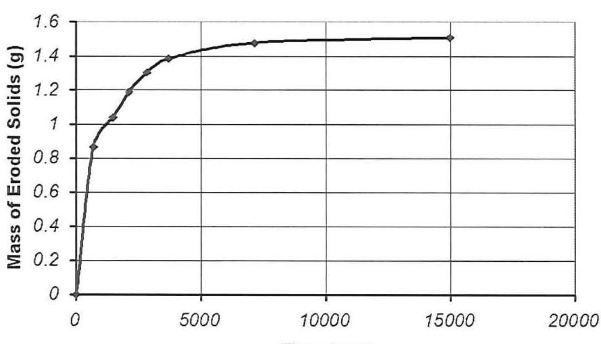

Figure 5 – Eroded mass versus time

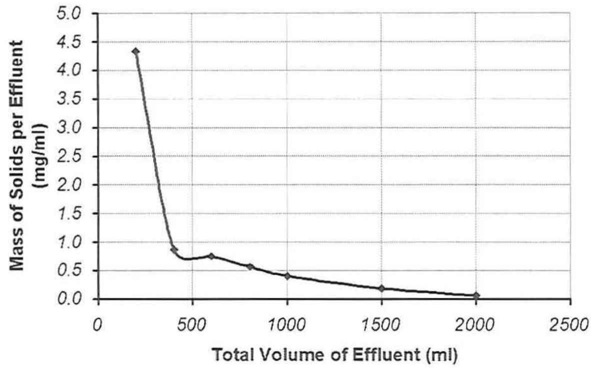

Figure 6 – Concentration of soil solids in effluent versus total effluent volume

Volumetric Behavior

As internal erosion occurs, the specimen volume decreases. Figures 7 and 8 show the total specimen volume reduction (in percentage of initial total specimen volume) with time and effluent volume, respectively. Also presented in both figures are the calculated specimen volume, which is based on the volume of the eroded particles and the pore volume that the eroded particles may construct. In the calculated volume prediction, it is assumed that the void ratio of the eroded fines (when they construct pores) is the same as the average void ratio of the entire specimen. Figures 7 and 8 both suggest that the extent of volume reduction appears to be minor, which is comparable to the degree of suffusion that occurred in the experiment — this test suffered only approximately 0.3% volume reduction due to an approximately 0.5% eroded soil mass. The results show that the volume change stabilizes in the early stage of the test while the suffusion continued throughout the test. It could be because loose and unsupported large particles near the base of the specimen eroded first, causing relatively large reduction in volume at the beginning of the test. After that, suffusion of finer particles did not cause measurable volume change. It is also learned from this exploratory tests that volume change due to suffusion may also depends on percentage of fine contents. Apparently 5.5% fines (< 0.075 mm) in the specimen caused little volume reduction as a result of the fines suffusion. Our ongoing experiments using the same methodology employ a smaller screen (U.S. #10 sieve, instead of #4 sieve) at the bottom. The new tests showed the volume reduction trend becomes shallower and volume reduction parallels the suffusion throughout the test (Shwiyhat, 2010). The results found a similar volume reduction (0.26%) with only 0.15% decrease in sample mass.

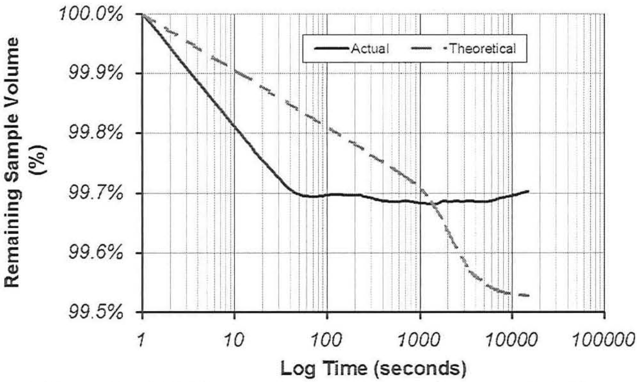

Figure 7 – Relative specimen volume with respect to time

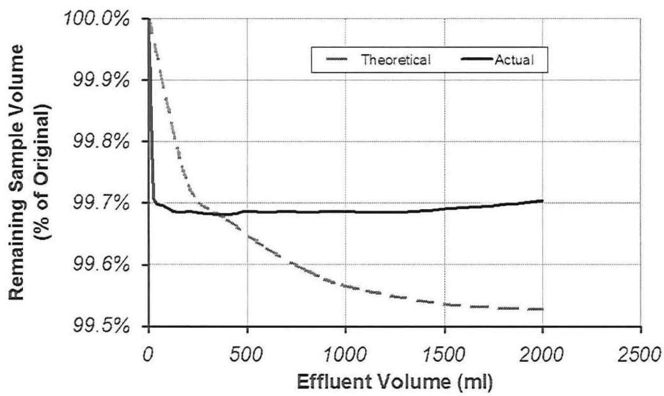

Figure 8 – Relative specimen volume with respect to total effluent volume

CONCLUSIONS

This paper presents the findings of a preliminary experimental investigation on the mechanical behaviors of a sandy soil that is subjected to suffusion. With approximately 5.5% fines in the sand, the test suggests that suffusion can occur and cause soil settlement. Suffusion of fine particles may also clog the downstream soil layer and results in permeability reduction. In this experiment, suffusion and volume reduction gradually diminish relatively quickly to an un-measurable level after 4 hours of seepage through the soil under a hydraulic gradient of approximately 20. A systematic experimental program by the authors, following the same methodology presented in this paper, continues to verify the preliminary findings through testing of poorly graded and gap-graded soils with various fine contents.

ACKNOWLEDGEMENT

The authors thank the support of this research by California State University, Fresno.

REFERENCES

Bendahmane, F., Marot, D., Alexis, A. (2008). "Experimental Parametric Study of Suffusion and Backward Erosion." *Journal of Geotechnical and Geoenvironmental Engineering,* 134 (1): 57-67

Foster, M., Fell, R., and Spannagle, M. (2000). "The Statistics of Embankment Dam Failures and Accidents." *Canadian Geotechnical Journal*, 37(5): 1000-1024.

Richards, K.S., and Reddy, K.R. (2008). "Experimental investigation of piping potential in earthen structures." Geosustainability and Geohazard Mitigation, Proceedings of GeoCongress 2008, ASCE Geotechnical Special Publication No. 178, 367-376. Reddy et al. (Ed). ASCE Geo-Institute.

Sanchez, R.L., Strutynsky, A.I., and Silver, M.L. (1983). "Evaluation of the erosion potential of embankment core materials using the laboratory triaxial erosion test procedure." Tech. Rep. GL-83-4, Army Engineer Waterways Experiment Station, Vicksburg, MS, Geotechnical Lab, Apr 1983.

Seed, R. B., Bea, R.G., Abdelmalak, R. I., Athanasopoulos-Zekkos, A., Boutwell, G.P., Bray, J.D., Cheung, C., Cobos-Roa D., Ehrensing, L., Harder Jr., L.F., Pestana, J.M., Riemer, M.F., Rogers, J.D., Storesund, R., Vera-Grunauer, X, ; and Wartman, J. (2008a). "New Orleans and Hurricane Katrina. II: the central region and the lower Ninth Ward." *ASCE J. of Geotechnical and Geoenvironmental Engineering*, 134(5): 718-739.

Seed, R. B., Bea, R.G., Abdelmalak, R. I., Athanasopoulos-Zekkos, A., Boutwell, G.P., Bray, J.D., Cheung, C., Cobos-Roa D., Cohen-Waeber, J., Collins, B.D., Harder Jr., L.F, Kayen, R.E., Pestana, J.M., Riemer, M.F., Rogers, J.D., Storesund, R., Vera-Grunauer, X, ; and Wartman, J. (2008b). "New Orleans and Hurricane Katrina. IV: Orleans East Bank (Metro) Protected Basin." *ASCE J. of Geotechnical and Geoenvironmental Engineering*, 134(5): 762-779.

Shwiyhat, N. (2010). "Effect of Suffusion on Mechanical Characteristics of Sand." MS thesis, Department of Civil and Geomatics Engineering, California State University, Fresno, Dec 2010.

Sills, G.L., Vroman, N.D., Wahl, R.E., Schwanz, N.T. (2008). Overview of New Orleans levee failures: lessons learned and their impact on national levee design and assessment. *ASCE Journal of Geotechnical and Geoenvironmental Engineering,* 134(5): 556-565.

Wan, C. F., Fell, R. (2004). "Investigation of Rate of Erosion of Soils in Embankment Dams." *Journal of Geotechnical and Geoenvironmental Engineering*, 130 (4): 373-380.

Wan, C. F., Fell, R., (2008). "Assessing the Potential of Internal Instability and Suffusion in Embankment Dams and Their Foundations". Journal of Geotechnical and Geoenvironmental Engineering, 134 (3): 401-407.

Hydraulic Erosion along the Interface of Different Soil Layers

R. Beguin[1], Y.-H. Faure[1], C. Guidoux[1,2], P. Philippe[3]

[1]Laboratoire d'étude des Transferts en Hydrologie et Environnement, University of Grenoble, BP53, 38 041 GRENOBLE Cedex 09, France ; email: remi.beguin@ujf-grenoble.fr
[2]Geophyconsult, Savoie Technolac BP. 73377 LE BOURGET DU LAC Cedex; email : cyril.guidoux@geophyconsult.com
[3]CEMAGREF, Aix-en-Provence, France ; email : pierre.philippe@cemagref.fr

ABSTRACT

Contact erosion occurs at the interface of two different soil layers when particles of the finer layer are removed by the flow and transported through the pores of the coarser layer. Whenever this kind of internal erosion occurs in embankment dams, dykes or in their foundations, severe consequences are likely. As contact erosion may be seen as a type of surface erosion, river erosion models have been used by previous authors to model this phenomenon, mainly for contact between sand and gravel layers. Thanks to a specific experimental device, these results are extended to finer soils, broadly-graded, made of clays, silts and sands. The available data for contact erosion is sum-up and the adequate laws for different situations are underlined. Then, the concept of erosion threshold, useful to evaluate dykes' safety, is discussed and linked with the erosion variability and evolution with time.

INTRODUCTION

At the interface between two different soil layers submitted to groundwater seepage, contact erosion is likely. Particles of the finer layer may be destabilized by the water flow and transported through the pores of the coarser layer. This requires two conditions. First, the coarse layer has to be geometrically open to the other layer, that is to say, to have pores sufficiently large so that fine particles can pass through them. Previous authors have tried to quantify this condition in terms of ratio of the grading of both soils and call it a filter criterion (Sherard et al., 1984). Second, the flow has to be sufficient to detach the particle but also to transport it. This is the hydraulic condition for erosion. The construction of earth embankment in fluvial valleys is a typical situation in which a coarse alluvial foundation can be in contact with a finer soil which constitutes the core of an earth structure. Nowadays, the filter criterion is normally fulfilled for the construction of new hydraulic structures, but the length of dykes often obliges the use of in-situ material and sometimes this material is not ideal. Moreover, many older dykes have been built without consideration of the filter criterion and no one knows how they will behave.

Therefore, contact erosion may be an important safety risk for dykes. This kind of erosion has been studied in the context of seaside dykes by various authors from the Netherlands (Bezuijen et al., 1987; Den Adel et al., 1994) and by (Brauns, 1985; Wörman et al., 1992). They usually consider the case of sand erosion, in the configuration of a coarse layer above a fine layer that will be called "Configuration

1" in this paper. This does not correspond to the majority of river dykes, usually made of a silt or clay core in contact with gravel layers, with the fine layer above the coarse layer, called here "Configuration 2". In this context, the work done by (Schmitz, 2007) provides measured flow velocities initiating erosion of a silt layer above a gravel layer. Nevertheless, the phenomena implicated seem to not be completely understood, and the model proposed by Schmitz only gives a tendency, without explaining all the variability of its data. Extrapolation of these results has to be done with caution.

To evaluate the safety of a dyke where interfaces without geometrical filter criteria are identified, it is fundamental to determine what is the hydraulic loading which will activate the erosion and what is the celerity of the process. Therefore, a suitable experimental device has been set-up to generate contact erosion in the laboratory, in order to identify the key phenomena involved, to quantify the process, and to determine the parameters controlling the erosion. This study focus on the layout of a horizontal interface separating two soil layers which do not verify the geometrical filter criteria. The global water flow is horizontal and tangent to the interface. Sand erosion was considered to compare the results to previous works, but also silt, clay and mixtures closer to soils that can be found in dykes have been used.

Experimental device

The experimental device is similar to the apparatus used by (Brauns, 1985) and (Schmitz, 2007). A granular interface is submitted to a control flow in order to produce contact erosion (see Figure 1).

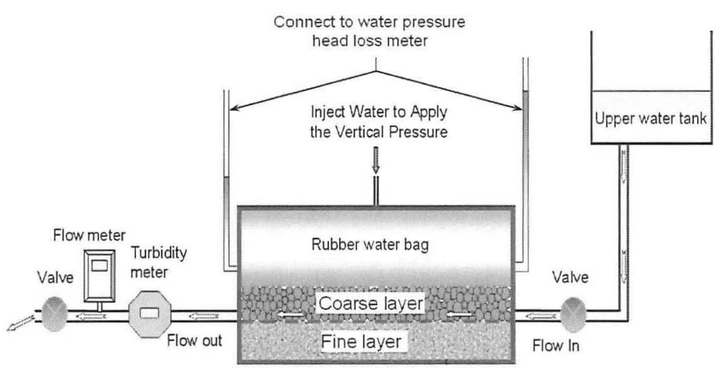

Figure 1. Experimental device set-up for Configuration 1 (the fine layer is above the coarse layer for Configuration 2)

A sample constituted of a fine soil layer and a coarse soil layer is set up in a steel cell of 300 x 700 x 265 mm. The fine soil is prepared at the Proctor optimum water content and compacted to reach a density of 90% of the Proctor maximum density. A rubber bag is put inside the cell, on the sample, and enables to apply a controlled static load. A constant hydraulic head is applied at the entry of the cell which is connected to a hydraulic system by two openings 5 mm height along the width of the cell. The sample is set-up so that the openings of the cell (inlet and outlet) coincide with the coarse layer and so that the flow is tangent to the fine soil surface. As the flow is considered to be influenced by boundary conditions at the entry and the exit, two pieces of geotextile inhibit erosion in these areas. The head loss in the sample is measured by a differential pressure sensor connected to the cell. A flowmeter and a turbidimeter are set up at the exit of the cell. The turbidity measurement is an estimation of the sediment concentration in the effluent, which indicates the amount of fine particles eroded and transported by the flow. Samples of the effluent were regularly taken in order to track the evolution of the grading of the eroded soil. One side of the cell is made from window glass, so that the interface can be observed during erosion process. However, this observation is limited to a small zone close to the window, influenced by side effects.

The fine soils tested are a uniformly graded sand (d_{50}=250μm, Cu=1.7), a broadly-graded silt (d_{50}=56μm, Cu=6), Illite (d_{50}=4μm, Cu=5.3), and gap-graded mixtures of 10% and 20% Illite with sand, with $Cu=d_{60}/d_{10}$ and d_x, the x%-percentile of the soil grain-size. The coarse soils tested are 4 different uniformly graded gravels (Cu < 2) with (D_{50}=3, 5.2, 9 and 17mm). Each gravel has been tested in combination with each fine soil, with 8 repetitions of the tests with the silt and between 1 and 3 repetitions for the other fine soils.

State of the art and theoretical framework

During contact erosion, focusing on one pore of the coarse layer just above the top of the fine layer (see Figure 2), we are confronted with a problem of surface erosion of the fine particles by the flow which develops into the pore.

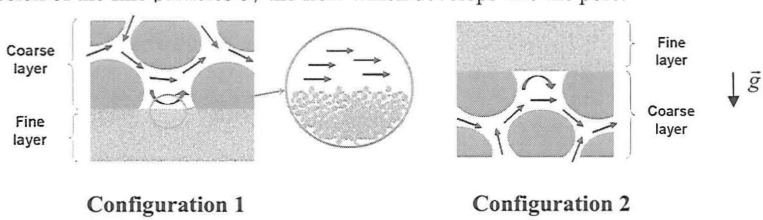

Figure 2. Contact erosion as a particular surface erosion ($\vec{g}$ is the gravity)

This phenomenon can be related to classical surface erosion in river context for example, but with many specificities linked to the presence of a coarse layer. The first difference is the characteristics of the flow, which can freely develop in a river but have to follow the numerous changes in section and direction of a pore. Second, a part of the fine layer surface is in direct contact with the coarse layer particles. This area is not directly submitted to the flow but is subjected to the stresses transmitted by the granular skeleton, mainly the weight of the soil column above the interface. Then, the coarse particles are obstacles to the flow, and also obstacle to the transport of the fine particles, and a straining mechanism can develop, enhance by electrostatic effects. Finally, contact erosion may appear with the fine layer above the coarse layer (Configuration 2, see Figure 2). Consequently, as the fine soil is eroded from below, the gravity is a destabilizing force for the fine particles and contributes to erosion at the opposite of the classical surface erosion. The methodology used by previous authors to model contact erosion is usually to adapt erosion law elaborated for surface erosion to this particular configuration. For example, to estimate the initiation of erosion, Bezuijen proposed an adaptation of classical (Shields, 1936) criterion in a similar manner than Brauns (Bezuijen et al., 1987). To calculate the shear stress on a particle, he considers that the shear velocity $u^* = \tau/\rho$ is linearly function of the pore velocity, e being the coefficient which link these velocities. He obtains a critical bulk velocity for erosion initiation (equation 1).

$$u_{cr} = \frac{n}{e}\sqrt{\theta}\sqrt{\left(\frac{\rho_s - \rho_w}{\rho_w}\right) g d_{50}} \tag{1}$$

With u_{cr} (m/s) the erosion initiation bulk velocity, n the porosity of the coarse layer, e an empirical parameter, θ the Shields parameter, ρ_s (kg/m3) the specific mass of the grains, ρ_w (kg/m^3) the specific mass of the fluid, d_{50} (m) the 50% percentile of the fine soil size distribution curve and g (m/s^2) gravity. Bezuijen's proposal of using an empirical parameter e illustrates that the main difficulty to adapt surface erosion law to contact erosion is to evaluate the hydrodynamic loading on the particle of the fine soil (Bezuijen et al., 1987). Next, to quantify the erosion and the celerity of the process, Wörman, starting from the Shields criterion, proposed a power law adjustment to model erosion transport (Wörman et al., 1992). With the same objective, Den Adel chose to use statistical distributions to model the hydraulic loading and the particles stability (Den Adel et al., 1994). All these studies have been established and are valid for sand erosion when the coarse layer is above the fine layer. If finer soils are considered as silt or clay, or if the fine soil is above the coarse soil, many differences appear. First, the adhesive forces will play an important role which is not taken into account in the previous models. In this case, it is proposed (Guidoux et al., 2010) to modify Brauns formula in order to extend the validity of this law for silts by adding a term which considers these adhesive contributions (equation 2).

$$u_{cr} = 0.7n\sqrt{\left(\frac{\rho_s - \rho_w}{\rho_w}\right) g d_H \left(1 + \frac{\beta}{d_H{}^2}\right)} \tag{2}$$

With d_H (m) the effective diameter proposed by (Kozeny, 1953), which conserves the specific area of the grading, and β (m^2) a coefficient function of the adhesive properties of the particles considered. Moreover finer particles will be transported by suspension in the coarse layer unlike sand which is transported by bedload. Bedload transport implies a shielding effect which limits erosion as the amount of sand transported increase. After a given length, the quantity of sand transported will reach equilibrium. For finer particles transported by suspension, this effect is very weak and usually no equilibrium is reached until the exit of erosion zone. In consequence, the transport model proposed by Wörman and Den Adel cannot be applied for silt and clay (Den Adel et al., 1994; Wörman et al., 1992). Transport concentration in the fluid is not enough high to reduce erosion. In this case, existing surface erosion model can be adapted (Bonelli et al., 2006). This model is a threshold law expressed in terms of shear stress applied to the eroded soil of the form:

$$\begin{aligned} &\varepsilon = k_{er}(\tau - \tau_c) \quad si \quad \tau > \tau_C \\ &\varepsilon = 0 \quad si \quad \tau \leq \tau_C \end{aligned} \tag{3}$$

k_{er} (s/m) is the coefficient of erosion which characterizes the kinetic of the phenomenon, τ (Pa) is the shear stress applied by the flow on the interface, τ_C (Pa) is the threshold shear stress of the fine soil and ε (kg/s/m^2) is the erosion rate per unit time and surface eroded. The shear stress is estimated by measuring the gradient i in the coarse layer, and evaluating its specific area A_s thanks to the size distribution curve and empirical formula, or deduced from permeability (equation 4).

$$\tau = \frac{n\rho_w g i}{A_S} \tag{4}$$

This expression correlates well to data obtained with our apparatus (see Figure 3).

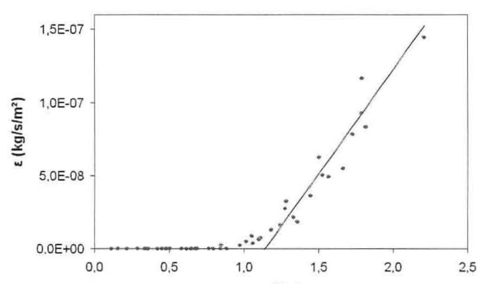

Figure 3. Experimental data for one couple fine soil/coarse soil and application of equation (3)

For the configuration 2, formula based on Shields criterion cannot be used. As the gravity has an opposite contribution, the phenomena involved are different and Schmitz proposed a model with two contributions: the mechanical shear resistance of the soil and the equilibrium of the soil consider as a dense fluid over the water (Schmitz, 2007). If the interface remain well define during the erosion process, erosion law of type (3) could also be used. In both configurations, fine layer above or below the coarse layer, the fine particles need to be transported trough the pores of the coarse layer after being detached. If not, the fine particles will accumulate until blocking the coarse layers pores. Transport of fines in a porous medium is a complex phenomenon which has been widely studied for many applications. It implies to take into account the hydrodynamic loading on the particle which will move the particle but also the possible trapping of the particle, geometrically in a small pore, hydraulically in a slow velocity zone, or by adhesion to the coarse grains, especially for clay with electrically charged particles.

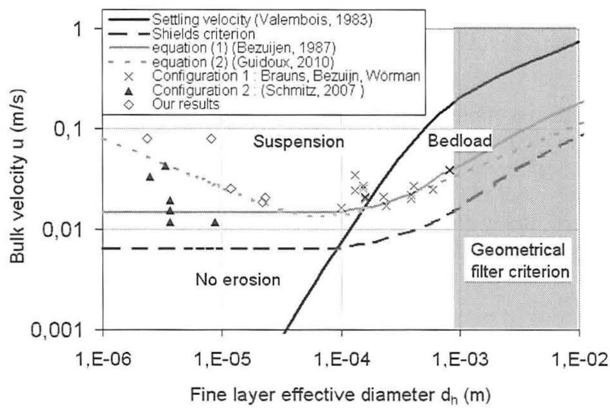

Figure 4. Critical bulk velocity for a coarse layer D_{50} around 20mm

As underlined, contact erosion is similar to classical surface erosion but also a complex combination of various phenomena. The knowledge about the initiation of contact erosion was summarized in Figure 4. Results are usually expressed in critical bulk velocity initiating the process, bulk velocity being a parameter easy to measure during experimentation and computable on the field if in-situ permeability is known. The criterion that defines the start of erosion differs from author to author : the first sediment observed visually in the effluent (Brauns, 1985), a chosen quantity transported (Bezuijen et al., 1987), a no null turbidity after 30 minutes for our experiments (Guidoux et al., 2010) and even no threshold (Wörman et al., 1992). As it can be seen, the threshold velocities are not so different and lay between 0.01 and 0.1m/s. These results are collected for data with a coarse layer of D_{50} close to 20 mm. If all the experimental data are plotted in function of the D_{50} regardless of the fine soil, it can be seen that the grading of the coarse layer has a weak influence on the critical velocity (see Figure 5). A tendency could be to a small increase of the critical velocity with increasing D_{50}. In terms of flow regime in the coarse layer, the limit of Darcy regime is always exceeded, and hence in a regime where inertial contribution cannot be neglected. Temporal fluctuations and turbulence seem to not be the criterion for initiation of erosion as sometimes evocated. These results seem to show that for a bulk velocity inferior to 10 mm/s no contact erosion is possible.

Indeed, among all the experiments done, only one critical value inferior to 10mm/s has been measured by Schmitz and this was only in configuration 2 (Schmitz, 2007). This have a great importance for dyke safety as it can provide a first order indication of erosion initiation. Nevertheless, it has been noticed that the notion of threshold depend on each author and two models, from Wörman and Den Adel, consider that there is no threshold but very small erosion rates for low velocity (Den Adel et al., 1994; Wörman et al., 1992). It means that for long duration as it is the case in-situ, eroded mass may be very large. This reveals an important question that has not been greatly considered concerning the evolution of the erosion with time.

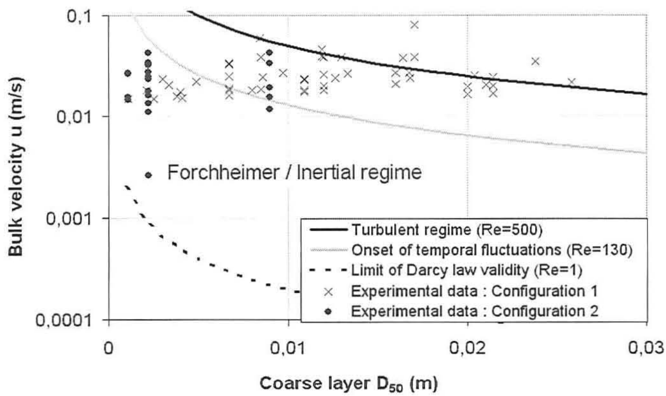

Figure 5. Critical bulk velocity for different fine soil in function of the D_{50} of the coarse layer and limits of flow regime linked with particle Reynolds number: $\mathrm{Re} = ud/\nu$**, with** u **(m/s) bulk velocity,** ν **(m²/s) viscosity of the fluid**

Evolution of erosion with time

The turbidimeter used in our experiment can follow the evolution in time of erosion with a measurement each second of the concentration in sediment of the effluent. Experiments done with various fine soils show a similar behavior. When increasing the velocity to a chosen value, a peak of turbidity is first observed and then a progressive decrease until reaching a null turbidity for low velocity or a, a priori constant, erosion rate when exceeding the critical velocity (see Figure 6). This means that even below the critical velocity a small amount of soil is eroded at the beginning of the step.

This can be explained using the statistical model proposed by (Den Adel et al., 1994). In the coarse layer, the flow is spatially variable due to the numerous changes in section and direction. This results in a variable hydraulic loading on the surface of the fine soil. Den Adel chose to use a log-normal distribution for the possibilities of destabilization of particles. Velocity measurements have been performed inside a refractive index matching porous medium, made of glass beads and mineral oil. Particle Image Velocimetry has been used to obtain velocity fields of the porous flow. Thanks to these results, shear-stresses could be estimated from measured velocity gradients. This study has shown that velocities and shear-stress are distributed following a log-normal law (see Figure 7). This distribution have a large extend along the high values that means that even for a low bulk velocity, local shear-stress can be quite important. This spreading of hydraulic loading exists for classical surface erosion but this effect is largely more pronounced in a porous flow.

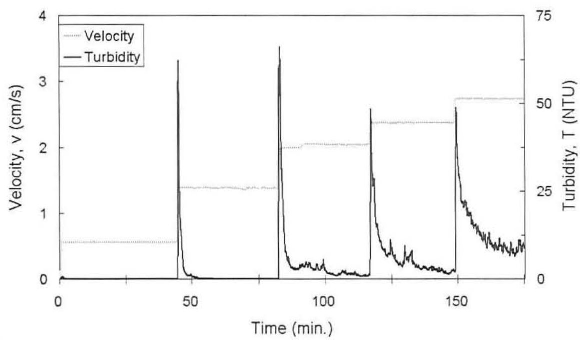

Figure 6. Classical result of contact erosion experiment, velocity and turbidity as a function of time

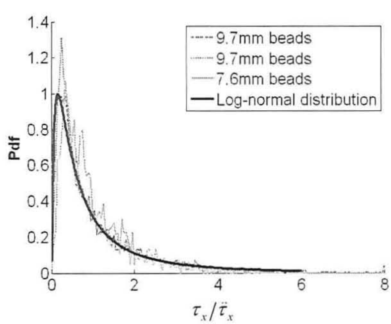

Figure 7. Shear stress distribution calculated from PIV measurement in a refractive index matching porous medium made of glass beads and mineral oil

Following the same argument, the stability of the fine particles can be expressed as a distribution (Grass, 1970). Particles hidden by others or with stronger adhesive links need a higher loading to be destabilized than others. The initial peak can be associated to the erosion of the particles more sensible to erosion. The following decrease is linked to a hardening of the eroded surface. The particles which have the stronger resistance are not eroded and stay in place, whereas the weakest are eroded. After a while, the global resistance of the surface increases until all the exposed particles cannot be eroded with the actual hydraulic loading. Soils with a wide size distribution curve are likely to exhibit such behavior. Additionally they may contain particles sufficiently big to be geometrically trapped in the pores of the coarse layer. Only fine soil which does not validate the geometrical filter criterion proposed by Sherard, based on the d_{85} has been considered, but this does not mean that all the particles can pass in the pores (Sherard et al., 1984). During the contact erosion process, if one coarser particle is trapped, it will start to clog the coarse layer. Experiments done with natural silt at a constant velocity during various hours have shown this phenomenon (see Figure 8). Grading measurement of the soil before and after the experiment confirmed this selective erosion of the fines (see Figure 9). This segregation is well known in surface erosion in river, and was noticed by (Wörman, 1996) for contact erosion. Wörman studied this phenomenon for different well-graded sand and proposed an expression of the evolution of the surface clogged with time. The same behavior was observed for experiments in configuration 2, which are affected inversely by gravity. After several hours, the erosion stops. This implies that even though a global classical geometrical criterion is not fulfilled, if there exists some particles sufficiently big to clog the pores of the coarse layer, erosion will stop after a certain amount of erosion. In terms of design of a hydraulic structure, if this erodible amount is sufficiently small to not modify the performance of the structure, it could be considered to not fulfill the geometrical criteria in this specific situation.

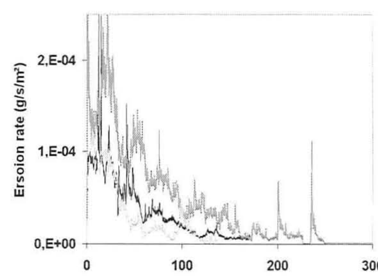

Figure 8. Evolution of erosion rate with time at constant velocity for 3 experiments with a natural silt in Configuration 1

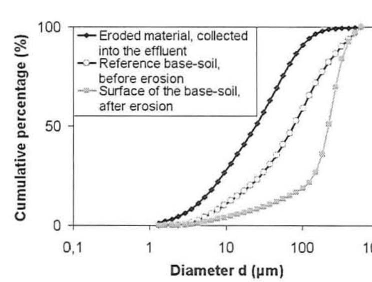

Figure 9. Size distribution curves of the natural silt used, before experiment, in the effluent and on the interface after the end of experiment

CONCLUSION

Contact erosion is a process similar to surface erosion but with many specifics linked to the presence of the coarse layer. A synthesis of studies undertaken on contact erosion has been conducted and coherence was found in the results but their field of validity is limited to sand. For finer soils, an adapted surface erosion model based on hydraulic shear-stress has been proposed and agrees with our data. It has also been noticed that no agreement exists in the literature on the existence of an erosion threshold and it has been shown that this can be attributed to the porous medium variability and the erosion evolution over time. Finally, it is experimentally observed that the erosion rate decrease with time for broadly graded soils due to the progressive clogging of the coarse soil. In consequence, for real structures, the entire size distribution of the soil is important and may eventually allow relaxation of the geometrical classical filter criteria.

REFERENCES

Bezuijen, A., M. Klein-Breteller, et al. (1987), Design criteria for placed block revetments and granular filters., in Proceedings of the 2nd international conference on coastal & port engineering in developing countries, Beijing, China.

Bonelli, S., O. Brivois, et al. (2006), On the modelling of piping erosion, CR Mecanique 334(8-9), 555-559.

Brauns, J. (1985), Erosionsverhalten geschichteten Bodens bei horizontaler Durchstromung, Wasserwirtschaft 75, 448-453.

Den Adel, H., Koenders, M.A. , Bakker, K.J. (1994), The analysis of relaxed criteria for erosion-control filters, Can. Geotech. J. 31(6), 829-840.

Guidoux ,C., Y.-H. Faure, R. Beguin, C.-C., Ho (2010) Contact erosion at the interface between granular filter and various base-soils with tangential flow, J. Geotech. Geoenviron. Eng. Vol. 136, No. 5, may 2010, pp 741-750.

Grass, A.J., 1970, Initial instability of fine bed sand, Proceedings of the American Society of Civil Engineers, Hydraulic Division, Vol.96, No.HY3, pp.619-632.

Kozeny, J. (1953). Hydraulik: Ihre Grundlagen und praktische anwendung. Springer-Verlag, Vienna.

Schmitz (2007). Zur hydraulischen Kontakterosion bei bindigen Basiserdstoffen. PhD thesis, Universität der Bundeswehr, Munich, Germany.

Sherard, J. L., Dunnigan, L. P., et al. (1984), Basic properties of sand and gravel filters., J. Geotech. Eng-ASCE 110(6), 684-700

Shields, A. (1936), Anwendung der Ähnlichkeitsmechanik und Turbulenzforschung auf die Geschiebebewegung, PhD thesis, Versuchsanstalt für Wasserbau und Schiffbau, 26, Berlin, Germany

Valembois, J., (1983) Calcul direct de la vitesse de chute d'un grain sphérique dans un fluide, La Houille Blanche, pp. 127–129

Wörman, A., Olafsdottir, R. (1992), Erosion in a granular medium interface, J. Hydraul. Res. 30(5), 639-655

Wörman, A. (1996). "Constitutive equation for filtration of well graded base soil with flow parallel to base/filter interface." *Proceedings of GeoFilters 1996*, Lafleur, J. and Rollin, A.L., Editors, Montreal, Canada, 295-304, ISBN-2-553-00561-x.

Identification of Descriptive Parameters of the Soil Pore Structure using Experiments and CT Data

Richard Binner[1], Ulrike Homberg[2], Steffen Prohaska[2], Ute Kalbe[1], and Karl-Josef Witt[3]

[1]BAM Federal Institute for Materials Research and Testing, Berlin, Germany, email: richard.binner@bam.de, ute.kalbe@bam.de
[2]Zuse Institute Berlin (ZIB), Berlin, Germany, email: homberg@zib.de, prohaska@zib.de
[3]Bauhaus-Universität Weimar, Weimar, Germany, email: kj.witt@uni-weimar.de

ABSTRACT

In this paper, methods are presented that combine experimental and micro tomographic information to derive parameters of the grain and pore structure of wide-gradated soils. For this purpose, samples based on a model soil were prepared for special experiments as well as for high-resolution CT imaging. Compacting and column experiments were developed to determine specific parameters of the pore and grain structure. Among others, the grain size and discharge quantity of potentially mobile grains were identified as well as characteristics of the supporting skeleton of the model.

The results of the compaction and column experiments provide suitable geometric parameters of realistic grain and pore structures for analyzing suffosive erosion phenomena, whereas the CT specimens support the description and visualization of representative pore structures. The presented methods contribute to a better understanding of the physical processes within the pore structure. As a part of the joint project "Conditions of suffosive erosion phenomena in soils", the results of this paper can be incorporated into pore-network models to verify and simulate existing transport models.

INTRODUCTION

Recent extreme flood events suggest that the vulnerability of river basins has increased over the past years as a consequence of climate change and engineering projects. One of the negative results is that any change of flow condition in the subground might trigger internal erosion processes. Any kind of particle displacement represents an evident problem for the stability of retaining constructions, embankment dams, dykes or tailing impontments. In case of unstable structure seepage force can displace the fines within the grain skeleton during groundwater flow. This process is called suffosion and characterizes the relocation and discharge of fine particles through the pore space. Soils with a relatively large degree of nonuniformity as well as gap graded soils are particularly prone to suffosion. Initially, the supporting granular skeleton will not be changed. The porosity and permeability of the soil, however, increase. Proceeding suffosion and additional external mechanical influences may cause instabilities of the supporting granular structure and subsequently, other types deformation may occur.

There are some studies on internal erosion (Bonelli et al. 2006, Burns et al. 2006, Fell and Fry 2005, Lachouette et al. 2008, Mattsson et al. 2008, Sjo¨dahl et al. 2008, Vaughan 2000). However, gradated soils have not been included. Furthermore, the combinations of CT analysis with experimental derivation of geometric parameters on pore structures of gradated soils have not been considered. Piping, as a type of internal erosion, was analyzed by (Bonelli et al. 2006, Bryan and Jones 1997, Faulkner 2006, Khilar et al. 1985, Lachouette et al. 2008, Ojha et al. 2001) taking into account only 1D and 2D considerations and ignoring spatial and realistic information on the pore space. Although the suffosion controlling parts of the pore structure, characterized by their constriction distribution, is essential to the explanation of suffosion processes (Witt 1986), only the grain size distribution has been used for this purpose in the framework of risk estimation regarding internal erosion.

In this study, spatial and realistic pore structures of gradated soils were investigated. This comprises the preparation of model test material and the generation of 3D CT data sets. Furthermore, experiments were developed in order two determine descriptive parameters on the supporting structure and the mobile fraction.

MATERIAL AND METHODS

Wide-gradated soils are characterized as coarse grained soils that exhibit an asymmetric grain size distribution. They are frequently prone to be suffosive, especially if they feature a gap grading or a non steady distributed grain size curve. Figure 1 illustrates the model grain size distribution (MGSD) of a suffosive noncohesive soil with a gap grading between 0.63 and 2.8 mm that was chosen for this study. This kind of distribution is typical for sedimentary soils in the medium course of a large river and is considered as a soil with a high risk for suffosion (Cistin 1967, Witt 1986, Ziems 1969). Model soil samples exhibiting this grain size distribution were processed by sieving. For this purpose, material was taken from a fluviatile soil of the Upper-Rhine river area.

Preparation of samples for CT analysis and column experiments

To investigate the spatial structure of gradated soils, samples based on the MGSD were prepared for CT analysis as well as for column experiments. For both approaches, the test samples have to fulfill the following two prerequisites: First, the samples should represent the natural bedding and density of the suffosive material as realistically as possible. Second, the sample volume should be representative and stable. For the CT analysis, the samples were embedded in epoxy resin (Figure 2).

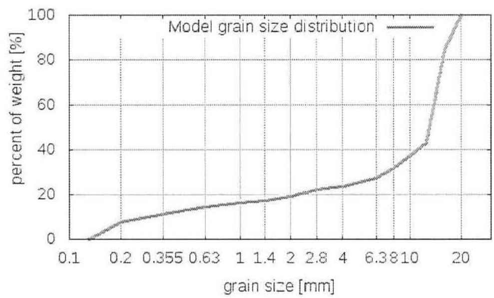

Figure 1: Grain size distribution of the investigated soil.

The individual preparation steps were:

1. Assembling the material: The grain fractions according to the MGSD were merged yielding a mass of 6000 g and filled into the column. The diameter of the column was 139 mm.
2. Compaction and homogenization: The sample was compacted and homogenized by rotating the column and compressing the material at the same time. This is necessary because the fine grain material has a high mobility in the uncompacted sample. The compaction was achieved by applying a uniform pressure of 2.5 N/cm2. For the compression, a plunger was constructed with four springs (Figure 2a–b).
3. Embedding the material: The sample was slowly embedded in epoxy resin from bottom to top in order to avoid air bubbles within the resin and to avoid the relocation of grains (Figure 2c).
4. Cutting the sample: The hardened cylindrical sample was cut to a size of 110 mm in diameter and 110 mm in height using water jet technique (Figure 2d), taking into account the requirements on the specimen size for CT scans.

A second preparation process was carried out for the column experiments. Step 1 and 2 are analog to the CT preparation steps. The further steps ensure that the column material is permeable to water.

1. Assembling the material.
2. Compaction and homogenization.
3. Inserting a perforated plate: Up to now, a synthetic liner had closed the column during the compaction and homogenization process. The column with the unstressed plunger was rotated and the liner was replaced by a perforated plate and funnel at the bottom of the column (Figure 3c). Both are needed for the column experiment.
4. Inserting a filter layer: A further condition for the experiment is a filter layer

upon the material. After rotating the column and replacing the plunger, the filter layer was inserted (Figure 3e-f). The filter consists of a perforated plate and a layer of glass spheres. The latter enables a laminar flow during the experiment.

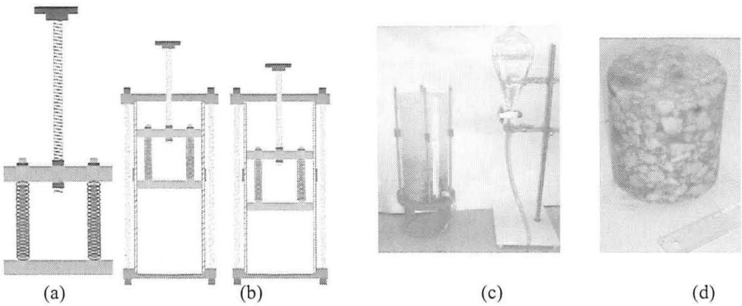

Figure 2: Preparation of specimens for the CT scan, a) detail of the plunger with the compression springs, b) compaction and homogenization, c) embedding in epoxy resin, d) cylindrical specimen.

CT Analysis

For analyzing and visualizing the spatial structure of the soil, specimens were prepared for CT analysis. In a previous study (Homberg et al. 2008), specimens of a height and a diameter of 6 cm each were used and acquired at a resolution of 35 μm for analyzing the grains structure. The results show that specimens of 6 cm diameter cannot be used to determine a representative picture of the geometric structure at the given resolution. Because there is a trade-off between spatial resolution and size of specimen, a double-stage CT acquisition was developed. In a first step, a cylindrical overview specimen of 11x11 cm was cut out from the original specimen using water jet technique and acquired at a resolution of 209 μm (Figure 4a-b). This specimen was cut into 6 parts (Figure 4c-d). The resulting parts had an edge length of 5.5 cm and were scanned at a resolution of 39 μm.

Compaction experiments: Determining the structure-bearing grain fractions

The aim of this experiment is to determine the grain size fractions that form the supporting skeleton. This experiment was performed assuming that the grain fractions which do not belong to the supporting skeleton will not change the filling height. The filling height h is the distance between the bottom and the plunger of the column (Figure 5). For this purpose, grain fractions of a 6 kg sample were split according to the MGSD. Then, the column was filled successively in top down order:

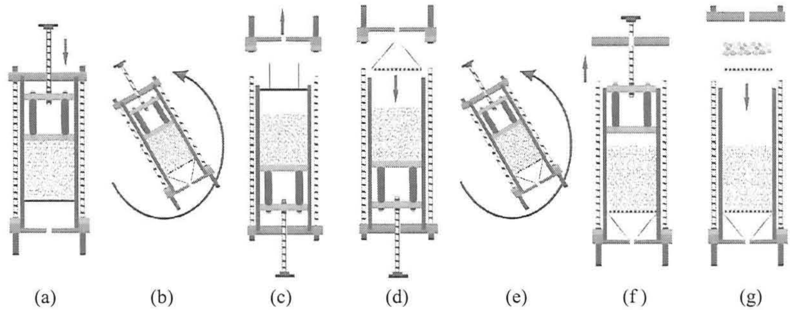

Figure 3: Workflow of column packing, a) homogenization and compaction, b) turning the column, c-d) replacing the synthetic liner by a perforated plate, e) turning the column, f) replacing the plunger by a perforated plate and g) inserting a filter layer of glass spheres and a cap with a water inlet.

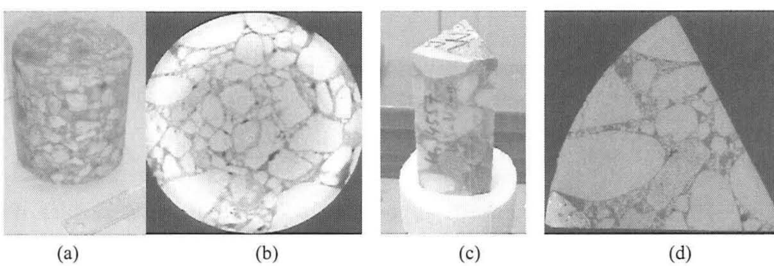

Figure 4: Double-staged CT scan, a-b) the overview specimen scanned at a resolution of 209 μm, c-d) a part cut out from the overview specimen scanned at a resolution of 39 μm.

from the large fractions to the finer fractions. After each adding step, the material in the column was homogenized and compacted as described in the CT sample preparation. Subsequently, the filling height of the compacted material was measured (Figure 5).

Column experiments: Identification of the mobile grain fractions

The objective of the experiment is to determine the mobile grain fractions of the MGSD. The assumption is that there are potentially mobile grains within the supporting skeleton and a possible discharge of these grains does not change the supporting skeleton. This experiment was carried out on two samples which were prepared as described in the preparation section. Note that the perforation size of the inserted perforated plate depends on the results of the compaction experiment. That is, the perforated plate has to retain the smallest grain of the supporting skeleton.

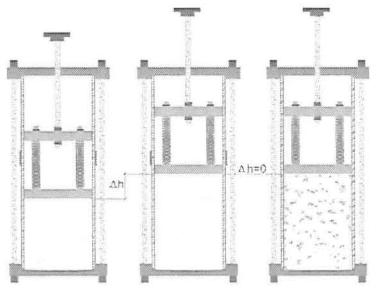

Figure 5: Scheme of the compaction experiment to determine the structure-bearing grain size fractions.

To move the potential mobile grains, water was supplied to the column using an immersion pump at a flow rate of 8.0 l/min (Figure 6). This flow rate corresponds to flow rates within embankment dams, which was found by (Cistin 1967). The discharge containing the mobile grains was collected in a 63 μm sieve, which was emptied after certain time intervals (5, 10, 30, 60 min, 24, 24, 24 h . . .). The experiment was finished when there was no material discharge for 24 h. Finally, the total discharge was analyzed according to (DIN-18123 1996) using sieving sizes of 0.2, 0.355, 0.63, 1.0, 1.4, 2.0, and 2.8 mm.

RESULTS

The compaction experiment was performed for three material samples of the MGSD. The final filling height (sample mass) in the column resulted in 18.9 cm (6034 g), 18.6 cm (5804 g), and 20.0 cm (6336 g) respectively. Figure 7 shows the filling height per fraction related to the total filling height. The different icons represent three replicates. Regarding the height percentages and the course of the filling height per fraction, one can distinguish three groups:

1. The large fractions 20/25 and 16/20 mm form the main part of the sample with about 80 %. They contribute a double-digit height percentage each.
2. The second group consists of the grain fractions of 12.5/16 mm to 4/6.3 mm. These fractions nearly complete the filling height up to 99 % in average, whereas each fraction makes up a few percent of the filling height.
3. Finally, there are the finer fractions. Two of the tests had already achieved the full height, whereas one test still converges to the full height. These fractions do not influence the filling height significantly.

The full filling height is composed of the first (20/25 and 16/20 mm) and the second (12.5/16 to 4/6.3 mm) group, whereas the third group smaller than 4 mm does not contribute to the filling height significantly. They are assumed to be potential mobile within the skeleton of course fractions. In the following, this size of 4 mm was used to prepare the perforated plate for the column experiment.

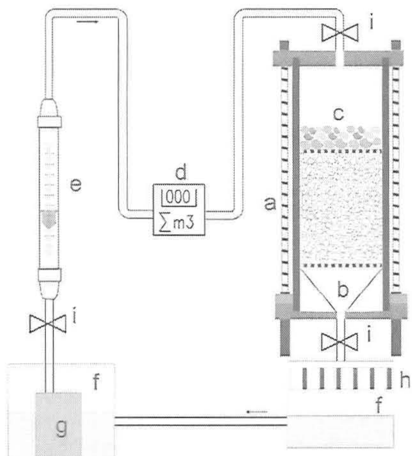

Figure 6: Setup of the column experiment, a) test sample with MSGD, b) perforated plate and funnel, c) layer of glass spheres and perforated plate, d) water meter, e) flow meter, f) water reservoir, g) electric pump, h) sieve, i) plug cock.

Two replicates of the column experiment were carried out, lasting about 70 h. Figure 8 shows the percentage per fraction that was discharged as well as the entire discharge related to the total sample mass. Again, one can distinguish three groups. In the first group, the discharge dominates. Nearly two-thirds and more than a half of the fine fractions 0/0.335 and 0.335/0.63 mm were discharged. That is, one-third to a half of these fractions was retained during the experiment. For the second group, the retained percentage dominates. It contains the fractions between 0.63 to 2.8 mm. The discharge ranges from 8 to 34 %. Third, the fraction 2.8/4.0 mm exhibit sparse discharges: 2.2 % and 1.4 %, respectively.

The prepared CT scans allow visualizing the structures of the investigated soil. The overview scan reveals the whole structure at a low resolution (Figure 4b). Finer structures can be viewed using the detailed scans, which contain the structure parts of the overview scan at a higher resolution (Figure 4d). Figure 9 shows 4 detailed slices out of a CT scan in lateral view, which represent 22x22 mm each and are taken from a range of 3.3 mm. The slices show 4 large grains of the fractions 12.5/16 and 16/20 mm. These large grains form cavities, wherein small grains of the fractions 0.335/0.63 to 2/2.8 mm were enclosed.

DISCUSSION

Considering the results of the experiments, the grains of the MGSD can be distinguished by their behavior during suffosion processes: structure-bearing, mobile, and retained grains. The compaction experiments showed which grain fractions influence the filling height and form the supporting skeleton, respectively.

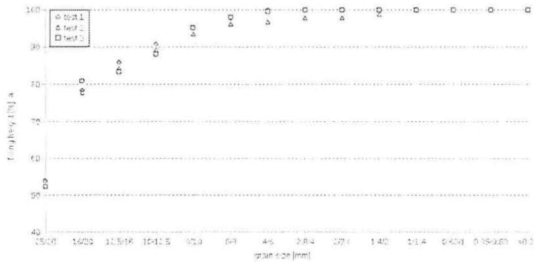

Figure 7: Compaction experiment: filling height per fraction related to the total filling height.

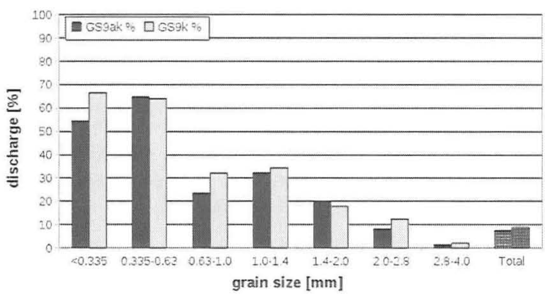

Figure 8: Column experiment: percentage of discharge per fraction and final discharge related to the total sample mass.

Transformed to erosion phenomena this test procedure corresponds to volume change due to a successive erosion of fines. As there is no or less volume change, the eroded particles are embedded within the space of the statical overall structure without fixing. The test shows that the supporting skeleton is dominated by the fractions from 20/25 to 4/6.3 mm. The grain of these fractions governs the structure. The remaining fractions are embedded and potential mobile. That is, they can be discharged or retained depending of the opening size of the structure. The column experiment identifies the mobile and the retained grains of the potential mobile fractions. The resulting groups of this experiment were distinguished by their discharged percentage. The first group exhibits the largest discharge and thus a high mobility. The pore structure mostly seems to consist of connected pore paths with constrictions equal or larger than 0.63 mm. The second group has a minor discharge and thus shows a lower mobility. This indicates that the pore structure contains only a few preferential paths with adequate sized constrictions related to the particular fractions. Considering possible boundary effects and measuring uncertainties, the discharge of the third group (fraction 2.8/4 mm) is too sparse to assign it to the mobile fraction.

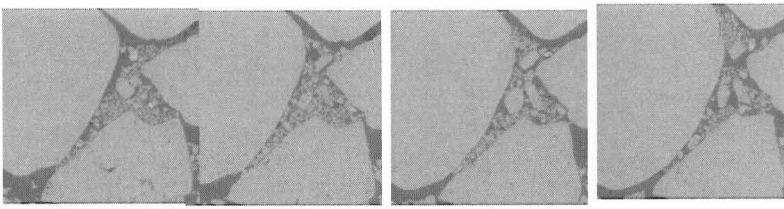

Figure 9: Potential mobile grains retained by structure-bearing grains in a detail of 22x22 mm at a resolution of 39 μm

That is, the largest mobile grains are 2.8 mm. The results of the column experiments suggest that the two smallest fractions are highly mobile in the entire pore space. The complete percentage of these fractions was not discharged. This is due to the irregular shape of real grains and their arrangement, possibly. The analysis of the CT scans encourages this suspicion (Figure 9). The large grains contain concave, convex, and flat surfaces that form cavities and gaps, which retain the potential mobile grains. The mobility could be investigated shape independent using samples of glass spheres to estimate the order of magnitude of this effect. As discussed above, the fraction of 2.8/4 mm can be assigned neither to the overall mobile fractions nor to the structure-bearing fractions. The fraction seems to be a transition between both of them embedded into the coarser pore space of the structure. Possibly, the boundary is located somewhere in this size range. To narrow down this boundary, this fraction could be subdivided into smaller fractions for further experiments. On the other hand, possible boundary effects may appear because the perforated plate does not represent the structure of soil and may impact the soil structure at the bottom of the sample and thus the discharge of this region. This could be investigated with different samples masses or different perforated plates. Furthermore, the results of the compaction experiments exhibit some uncertainty in the range of the lower skeleton boundary and should be validated by further experiments.

CONCLUSIONS

Methods for preparing soil samples and generating CT data as well as experiments that determine geometrical parameters of gradated soils were presented. A compaction experiment was designed and replicated to approximate the lower size boundary of the statically structure-bearing grain fractions. It separates the structure-bearing fractions that might be the effective grain size distribution related to the common criteria from the potentially mobile fractions which not contribute to the structure. This boundary further was used to design the column experiment. By means of the column experiment, the potentially mobile fractions were analyzed by determining the percentages of the mobile and the retained grains. This led to the size of the largest mobile grains within the soil structure and moreover to a size boundary between high mobile and less mobile fractions. In turn, this allows drawing conclusions on the relevant pore structure concerning its connectivity and constriction sizes. The double-staged CT scans allow capturing large and representative specimens at a high resolution. By transforming the scans into a mathematical and numerical model this technique can be used to estimate and analyze the spatial soil structures visually.

ACKNOWLEDGEMENTS

The authors thank the German Research Foundation (DFG) for supporting the research project "Conditions of suffosive erosion phenomena in soil".

REFERENCES

Bonelli, S., Brivois, O., Borghi, R., and Benahmed, N. (2006). "On the modelling of piping erosion." Comptes Rendus M´ecanique, 334(8-9), 555-559.

Bryan, R. B. and Jones, J. A. A. (1997). "The significance of soil piping processes: inventory and prospect." Geomorphology, 20(3-4), 209-218.

Burns, B., Barker, R., and Ghataora, G. S. (2006). "Investigating internal erosion using a miniature resistivity array." NDT & E International, 39(2), 169-174.

Cistin, J. (1967). „Zum Problem mechanischer Deformation nichtbindiger Lockergesteine durch die Sickerwasserstr¨omung in Erdd¨ammen." Wasserwirtschaft Wassertechnik, 2, 45-49. DIN-18123. (1996)., Bestimmung der Korngr¨oßenverteilung." DIN Deutsches Institut fu¨r Normung e.V., 11.

Faulkner, H. (2006). "Piping Hazard on Collapsible and Dispersive Soils in Europe." Soil Erosion in Europe, J. B. a. J. Poesen, ed., 537-563.

Fell, R. and Fry, J.-J. (2005)."Internal Erosion of Dams and their Foundations." Aussois. Homberg,

U., Binner, R., Prohaska, S., Dercksen, V. J., Kuß, A., and Kalbe, U. (2008). "Determining Geometric Grain Structure from X-Ray Micro-Tomograms of Gradated Soil." In Witt, K.-J. editor (2008), Proc. Work. Internal Erosion, Weimar.

Khilar, K. C., Fogler, H. S., and Gray, D. H. (1985). "Model for Piping-Plugging in EarthenStructures." Journal of Geotechnical Engineering, 111(7), 833-846

Lachouette, D., Golay, F., and Bonelli, S. (2008). "One-dimensional modeling of piping flow erosion." Comptes Rendus M´ecanique, 336(9), 731-736.

Mattsson, H., Hellstr¨om, J. G. I., and S., L. T. (2008). "On Internal Erosion in Embakment Dams." University of Technology, Lulea.

Ojha, C. S. P., Singh, V. P., and Adrian, D. D. (2001). "Influence of porosity on piping models of levee failure." Journal of geotechnical and geoenvironmental engineering (12), 1071-1074.

Sj¨odahl, P., Dahlin, T., Johansson, S., and Loke, M. H. (2008). "Resistivity monitoring for leakage and internal erosion detection at H¨allby embankment dam." Journal of Applied Geophysics, 65(3-4), 155-164.

Vaughan, P. R. „Internal Erosion of Dams Assessment of Risks." Filters and Drainage in Geotechnical and Environmental Engineering on the 3th International Conference Geofilters, Warszawa, Rotterdam, 349-356.
Witt, K.-J. (1986). „Filtrationsverfahren und Bemessung von Erdstofffiltern." Universit¨at Karlsruhe, Karlsruhe.
Ziems, J. (1969). „Beitrag zur Kontakterosion nichtbindiger Erdstoffe." TU Dresden.

Slurry Induced Piping Progression of a Sand

Exequiel Sinco[1], Ming Xiao[2], Louay M. Owaidat[3], and Larry Smith[4]

[1] Graduate Student, Department of Civil and Geomatic Engineering, California State University, Fresno, CA, USA. Email: esinco@csufresno.edu
[2]Assistant Professor, Department of Civil and Geomatic Engineering, California State University, Fresno, CA, USA. Email: mxiao@csufresno.edu. Phone: (559) 278-7588.
[3] President, Magnus Pacific Inc., Roseville, CA, USA.
[4] Chief of Construction and Area Engineer, U.S. Army Corps of Engineers, Sacramento, CA, USA.

Abstract

The motivation and the first objective of this laboratory experimental research is to study whether bentonite slurry, as a permeating fluid in levees during slurry cutoff wall installation, can induce further piping progression. The second objective of this research is to study the piping progression of a sand under different permeating fluids, which are often observed in the field where seepage carrying fine, suspended particles that are eroded from the upstream soil matrix permeates through a downstream piping channel. A simple constant-head hole-erosion test is used to study the piping progression of the sand subjected to three types of permeating fluids: water, slurry with 6% bentonite, water mixed with 1% fines of the same sand that pass the U.S. #200 sieve. A piping hole is preformed in the sand specimen and a constant hydraulic gradient induces concentrated seepage through the hole. Soil erosion rate and seepage with time and the total soil loss are monitored and measured. The diameters of the piping channels at the end of the tests using the three permeating fluids are quantified and compared. Our experimental results found that higher density of a permeating fluid does not induce more erosion. On the contrary, permeating fluids with fines reduce the eroded soil mass by an average of 90% and the average piping hole enlargement by 88%, compared with the results using water alone as a permeating fluid. The size distributions of the soils remaining on the inner wall of the piping channels are similar under the three permeating fluids. The agreement of the three particle size distributions suggests that particle deposition on the wall may not occur and is not a mechanism that accounts for the erosion difference.

Introduction

Subsurface erosion in the form of piping has been one of the most prevalent causes of catastrophic failure of levees and earth dams. Such examples include the 1972 failure of the Buffalo Creak dam in West Virginia (Wahler & Associates, 1973) and the 1990 collapsing of an embankment earth dam in South Carolina (Leonards and Deschamps, 1998). During Hurricane Katrina, three levee breaches were possibly caused by underseepage-induced failure due to piping (Seed et al., 2008a, 2008b).

Piping is an internal erosion process in which soil particles inside the soil matrix are entrained and washed out of the matrix by concentrated seepage, forming a tubular pipe that progresses from downstream to upstream; the pipe can develop into a large tunnel that may collapse. Erosion tests are used to study the erodibility of soils and to quantify erosion parameters. Common experimental methods for internal erosion include pinhole erosion test (Sherard and Dunnigan, 1989; ASTM, 2006), hole erosion test (Wan and Fell, 2004; Leonards et al., 1991; Reddi et al., 2000; Burns and Ghataora, 2007), and slot erosion test (Sherard et al., 1984; Kohno et al., 1987; Wan and Fell, 2004). In these tests, a hole or a slot is formed in the soil sample housed in a rigid column; the soil is then subjected to a constant hydraulic gradient that induces concentrated seepage through the preformed piping channel.

Dislodging of soil particles is a result of complex hydrodynamic force interactions including electrical forces and stresses between particles, gravity of particles, water pressure around particles and shear stress around particles (Briaud et al., 2008). Kakuturu and Reddi (2006) formulated the hydraulic shear stress (τ) that exerts on the wall of a piping hole as:

$$\tau(t) = \frac{4Q\eta}{\pi \cdot r_{cc}^3} \tag{1}$$

where Q = flow rate, η = dynamic viscosity of the permeating fluid, r_{cc} = radius of the idealized cylindrical core crack. The equation indicates that the physical characteristics of the permeating fluid influence the erosion process. An example is the installation of slurry cutoff walls, which are often used to prevent or remediate internal erosion and reduce seepage in or beneath levees. Slurry, a mixture of water and bentonite, keeps the trench open before the cemented soils are backfilled. When the trench that is filled with slurry intercepts a piping channel, the slurry may displace water and seep through the piping hole. Due to the higher density and viscosity of the slurry than that of water, the slurry may exert higher shear stress and facilitate the internal erosion. Consequently, an enlarged channel is created, causing much higher concentrated seepage. The motivation and the first objective of this research is to study whether bentonite slurry, as a permeating fluid in levees during slurry cutoff wall installation, can induce further piping hole development. The second objective of this research is to study the piping progression of sand under different permeating fluids, which are often observed in the field where seepage carrying fine, suspended particles that are eroded from the upstream soil matrix permeates through a downstream piping channel.

Materials and Methodology

In the series of experiments, a sandy soil is used. The poorly graded sand has fine content (passing U.S. #200 sieve) of 17.6%, and C_u = 10, C_c = 4. The sand is reconstituted in a Plexiglas column. The diameter of the specimen is 9.5 cm (3.74 inch) and the length is 30.5 cm (12 inch). The sand is compacted in 12 uniform layers at 95% of the maximum dry density (ρ_{dmax} = 2.00 g/cm^3) at the optimum water content (w_{opt} = 8.5%) (based on the modified Proctor test). A hole of 0.64 cm (1/4 inch) diameter that penetrates the entire specimen is formed during the specimen compaction using a rod of the same diameter. Our preliminary test found that the wall of the pre-made piping hole collapsed during the saturation process when the hole was filled with still water. To study the soil erosion only due to concentrated seepage, 5% (by mass) kaolinite is mixed with the sand to increase its plasticity. When the sand-clay mixture is compacted at 95% of the new ρ_{dmax} (2.10 g/cm^3) at the new w_{opt} (8.4%), the preformed piping hole remained open and the soil particles that detached from the wall of the piping hole during saturation was 1.7 g. The sand-clay mixture is used throughout the experiments.

Table 1. Hole-erosion test program

Permeating fluid	Measurements in tests of running time = 10 min	Measurements in tests of running time = 40 min
De-ionized water De-ionized water with 6.0% bentonite (slurry) De-ionized water with 1.0% fines that pass U.S. #200 sieve	• Erosion rate ~ time • Seepage ~ time • Particle size distributions of soils on the wall of piping hole	• Total dry soil loss • Piping hole shape and dimension at the end of test

A simple constant-head hole-erosion test is used to study the piping progression of the sand subjected to three types of permeating fluids. The test program is summarized in Table 1. 6% of bentonite by mass in slurry is commonly used in slurry walls in the field. The fines in the permeating fluid simulate the suspended particles that are eroded from the upstream section of the same soil. So the fines are obtained by sieving the sand from the same batch that is used to reconstitute the specimens. The fines are mostly silt and non-plastic. The fines concentration in the permeating fluid is 1.0% by mass. Figure 1 is a photo snapshot of the experimental setup. The water-fines mixture of a specified concentration is prepared in a bucket, in which a submersible pump pumps the mixture into a constant-head reservoir above the specimen. The overflow of the fluid returns back to the bucket. A mechanical stirrer is used to keep the solids (bentonite or fines) in suspension in the bucket and in the upstream reservoir, in an effort to keep the suspended solids concentration as close to the prescribed value as possible. Sufficient amount of permeating fluid is prepared: for the test running time of 40 min, approximately 110 liters of fluid is needed. To prevent the direct impact of the fluid on the inlet of the piping hole, a layer of uniform glass beads is laid on top of the specimen. The outlet of the piping channel opens to the atmosphere. The constant hydraulic gradient is 2.2. For each permeating fluid, two test periods are used: 10 min and 40 min. The 10-min period is chosen as a preliminary trial period; then the 40-min period is chosen because the top portion of the piping channel under de-ionized water enlarged to the perimeter of the mold and the test is stopped at 40 min. In the 10-min tests, the effluent with eroded solids is collected in each 2-min interval. The volume of the effluent is measured and then the effluent is oven-dried to obtain the eroded solid mass. In the 40-min erosion tests, only the dry mass of the eroded solids is obtained by subtracting the dry mass of the specimen after the erosion test from that before the erosion test.

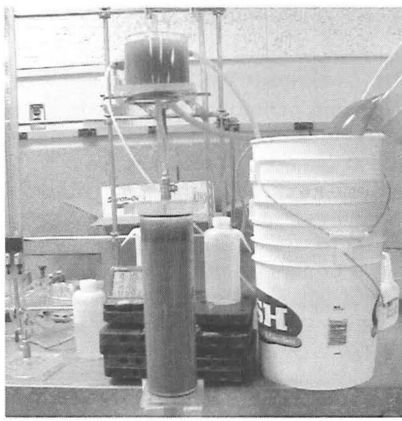

Figure 1. Experimental setup of the hole-erosion tests using different permeating fluids (the fluid shown in the photo contains 1% fines that pass #200 sieve)

In the complex interaction of the suspended fines in the permeating fluid and the soil particles on the wall that is exposed to the permeating fluid, the suspended fines may deposit on the wall and consequently protects the piping channel or they may detach the finer solids on the wall (possibly due to the abrasive force) and leave the coarser particles on the wall. To study the effect of different permeating fluids on the fate of the solids on the piping wall and account for the erosion differences under the different permeating fluids, a thin layer (about 2 mm, the accumulative mass is approximately 20 g) of the solids is carefully scraped from the wall at the end of each 10-min erosion test. Then wet sieving and hydrometer tests are conducted on the collected solids from the walls to obtain and compare the particle size distributions of the soil particles left on the walls.

To precisely record the dimension and shape of the piping channel at the end of each test (with the running period of 40 min), additional piping tests of the same test condition are performed. At the end of each test, a silicon rubber fluid (OOMOO®

25 Silicone Rubber, Smooth-On Inc., Easton, PA) is slowly injected into the piping hole. The fluid occupies the entire voids in the piping channel and solidifies in 75min at room temperature. The OOMOO® 25 silicon rubber is used for a variety of art-related and industrial applications including making molds for sculpture and prototype reproduction. The product has low viscosity (4250 cps) for easy mixing and pouring, and vacuum de-aeration is usually not necessary. It has negligible shrinkage and good tear strength. The solidified silicon rubber can be easily detached from the soil and it accurately represents the shape of the piping hole under different permeating fluids.

Results and Discussion

In the series of erosion experiments with running time of 40 min, significant erosion is observed when the permeating fluid is de-ionized water — the hole progresses to the perimeter of the mold at 40 min at the top portion of the specimen and the test is terminated at that time. When using the other fluids with bentonite or non-plastic fines, no noticeable piping progression is observed. The dry soil masses eroded are listed in Table 2. Contrary to our initial hypothesis, fluids with non-plastic fines result in much less soil erosion, even less than that from the bentonite slurry. The permeating fluids with bentonite or fines passing #200 sieve reduce the eroded soil mass by an average of 90%, compared with the erosion tests using water as permeating fluid.

Table 2. Piping erosion results (40-min erosion period)

Permeating fluids	Dry soil mass eroded (g)
De-ionized water	447.9
De-ionized water with 6.0% bentonite (slurry)	51.2
De-ionized water with 1.0% fines that pass U.S. #200 sieve	38.1

In the series of erosion tests with 10-min running time, similar piping progression and erosion trend are observed as in the tests of 40-min running time. The seepage variations with time through the specimens under the three permeating fluids are presented in Figure 2. The permeating fluids with bentonite or fines have similar seepage quantity. The progressively increased seepage of water with time is obviously due to the enlarged piping hole as a result of increased erosion.

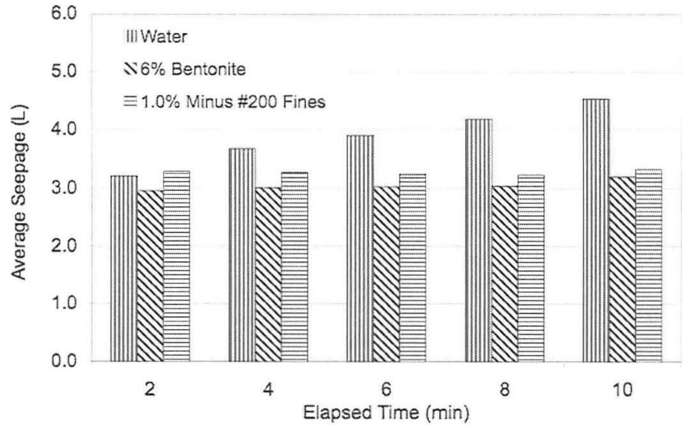

Figure 2. Seepage variations with time in erosion tests of 10-min running time

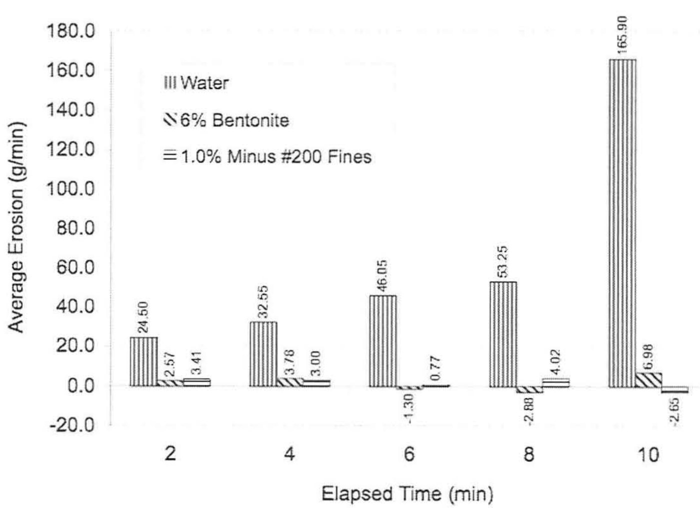

Figure 3. Variations of erosion rate with time in erosion tests of 10-min running time

We also attempted to measure the variation of erosion rate (dry eroded soil mass per minute) with time in the three tests of running time of 10 minutes. The results are shown in Figure 3. The effluent with eroded soils and the fines (or bentonite) that are initially in the fluid is collected in every two minutes and oven-dried. The dry eroded soil mass is calculated by subtracting the mass of bentonite or fines from the total dry mass collected. An assumption is made in calculating the mass of bentonite or fines in the effluent, i.e., the concentration of the bentonite or fines is constant in the permeating fluid throughout the test. The concentration of the bentonite or fines in the permeating fluid is found by (1) subtracting the total dry mass of the bentonite or fines (including that left in the unused fluid, left in the upstream reservoir, and accumulated in the glass beads and on top of the specimen) from the total dry mass of bentontie or fines used in the permeating fluid preparation, and (2) measuring the total volume of the effluent. The results indicate that the concentrations for bentonite and 1.0% fines passing #200 sieve are slightly different from the prescribed values and consequently cause negative erosion values as shown in Figure 3. The seepage of water is much higher than the other permeating fluids, due to increased piping hole. The increase of the seepage of water indicates a progressively increased piping toward failure.

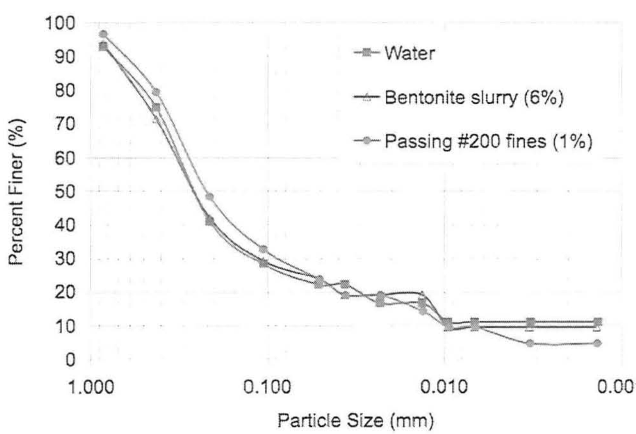

Figure 4. Particle size distributions of soils on the wall of piping hole (10-min running time)

In order to examine whether the slurry or fines deposit on the wall of the piping channel during the erosion test and consequently protect the wall from further erosion, the size distributions of the grains left on the wall at the end of each 10-min erosion test are obtained and shown in Figure 4. The particle size distributions (PSDs) from the tests using water, bentonite slurry, or fluids containing fines show no noticeable difference, indicating bentonite or fine particles in the permeating fluid did not deposit on the walls. Agreement of the three PSDs in Figure 4 suggests that particle deposition on the wall may not occur and is not a mechanism that accounts for the erosion difference.

To further investigate the effect of different permeating fluids on the piping progression of the sand, the shapes of the inner piping holes that are molded by the silicon rubber at the end of the 40-min erosion tests are shown Figure 5. We observed that the final shapes of the piping holes in the tests using bentonite and fines have no measurable difference. Therefore, only the silicon rubber from the bentonite slurry erosion test is compared with that from the water erosion test. The bumps on the rubber indicate the non-uniform erosion due to the non-uniform density caused by the specimen compaction in 12 layers. The measurements of the diameters of the piping holes are listed in Table 3. The data show that permeating fluids with fines reduce the average piping hole enlargement by 88%, compared with the results using water as permeating fluid.

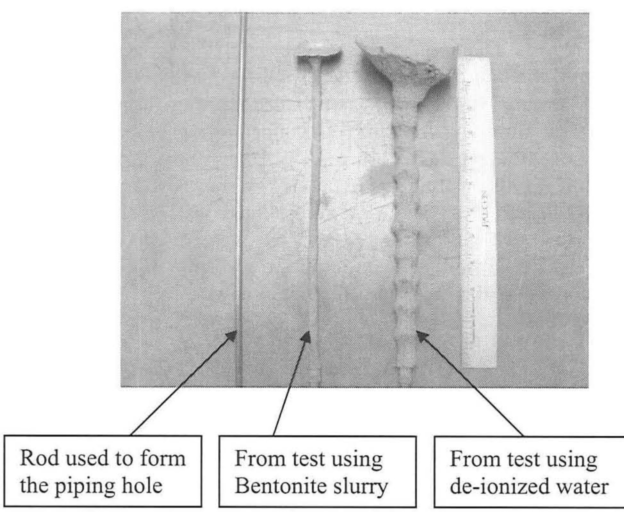

Figure 5. Shapes of piping holes represented by silicon rubber

Table 3. Final diameters of the piping holes in tests with 40-min erosion period

Permeating fluids	Initial hole diameter (mm)	Average hole diameter after test (mm)	Hole diameter enlargement (mm)
De-ionized water	6.4	20.5	14.1
Bentonite slurry	6.4	8.1	1.7

Using the same methodology, we are carrying out a comprehensive experimental program to reveal and quantify the effects of the characteristics of different permeating liquids (in terms of particle sizes, concentrations, and plasticity of fines) on the piping channel progression. Then we will move on to explore the fundamental mechanisms that account for the different piping progression under different permeating fluids.

Conclusions

This paper reports a laboratory investigation of the piping progression of a sandy soil under three types of permeating fluids. Our experimental results found that higher density of a permeating fluid does not induce more erosion. On the contrary, permeating fluids with slurry or fines of 1% concentration reduce the eroded soil mass by an average of 90% and reduce the average piping hole enlargement by 88%, compared with the results using water alone as permeating fluid. The size distributions of the soil particles remaining on the inner wall of the piping channels are similar for the different permeating fluids. The agreement of the particle size distributions suggests that particle deposition on the wall may not occur and is not a mechanism that accounts for the erosion difference.

Acknowledgements

This research is supported by Magnus Pacific, Inc (Roseville, CA) and the NSF Louis Stokes Alliance for Minority Participation (NSF-LSAMP) Program (grant number: HRD-0802628-515291) at California State University.

References

American Society for Testing and Materials (ASTM) (2006). Standard test method for identification and classification of dispersive clay soils by the pinhole test. 2006 Annual Book of ASTM Standards, Soil and Rock (I), Section 4, Volume 04.08. Designation: D 4647-93. ASTM International.

Briaud, J.-L., Chen, H.-C., Govindasamy, A.V., Storesund, R. (2008). Levee erosion by overtopping in New Orleans during the Katrina Hurrican. Journal of Geotechnical and Geoenvironmental Engineering, 134(5):618-632. 2008.

Burns, B., and Ghataora, G.S. (2007). Internal Erosion of Kaolin. GSP 162, Problematic Soils and Rocks and In Situ Characterization. GeoDenvor, 2007.

Kakuturu, S., and Reddi, L.N. (2006). Mechanistic model for self-healing of core cracks in earth dams. Journal of Geotechnical and Geoenvironmental Engineering, 132(7):890-901.

Kohno, I, Nishigaki, M, and Takeshita, Y. (1987). Levee failure caused by seepage and preventive measures. *Natural Disaster Science*, 9(2):55-76.

Leonards, G.A., and Deschamps, R.J. (1998). Failure of Cyanide overflow pond dam. *J. of Performance of Constructed Facilities*, 12(1):3-11.

Leonards, G.A., Huang, A.B., and Ramos, J. (1991). Piping and erosion tests at Conner Run Dam. *J. of Geotechnical Engineering*, 117(1):108-117.

Reddi, L.N., Lee, I-M., and Bonala, M.V.S. (2000) Comparison of internal and surface erosion using flow pump tests on a sand-kaolinite mixture. *Geotechnical Testing Journal*, 23(1):116-122.

Seed, R. B., Bea, R.G., Abdelmalak, R. I., Athanasopoulos-Zekkos, A., Boutwell, G.P., Bray, J.D., Cheung, C., Cobos-Roa D., Ehrensing, L., Harder Jr., L.F., Pestana, J.M., Riemer, M.F., Rogers, J.D., Storesund, R., Vera-Grunauer, X, ; and Wartman, J. (2008a). New Orleans and Hurricane Katrina. II: the central region and the lower Ninth Ward. *ASCE J. of Geotechnical and Geoenvironmental Engineering*, 134(5): 718-739.

Seed, R. B., Bea, R.G., Abdelmalak, R. I., Athanasopoulos-Zekkos, A., Boutwell, G.P., Bray, J.D., Cheung, C., Cobos-Roa D., Cohen-Waeber, J., Collins, B.D., Harder Jr., L.F, Kayen, R.E., Pestana, J.M., Riemer, M.F., Rogers, J.D., Storesund, R., Vera-Grunauer, X, ; and Wartman, J. (2008b). New Orleans and Hurricane Katrina. IV: Orleans East Bank (Metro) Protected Basin. *ASCE J. of Geotechnical and Geoenvironmental Engineering*, 134(5): 762-779.

Sherard, J.L., Dunnigan, L.P. (1989). Critical filters for impervious soils. *ASCE J. of Geotechnical Engineering*, 115(7):927-947.

Sherard, J.L., Dunnigan, L.P., Talbot, J.R. (1984). Basic properties of sand and gravel filters. *ASCE J. of Geotechnical Engineering*, 110(6):684-700.

Wahler, W.A. and Associates. (1973). Analysis of coal refuse dam failure, Middle Fork Buffalo Creek, Saunders West Virginia. National Technical Service Rep. PB-215, Washington, D.C., 142-143.

Wan, C.F., and Fell, R. (2004). Laboratory tests on the rate of piping erosion of soils in embankment dams. *ASTM Geotechnical Testing Journal*, 27(3):295-303.

Experimental Bench for Study of Internal Erosion in Cohesionless Soils

D. Marot, Y. Sail and A. Alexis

University of Nantes, Institut GeM, BP 420 44606 Saint-Nazaire Cedex, France; email : didier.marot@univ-nantes.fr, yacine.sail@univ-nantes.fr, alain.alexis@univ-nantes.fr

ABSTRACT

Under the internal flow, hydraulic earth structures (dikes, levees, or dams) can incur a migration of particles that can induce a modification of hydraulic and mechanic characteristics.

With the objective to characterize this phenomenon named internal erosion and its consequences on mechanical behaviour of granular materials, a large oedo-permeameter device is developed. An axial load is applied on specimen and also a downward flow with a constant hydraulic gradient. During the testing time, the bench can measure the spatial variability of density and of interstitial pressure along the specimen. Axial deformation, injected flow and eroded mass are also measured during the testing time.

Erosion of fine particles on downstream specimen part is accompanied by fine particles migration in the specimen. This migration induces a settlement and an increasing of interstitial pressure. Afterwards a localized instability appears and triggers specimen deformation.

INTRODUCTION

Within earth structure such as dam, dike or levee, seepage can induce a detachment and a transport of fine particles from the structure or from its foundation. This process named internal erosion can modify hydraulic properties of soil as permeability but internal erosion can also modify mechanical behaviour. Finally these modifications can induce instability of the earth structure. The occurrence of failures in new earth structures demonstrates the need of improving the knowledge of these phenomena and its consequences on mechanical behaviour of soil.

In uncracked soils, the two main phenomena of internal erosion are suffusion and backward erosion. Suffusion is the detachment and transport process of only fine particles whereas backward erosion concerns all grains. Initiation of internal erosion processes is influenced by geometric conditions as grain size distribution, porosity of soil (Kenney and Lau, 1985) and grain shape (Li, 2008) and by loading conditions as effective stress (Li, 2008) and hydraulic gradient (Skempton and Brogan, 1994). Depending on the process of internal erosion, confinement stress has a complex effect on internal erosion development (Bendahmane et al., 2008).

A new experimental bench is developed in order to characterize initiation and development of internal erosion. This device is described and a test procedure is performing for a specimen composed by a gap gradation of glass beads. Hydraulic and mechanical response of the specimen to an increasing hydraulic gradient is presented.

OEDO-PERMEAMETER DEVICE

The main bench characteristics are summarized in Figure 1. Device is configured to enable specimen preparation which is saturated and consolidated in oedometric condition. Specimen is subjected to seepage flow under a hydraulic gradient that increases by stages.

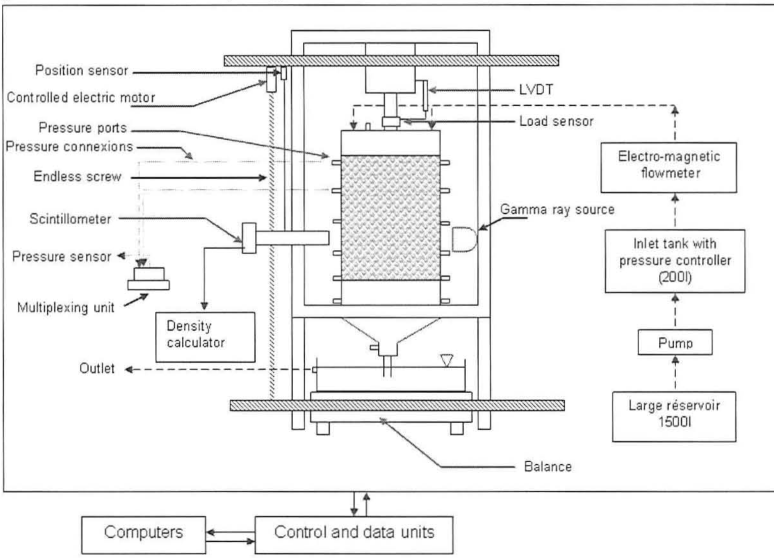

Figure 1. Schematic diagram of oedo-permeameter device

The bench is composed of an oedo-permeameter cell with a funnel-shaped draining system which is connected to a collection system. The bench comprises also an axial loading system, a hydraulic control system and a gammadensitometric system. The control and acquisition part is provided by two units connected to two computers. All these components are detailed below.

Oedo-permeameter cell

With the aim to observe specimen during testing time, the rigid wall cell is made of Plexiglas tube. Internal cell diameter is $\Phi_{cell} = 275$ mm and the specimen height can reach 600 mm. It can be noted that oedo-permeameter cell allows testing specimen with a maximum grain size $D_{max} = 9$ mm (equivalent to a cell factor $D_{max}/\Phi_{cell} = 30$) and a slenderness ratio of 2. The two ends of Plexiglas tube are reinforced by stainless steel plate. Cell wall is equipped with twelve pressure ports (two arrays of six pressure ports on opposite cell sides, two by two pressure ports at the same elevation and vertical spacing of 100 mm between pressure ports), a pressure port is placed on piston base plate (see below axial loading system) and a fourteenth port is positioned below specimen on draining system. In order to avoid discrepancy between two pressure transducers, pressure ports are connected to a multiplex unit which is connected to a pressure sensor (Alexis et al, 2004).

Thanks to several specimen supports, specimen with different heights can be tested. A stainless steel mesh screen is placed on specimen support. This 15 mm thick mesh screen has 10 mm pore opening size in order to allow the migration of all grains. With a rim, different wire meshes can be fixed on the mesh screen in order to take into account the effect of pore opening size on internal erosion (Marot et al, 2009). To eliminate any preferential flow between mesh screen and cell, a geotextile is placed between wire screen edge and rigid wall of cell.

Top plate has two inlet ports 10 mm in diameter and the base plat has a vertical funnel-shaped draining system which is specially designed to avoid clogging. The opening of draining system is controlled by a pneumatic gate. Outlet pipe is in glass in order to permit the measurement of effluent transparency by means of an optical sensor (Bendahmane et al., 2008).

Collection system

The collection system is composed of an effluent tank which has an overflow outlet with a 0.08 mm mesh in order to catch the fine eroded particles. Effluent tank can be continuously weighing or can contain several beakers for the effluent sampling.

Axial loading system

A piston, a pneumatic cylinder and a reaction frame compose the axial loading system. Piston comprises two perforated plates which are made of 15 mm thick stainless steel. A 61 mm thick layer of gravel separates the two plates in order to diffuse the injected fluid on the specimen contact interface uniformly. Two joints are bonded to the piston edge to avoid any parasitic particle displacements between piston and cell wall.

Axial effective stress on the top surface of specimen is generated by a pneumatic cylinder (capacity: 11.5 kN) which has a 200 mm stroke in order to maintain the axial stress even in the case of a great specimen settlement. A load cell measures the axial force on the loading rod. The piston displacements and thus the specimen settlements are measured by a Linear Variable Differential transducer (LVDT) (stroke: 200 mm).

The pneumatic cylinder is mounted on a framework. This framework supports also the oedo-permeameter cell which is mounted on a large ball bearing for the axial cell rotation.

Hydraulic control system

Hydraulic system is composed of two reservoirs and a pump. A 1500 litre storage reservoir is supplied by public water system and placed in a temperature-controlled chamber.

With a pump, this reservoir supplies a 200 L tank which is equipped with a pressure controller. A pressure transducer connected to the pressure port on the piston base plate allows controlling the water head applied on specimen top face. The connexion between controlled pressure tank and eodo-permeameter cell includes two electromagnetic flowmeters (120 L/min and 480 L/min of capacity) for the measurement of seepage flow.

Gamma-densitometric system

The gammadensitometric bench was developed by Alexis et al. (2004). It comprises a radioactive gamma-ray source and a scintillation counter on the opposite cell side. These components are bonded on a carriage which can move in vertical direction thanks to an endless screw and a controlled electric motor. The position of the carriage is measured by a position transducer. According to a previous gauging data, a density calculator counts the scintillometer impulses and calculates the density.

Monitoring and data acquisition system

The control and acquisition part is provided by two data units. One principally controls the gammadensitometric bench motor and the multiplex unit. It is also in charge of the acquisition of: density measurements, position carriage and water head. Two velocities of travelling motion are used, a cruising speed and an approach speed to limit both travelling duration and position discrepancy. This unit drives the run of the second data acquisition unit.

The second data unit carries out the measurements from load sensor, settlement sensor, mass balance and seepage flowmeters.

TEST PROCEDURE AND TESTED MIXTURE PROPERTIES

The tested material is a mixture of glass beads. This cohesionless material allows to compare our results with an experimental campaign performed by Moffat and Fannin (2006) with a large permameter.

Grain size distribution of mixture

Figure 2 plots the grain size distribution of tested mixture (named G4-C by Moffat and Fannin, 2006) and the grain size distributions of the mixture components (coarse fraction C and fine fraction F).

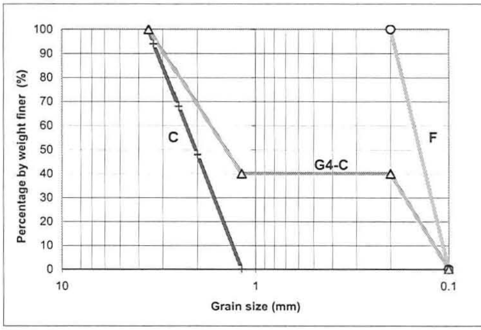

Figure 2. Grain size distribution of tested mixture.

According to Moffat and Fannin (2006), fine fraction F is equivalent to fine sand with a coefficient of uniformity Cu = 1.4 and d_{85} = 0.19 mm (where d_{85}: sieve size for which 85% of the weighed soil is finer). Fraction C is equivalent to coarse sand with Cu = 1.7 and d_{10} = 1.4 mm. Gradation G4-C is composed of 40% by weight of F and 60% of C and it is characterized by a gap. The mixture preparation phase is divided in four steps: positioning alternatively a series of coarse and fine fractions layers in mixing machine with 10% of water content, mixing during 3 minutes and homogeneity verification by size distribution measurements.

Test procedure

A wire mesh with a 1.25 mm pore opening size is fixed on wire mesh screen in order to allow only the migration of particles F.

The cell is filled with water to saturate by gravity flow: the pressure connexions, the multiplex unit and the pressure sensor.

In conformity with specimen reconstitution technique used by Moffat and Fannin (2006), specimen is prepared in several layers by slurry deposition. The total dry mass of glass beads in specimen is 51.64 kg and the initial specimen height is 45 cm. An upper wire mesh of 0.08 mm is placed on specimen face to avoid fine particles migration in the piston. Specimen consolidation occurs under 25 kPa axial loading and with double drainage condition (dissipation of excess interstitial pressure in upward and downward direction).

Data acquisition is started afterwards specimen is submitted to a downward seepage under a first value of hydraulic gradient. Hydraulic gradient is increased by increments about unity until specimen failure. Each stage of hydraulic gradient is applied during 60 minutes. During testing duration, data are recorded with a periodicity of 1 second and the effluent sampling is performed with a 6 minutes period.

For this specimen height, Figure 3 shows the position of used pressure ports (number 1 to 11) and the distance from the specimen bottom of density measurement stations (section 1 to section 6).

At the end of each hydraulic gradient stage, the specimen is isolated by simultaneous closing of upstream and downstream gates and the controlled pressure tank is filled.

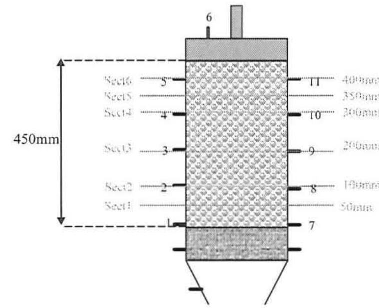

Figure 3. Position of interstitial pore pressure ports and stations of density measurement.

TEST RESULTS AND DISCUSSION

Moffat and Fannin (2006) detected the onset of failure for a value of hydraulic gradient i = 8.3. About half of this value was chosen for the first stage of hydraulic gradient (i = 3.6) and two other stages could be applied on specimen before failure: 4.6 and 5.6 respectively.

Initial state of specimen

At the end of specimen preparation, a loss of fine particles is measured which represents around 2.7% of total fine mass. The upward and downward profiles of density measurement (cf. Figure 4) show a density which decreases in downward direction from 2 g/cm^3 to 1.95 g/cm^3.

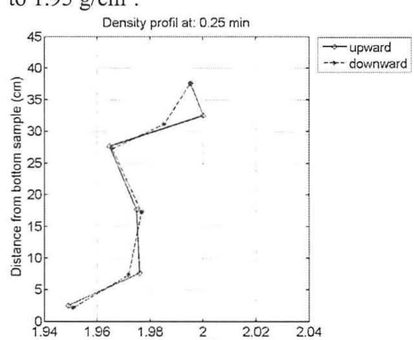

Figure 4. Initial profiles of density.

The low discrepancy between these two density profiles shows that repeatability of density measurement is fairly good as the two profiles are very close.

Injected flow and permeability

During the first hydraulic gradient stage ($i_1 = 3.6$), the seepage flow is 1.3 L/min. For the second stage ($i_2 = 4.6$), the flow reaches 1.7 L/min and its value is 2 L/min during 20 minutes of third stage ($i_3 = 5.6$). For these three stages, the specimen hydraulic conductivity is $k = 1.10^{-4}$m/s.

At t = 20 min for the third stage, flow suddenly increases and finally it exceeds the flowmeter capacity (> 8 L/min). So the specimen hydraulic conductivity is higher than 4.10^{-4}m/s. An instability characterized by no particle F can be observed along the cell (see Figures 5(a) and 5(b)).

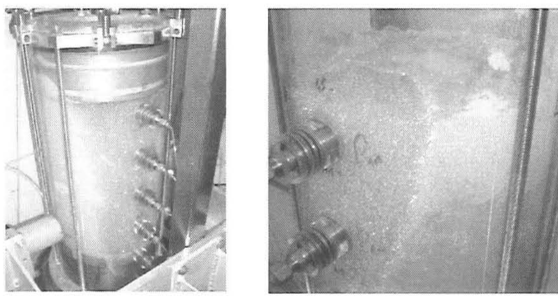

(a) (b)

Figure 5. Localized instability: (a) general view, (b) detail near pore pressure ports number 11 and 10 ($i_3 = 5.6$ m/m, t > 20 min).

The initiation of this instability is observed at the specimen top interface and it progresses in downstream direction along the positions of pressure ports number 11, 10, 9, 8 and finally 7.

Eroded mass and settlement

Application of the two first stages of hydraulic gradient induces a small erosion of fine particles (for $i_1 = 3.6$, eroded mass $m_{F\ eroded} = 140$ g, that represents a relative erosion $m_{F\ eroded}/m_{Finitial} = 0.7\%$; for $i_2 = 4.6$, $m_{F\ eroded} = 250$ g, $m_{F\ eroded}/m_{Finitial} = 1.2\%$).

The measured settlements are similar for the two stages: for each stage around 2.4 mm (that corresponds to a 0.5% axial deformation).

During the first twenty minutes of the third stage ($i_3 = 5.6$) (which corresponds to the first fifteen minutes of effluent sampling) the increasing of settlement is quite similar to the settlement increasing in the course of previous stages and eroded mass is $m_{F\ eroded} = 200$ g ($m_{F\ eroded}/m_{Finitial} = 0.9\%$). At t = 20 min, settlement suddenly increases to reach 13 mm (axial deformation of 3%) and the cumulative eroded mass increases by 2.4 kg ($m_{F\ eroded}/m_{Finitial} = 11\%$).

Figure 6 represents the instantaneous variations of eroded mass and settlement during the three stages.

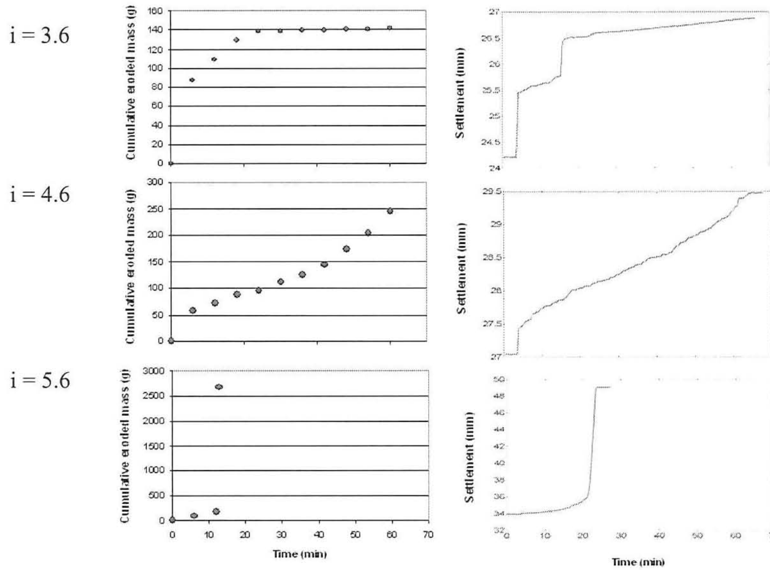

(a) (b)

Figure 6. Instantaneous variations of: (a) eroded mass, (b) settlement during the three stages.

It can be noted the similar kinetics of increasing for eroded mass and settlement. Two hypotheses about the process can be considered:

-fine particles erosion at specimen bottom induces a migration of fine particles which concerns the whole specimen and causes the settlement

-fine particles erosion at specimen bottom induces an instability located on downstream part and which causes a specimen translation without any migration of fine particle in the specimen centre.

Density variations

Two types of density variations are measured during the two first stages of hydraulic gradient:

-decrease of density in the downstream part of specimen (sections 1, 2 and 3) with a relative variation in comparison to initial density between -0.5% and -1.5%

-increase of density in the upstream part (sections 5 and 6) with a relative variation between +0.25% and +2.4%.

During the third stage, only the density values on downstream part evolve (-1% for sections 1, 2 and 3). It must be noted that the localized instability was developed outside of the measurement zone of gammadensitometer (see Figure 5(a)).

Local hydraulic head variations

Spatial and time evolutions of local hydraulic head during hydraulic gradient stages 1 and 2 don't evolve significantly.

Figure 7 represents profiles of hydraulic head during the third stage. At t = 5 min hydraulic head decreases because of the downstream gate opening. At t = 10min, the hydraulic head on pressure port number 11 slightly increases. 5 minutes later, a fast increasing of hydraulic head on pressure port number 10 of about $\Delta h_{10} = 35$ cm is detected (that corresponds to an overpressure of 3.5 kPa).

At t = 17 min the hydraulic head on point 9 increases about $\Delta h_9 = 55$ cm and one minute later on point 8: $\Delta h_8 = 20$ cm. This increasing of interstitial pressure which appears in the specimen centre and progresses in downstream direction may be due to clogging. At t = 20 min, hydraulic head profiles decrease suddenly and this evolution appears at the same time as increasing of: seepage flow, settlement and eroded mass.

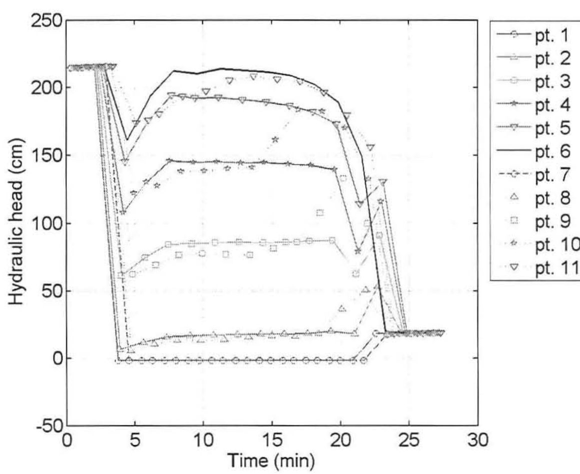

Figure 7. Instantaneous variations of hydraulic head (during third stage).

Thus a clogging which induces an interstitial overpressure appears (at point 10) 5 minutes before the initiation of localized instability. This observation confirms the first hypothesis of a fine particles migration in the whole specimen.

CONCLUSION

An experimental bench is designed to study initiation and development of internal erosion and its consequences on the hydraulic and mechanical behaviour of cohesionless soils. The device and experimental procedure are detailed. Results of a test performed on gap graded glass beads specimen are reported. On the downstream specimen part, an erosion of fine particles is detected and causes a migration of fine particles in the whole specimen. This evolution induces specimen settlement and a localized interstitial overpressure. This overpressure may be due to clogging and may be the cause of a localized instability. Finally the hydraulic conductivity is four times higher and the axial deformation reaches 4%.

The experiment setup could be used on different soils with varying particle fractions, in order to improve our understanding of the internal erosion mechanism.

ACKNOWLEDGEMENT

The authors wish to acknowledge the support of the French National Research Agency (project ANR-ERINOH) and the support of the French Institute for Applied Research and Experimentation in Civil Engineering (IREX) for this research.

BIBLIOGRAPHY

Alexis A., Le Bras G., Thomas P. (2004)."Experimental bench for study of settling-consolidation soil formation." *Geotechnical Testing J.* 27 (6): 557-567.

Bendahmane F., Marot D., Alexis A. (2008). "Parametric study of suffusion and backward erosion." *J. of Geotechnical and Geoenvironmental Engineering (ASCE)*, 134 (1): 57-67.

Kenney T.C., Lau D. (1985). "Internal stability of granular filters." *Canadian Geotechnical J.* 22 (2): 215-225.

Li M. (2008). "Seepage induced instability in widely graded soils." *PhD Thesis*, University of British Colombia, Vancouver, Canada, 300 p.

Marot D., Bendahmane F., Rosquoet F. Alexis A. (2009). "Internal flow effects on isotropic confined sand-clay mixtures." *Soil & Sediment Contamination, an Int. J.* 18 (3): 557-567.

Moffat R., Fannin R.J. (2006). "A large permeameter for study of internal stability in cohesionless soils." *Geotechnical Testing J.* 29 (4): 1-7.

Skempton A.W., Brogan J.M. (1994). "Experiments on piping in sandy gravels." *Géotechnique* 44 (3): 449-460.